Décolmatage des sédiments fins dans le lit d'une rivière à graviers

Action dans le cadre de l'accord agence de l'Eau / Irstea – 2015.

Table des matières

Personnes impliquées

Céline Berni	chargée de recherche
Albert Herrero	post-doctorant
Emeline Perret	doctorante
Benoît Camenen	chargé de recherche
Fabien Thollet	ingénieur d'étude

1 Projet soumis

1.1 Contexte

La Directive Cadre sur l'Eau donne comme objectif aux Etats européens d'atteindre un « bon état » écologique des cours d'eau à l'échéance de 2015. De nombreuses rivières à graviers des Alpes françaises transportent de grandes quantités de sédiments fins dont le flux est perturbé par des ouvrages (centrales hydroélectriques ou digues par exemple). Le déséquilibre engendré a un fort impact écologique car il peut notamment favoriser l'infiltration de sédiments fins (ou colmatage des lits) qui nuit à la qualité des habitats (manque d'oxygène, lieux de ponte altérés). Une meilleure maîtrise de la dynamique des sédiments fins sur une matrice graveleuse semble donc fondamentale quant à l'atteinte ou le maintien d'un bon état écologique des rivières.

1.2 Objectifs

L'objectif de cette action est de proposer des préconisations en termes de débit, de concentration et de forme d'hydrogramme pour le décolmatage par chasse hydraulique de rivières à graviers à l'aval d'un barrage. Nous chercherons à comprendre les processus physiques de décolmatage et notamment à répondre aux questions suivantes :

1. Sans mobiliser la matrice grossière, jusqu'à quelle profondeur peut-on décolmater un lit colmaté ?
2. Quel est l'impact de la mobilisation de la matrice grossière sur la profondeur de décolmatage du lit ?
3. Comment optimiser la forme d'un hydrogramme pour maximiser le décolmatage à volume d'eau constant (i.e. à coût constant) ?

1.3 Intérêt opérationnel

Si la problématique de colmatage « anthropique » est courante sur les rivières à graviers des Alpes françaises (voir l'annexe 1), les processus d'infiltration et surtout de remise en suspension de ces sédiments fins sont encore peu maitrisés et l'efficacité d'opérations de chasse d'eau claire est incertaine. Ainsi malgré leur potentiel, il n'existe pas actuellement de méthodologie claire de décolmatage en utilisant uniquement la force de l'eau et certains gestionnaires finissent généralement par opter pour une solution mécanique couteuse. Cependant, l'agence de l'eau a participé à des opérations successives de décolmatage de la Durance, entre 2007 et 2013 et il a été montré, qu'un décolmatage efficace peut avoir un impact positif important sur des populations piscicoles, même si son effet est de courte de durée, en effectuant le lâcher régulièrement juste avant la période de reproduction des espèces patrimoniales cibles. Il semble alors important d'optimiser la remise en suspension des sédiments fins par lâchers. Les tests grandeur nature sont coûteux et ne permettent pas d'optimiser facilement plusieurs paramètres à la fois. Les

sept années d'essais sur la Durance ont permis de déterminer le débit efficace minimal mais ni la durée, ni la forme de l'hydrogramme, ni la fréquence des lâchers optimales. Les lâchers ont par ailleurs conduit à un décolmatage significatif du lit mais un contrôle le mois suivant montre un retour à un état proche de celui avant lâcher. Ce projet combinant expériences en canaux et sur le terrain va contribuer à une meilleure compréhension de la dynamique des sédiments fins pendant et après les lâchers et mener à un guide de bonnes pratiques précis pour la conduite de chasses optimisant leur efficacité et la durée de leurs effets.

1.4 Description de l'opération

L'action proposée se réalisera dans la continuité des travaux in-situ déjà réalisés par l'équipe HHLY d'Irstea Lyon (coordination Benoît Camenen) et des travaux réalisés dans le canal à pente variable du hall hydraulique du centre d'Irstea Lyon (coordination Céline Berni). Elle se basera sur une étude en laboratoire permettant de tester plusieurs situations contrôlées et sur des mesures de terrain dans une rivière torrentielle : l'Arc en Maurienne. Ces mesures de terrain permettront de valider les hypothèses sous-jacentes au modèle physique. Des expériences de laboratoire en cours (postdoc d'Albert Herrero) permettent, préalablement à ce projet, de comprendre les processus d'infiltration de limons dans un lit de gravier. A leur suite seront réalisés, dans le cadre de ce projet, des tests dans le canal à pente variable. Nous envisageons 5 expériences combinant deux débits, deux concentrations et deux formes d'hydrogramme différentes (avec un temps de monté supérieur au temps de décrue et inversement). Les différentes expériences seront réalisées avec un même volume d'eau pour évaluer les conditions de chasse optimales à coût constant. Nous chercherons ainsi à quantifier l'influence de ces paramètres sur l'efficacité de la chasse, *i.e.* sur la quantité de sédiments fins évacués. Emeline Perret (doctorante à partir de Sept. 2014, co-encadrement EDF avec K. El Kadi, collaboration avec EDF/CIH) travaillera sur la contrainte critique de mise en mouvement de la matrice grossière colmatée. Cette étude permettra de mieux appréhender si (et à quel point) mouvement des grossiers et décolmatage vont nécessairement de pair. En parallèle, des mesures de terrain seront réalisées sur l'Arc en Maurienne pendant la période de fonte et pendant une chasse de barrage afin de mieux transposer les résultats de laboratoire au terrain (infiltration et remise en suspension de fines, impact sur les déplacements de galets tracé). La chasse de 2014 a déjà fait l'objet d'une telle étude. Le protocole utilisé ainsi que son adaptation aux futures campagnes est présenté en annexe. Ces travaux permettront ainsi de proposer des préconisations pour les chasses (détermination de la gamme de débit et de concentration maximale appropriée, de la forme de l'hydrogramme de chasse, de la fréquence d'intervention etc.).

1.5 Rattachement aux orientations thématiques de l'accord

Q6 Quelle efficacité des travaux de restauration et coûts associés ? Dans ce projet, nous n'allons pas chercher à quantifier le coût d'une restauration mais à qualifier à coût constant, l'efficacité d'une chasse de barrage sur le colmatage d'une rivière en fonction de quelques paramètres choisis. Cette restauration physique est en effet importante pour la qualité des habitats piscicoles notamment.

1.6 Résultats et indicateurs de suivi

L'action proposée fournira des préconisations de gestion des débits d'ouvrage ou bifurcation pour optimiser le décolmatage de rivières à graviers ainsi que des préconisations pour le suivi de ces opérations.

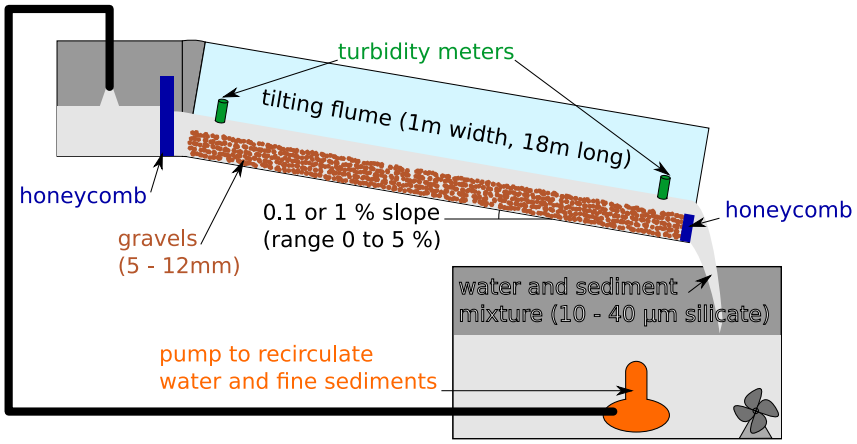

FIGURE 1 – schéma des expériences menées dans le canal inclinable

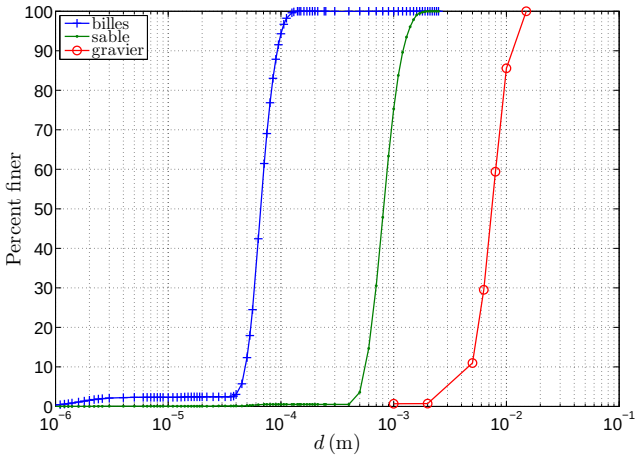

FIGURE 2 – Granulométrie des sédiments utilisés

2 Moyens mis en oeuvre

2.1 Protocole des expériences de laboratoire

Nous avons réalisé plusieurs expériences dans le laboratoire d'hydraulique et d'hydromorphologie d'Irstea Lyon-Villeurbanne (HHLab). Ces expériences ont été menées dans le canal dit inclinable, de 1 m de long, 18 m de large avec une pente réglable de 0 à 5 %, schématisé figure 1. Selon les expériences, le débit pouvait être constant ou variable et l'eau chargée ou non. Un débitmètre électromagnétique permet de mesurer le débit tout au long des expériences. Dans la suite, nous noterons x la coordonnée longitudinale, dans le sens de l'écoulement, $x = 0$ étant l'amont du canal ; y la coordonnée transversale, perpendiculaire à l'écoulement ; z la coordonnée verticale, perpendiculaire au fond. Nous avons utilisé 3 types de sédiments. Les courbes granulométriques correspondantes sont présentées figure 2. Les diamètres médians des billes, du sable et du gravier sont respectivement 66 microns, 813 microns et 7.5 mm.

2.1.1 Etat initial : expériences d'infiltration

Avant chaque expérience un lit de graviers est installé et aplani de manière à avoir une hauteur de fond sédimentaire constante le long du canal (8 cm). Chaque expérience de décolmatage est précédée d'une expérience d'infiltration. Cela consiste à soumettre le lit de graviers à un écoulement chargé en sédiment fin à un débit plus faible que celui permettant la mise en mouvement des graviers. Pour l'expérience AE1, le sédiment fin utilisé était très fin (billes de verre de 66 microns) et la mise en suspensions dans la bâche efficace. Tout au long de l'expérience d'infiltration (de 10 à 20 h environ) des billes ont été ajoutées dans le réservoir en sous-sol et mises en suspension par un agitateur. Le mélange eau+sédiment était ensuite pompé pour alimenter le canal en eau chargée.

Pour les expériences suivantes, nous avons voulu ajouter également du sable. Le même protocole a été appliqué pour les billes mais le sable s'est avéré trop lourd pour être efficacement mis en suspension dans le réservoir. A l'amont du lit de gravier, nous avons donc installé un stock de sable (lit de sable de la même épaisseur que le gravier sur 5 m). Ce lit de sable était érodé au fur à mesure de l'expérience et rechargé. Nous obtenions ainsi durant l'expérience d'infiltration une alimentation constante en sable sur le lit de gravier, sous forme de charriage et de suspension graduée. Ce réservoir de sable occupant la première partie du canal, l'analyse des expériences de décolmatage mettant en jeu du sable ne se fera que sur la partie aval.

Lorsque que seules des billes ont été utilisées comme sédiment fin (expérience AE1), celles-ci se sont infiltrées dans le lit sous l'effet de la gravité jusqu'à ce que l'ensemble des pores de la matrice grossière soit bouchés. Le lit obtenu était un lit colmaté sur toute la profondeur compte tenu de de la différence de diamètres importante. Les pores dans le lit de graviers sont trop gros pour pouvoir retenir le sédiment fin. La vitesse de colmatage du lit a été étudiée en détails. Elle est relativement bien prédite par la formule élaborée par Einstein (1968) pour peu qu'on prenne en compte la porosité du milieu. Ainsi, le flux de sédiment J_z par unité de surface, qui s'infiltre dans le lit, peut s'exprimer comme

$$J_z = C\theta v_s$$

où C est la concentration en sédiment fin juste au-dessus de l'interface, v_s la vitesse de chute et θ la porosité du lit. Dans les expériences que nous avons faites, nous obtenons un flux de sédiment de l'ordre de $0.5 \cdot 10^{-3}$ kg s^{-1} m^{-2}. Les résultats expérimentaux ont été présentés notamment lors du congrès IAHR (voir annexe A.2). Leur analyse plus approfondie ainsi que le développement d'un modèle a été réalisé en collaboration avec des collègues Australiens et un article devrait être soumis prochainement.

Les expériences avec du sable ont au contraire mené à un colmatage mixte, avec une part du sédiment qui s'est infiltrée jusqu'au fond du canal (les billes principalement) et une autre part qui est restée dans une couche à surface du lit (en majorité du sable). Ces deux types d'infiltrations sont illustrés figure 3. Un modèle géométrique simple a été développé durant ce projet et permet de prédire l'occurrence de l'un ou de l'autre type d'infiltration. Il a fait l'objet d'une publication soumise en Juin 2016 à *Water Resources Research*. La version soumise est présentée en annexe A.1.

Le tableau 1 récapitule les conditions d'infiltration des expériences d'infiltration qui ont précédé les expériences de décolmatage. Ces différentes conditions ont été investiguées afin de mieux comprendre les processus d'infiltration. Le colmatage par les sables et les billes a été réalisé en deux étapes pour les expériences préalables aux expériences AE2, AE3 et AE4, ou en alimentant le canal avec ces deux types de sédiments en même temps pour les expériences préalables à AE5 et AE6. Deux conditions de débits et de pente ont été étudiées. Elles conduisent à des colmatages légèrement différents. Ainsi, les dunes de sables formées lors de l'infiltration peuvent être de tailles différentes.

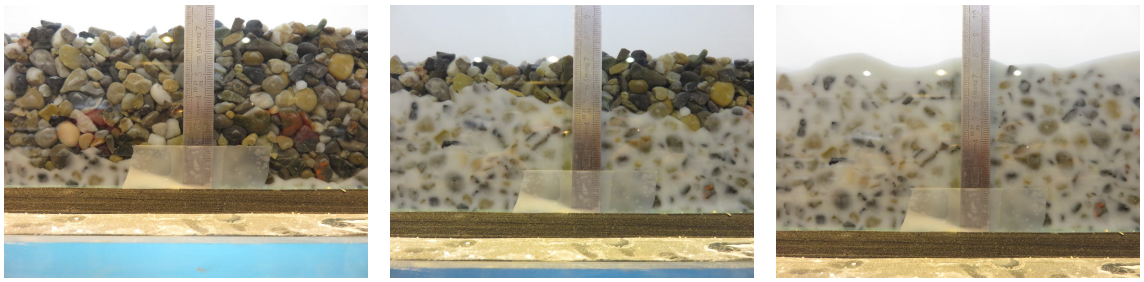

(a) Graviers + billes : colmatage sur toute la profondeur

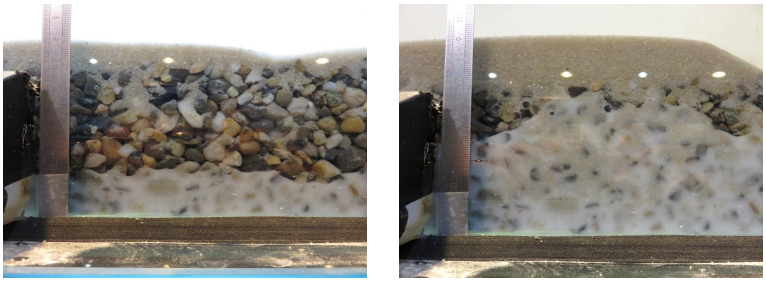

(b) Graviers + sable + billes : colmatage mixte

FIGURE 3 – Deux types d'infiltration. Photos vue de côté du canal à différents instants durant une expérience d'infiltration. De gauche à droite, le temps d'exposition du lit augmente.

TABLE 1 – Expériences d'infiltration préalables aux expériences de décolmatage

Expérience décolmatage qui suit	**Concentration**	**Débit**	**Pente**	
AE1	2.91 g/L	30 L/s	0.1 %	infiltration billes sur lit de graviers
AE2		50 L/s	0.1 %	infiltration sable sur lit de graviers
	1.39 g/L	20 L/s	0.1 %	infiltration billes sur le lit graviers + sable
AE3 et AE4		40 L/s	1 %	infiltration sable sur lit de graviers
	1.13 g/L	20 L/s	0.1 %	infiltration billes sur lit graviers + sable
AE5	0.95 g/L	50 L/s	0.1 %	infiltration billes et sable sur lit de graviers
AE6	0.78 g/L	40 L/s	1 %	infiltration billes et sable sur lit de graviers

2.1.2 Expériences de décolmatage

Le tableau 2 récapitule les conditions des différentes expériences menées pour ce projet. La figure 4 présente les séries temporelles des expériences AE2 à AE6. Nous ne disposons pas de l'enregistrement du débit de l'expérience AE1. Elle a été conduite identiquement à l'expérience AE2.

Table 2 – Tableau récapitulatif des expériences

Expérience		Débit	Ecoulement	Pente	Durée	Sédiments
AE1	29/05/2015	constant : 25 L/s	eau claire	1%	30 min	gravier + billes
AE2	01/09/2015	constant : 25 L/s	chargé à 3 g/L	1.03%	30 min	gravier + sable + billes
AE3	09/10/2015	constant : 45 L/s	chargé à 2 - 5 g/L	0.97%	17 min	gravier + sable + billes
AE4	13/10/2015	paliers : 45L/s, 50L/s, 55L/s	chargé à 2 - 5 g/L	1.04%	40 min	gravier + sable + billes
AE5	06/11/2015	hydrogramme montant	chargé à 0.2 - 0.7 g/L	1.06%	30 min	gravier + sable + billes
AE6	03/12/2015	hydrogramme descendant	chargé à 0.3 - 0.8 g/L	1.04%	30 min	gravier + sable + billes

L'écoulement peut être chargé ou non en sédiment fins. La concentration en sédiments présentée dans le tableau 2 a été déterminée par filtrage et pesée d'échantillons récoltés manuellement à l'amont et à l'aval du canal. Il n'y a pas d'alimentation solide en gravier durant les différentes expériences.

Nous avons effectué un jeu de 4 expériences à volume d'eau total déversé constant, les expériences AE2, AE3, AE5 et AE6 dans le but d'optimiser la forme d'hydrogramme qui décolmate le plus efficacement un lit colmaté. Une expérience longue à faible débit, une courte à plus fort débit, un hydrogramme montant avec une descente rapide et un hydrogramme descendant avec une montée rapide ont ainsi été comparés (voir figure 4). Le lit initial pour ces quatre expériences était constitué de gravier infiltré de sable et de billes (colmatage mixte, voir figure 3b), l'eau était chargée en sédiments fins et du sable pouvait être également transporté sous forme de charriage ou suspension graduée. L'expérience AE2 peut être comparée à l'expérience AE1, pour laquelle, l'eau entrant dans le canal était claire, et le lit colmaté sur toute la profondeur, avec des billes seulement. L'expérience AE4 fait suite à l'expérience AE3. Elle avait pour but de qualifier la mobilité du gravier après décolmatage.

Lors de ces expériences, nous avons qualifié l'état du lit de différentes façons. Nous avons effectué des prélèvements avant et après une expérience. Nous avons pris des photographies de l'état de surface et du lit par côté à travers les parois vitrées du canal pour évaluer le niveau du colmatage. Un scanner 2D (scanCONTROL 2900) a été déployé afin d'obtenir des profils d'élévation du lit. Ceux-ci ont pu être utilisés pour calculer des rugosités (écart type de l'élévation) selon différentes directions et sur des distances plus ou moins longues. Nous avons également utilisé ces résultats pour obtenir des modèles d'élévation numériques (DEM) sur de petites zones de $10 \times 40\,\text{cm}$.

2.2 Sur le terrain

Deux expériences ont été menées lors de la chasse de l'Arc, en 2014 et 2015. Le débit atteint n'a pas été suffisant pour mettre en mouvement le banc de galet étudié. De forts dépôts ont été observés, dont une partie a été reprise par l'écoulement durant l'évènement, ce qui s'est traduit par des chenaux visibles à la fin de la chasse (voir figure 5). Les résultats de cette expérience

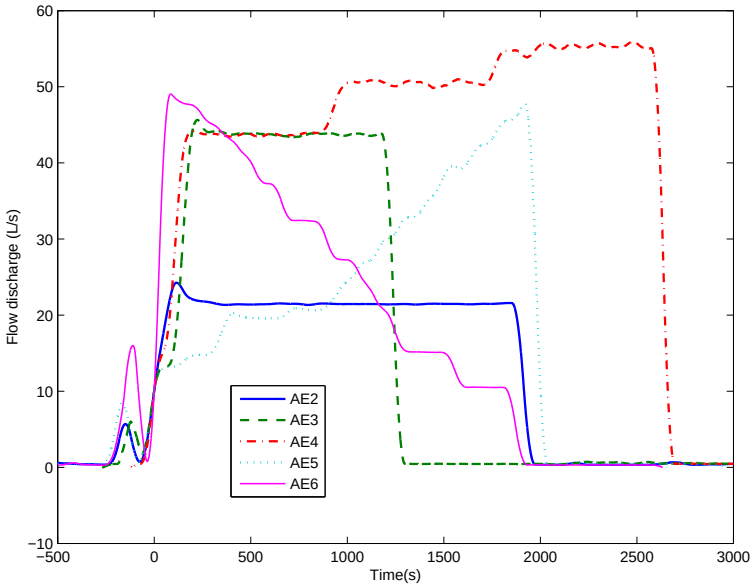

FIGURE 4 – Débit liquide en fonction du temps lors des expériences 2 à 6.

ont notamment été présentés au congrès de l'IAHR, voir annexe A.3. Ces résultats semblent indiquer que la quantité de sédiments déposés est relativement bien prédite par la formule d'Einstein modifiée, telle qu'elle a été validée lors des expériences en canal. Il faut cependant préciser que la distribution granulométrique de ces dépôts n'est pas très bien prédite.

FIGURE 5 – Photo du banc de l'Arc après la chasse

3 Résultats

Nous présenterons dans cette partie les résultats obtenus pour les diverses expériences, qui seront discutés et comparés par la suite.

3.1 Expérience AE1

L'expérience AE1 a consisté à soumettre un lit de graviers colmaté entièrement de billes (voir figure 3a) à un écoulement d'eau claire de 25 L/s avec une pente de 1 % pendant 30 minutes. La figure 6 présente une photo de l'état de surface du lit avant et après l'expérience. Les zones blanches indiquent la présence de billes et correspondent à un colmatage de surface. Lors de cette expérience, le colmatage de surface est entièrement lessivé. Alors que l'élévation du lit initiale présente des étendues lisses (voir figure 7a), des grains sont visibles sur toute l'étendue du relevé à la fin de l'expérience (voir figure 7b). On peut reconnaître des grains d'un relevé à l'autre, attestant que le transport des graviers était quasi inexistant lors de cette expérience. La même analyse peut être faite à partir des profils transversaux présentés figure 8, sur laquelle chaque pic représente un grain, dont les contours se précisent après le décolmatage. L'analyse des profils scanner révèle que la rugosité a augmenté durant cette expérience, de l'ordre de 2.2 à 2.6 mm. A titre de comparaison, la rugosité moyenne d'un lit de graviers seuls est de l'ordre de 3.2 mm. Après décolmatage, on s'approche de cette rugosité, notamment dans la partie amont. On peut aller plus loin dans l'analyse de la rugosité du lit en regardant comment celle-ci évolue le long du canal. Sur la figure 9, sont présentées les rugosités locales du lit initial de cette expérience, du lit final, et de 2 lits de graviers seuls. Ces rugosités sont obtenues à partir de l'écart type d'un profil d'élévation scanner de 10 cm de long environ comme présenté figure 8. Huit profils ont été réalisés dans la largeur du canal, l'écart-type moyen pour ces huit profils est présenté. La rugosité du fond a augmenté sur l'ensemble du canal. Elle était cependant légèrement moins élevée initialement dans la partie aval. Ceci indique que le colmatage du lit est moins marqué dans cette partie. Nous verrons par la suite que c'est le cas d'une majeure partie des expériences. Le colmatage est en effet fonction de la concentration et celle-ci diminue le long du canal durant les expériences d'infiltration. Le lit se colmate toujours un peu plus lentement à l'amont qu'à l'aval du canal.

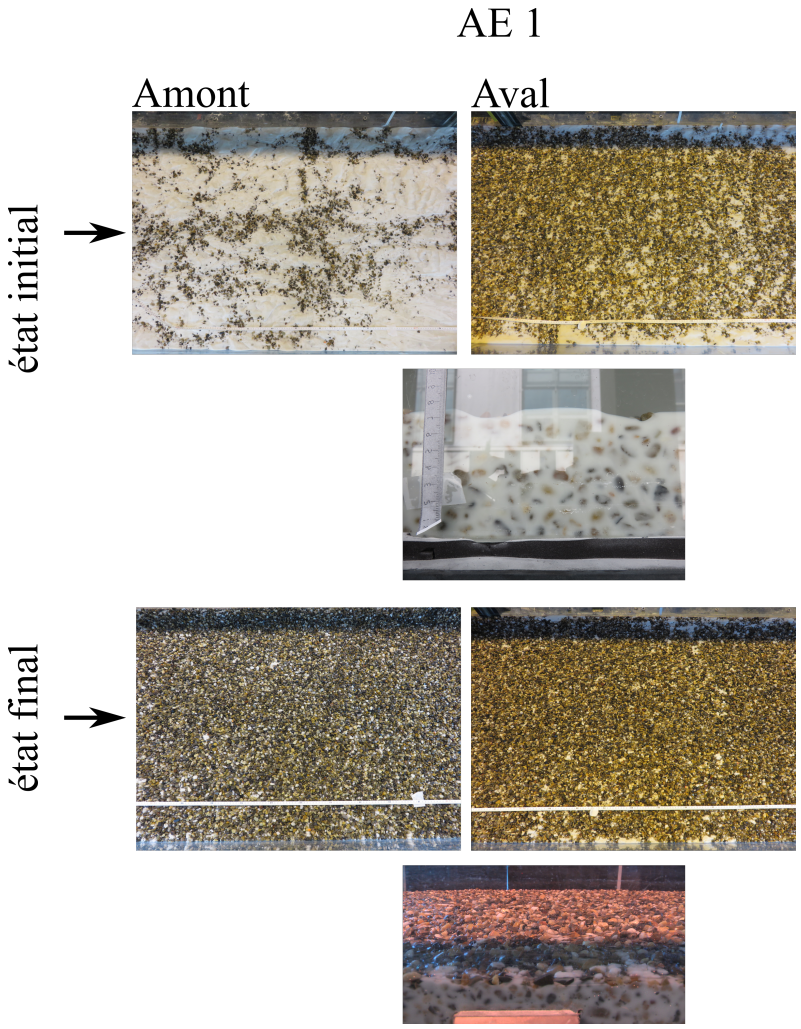

FIGURE 6 – Photographies de l'état de surface et par côté de l'expérience AE1, à l'état initial et à l'état final. La flèche indique le sens de l'écoulement. Les deux photos alignées horizontalement sont des vues de dessus, la photo en dessous une vue de côté à travers la vitre du canal.

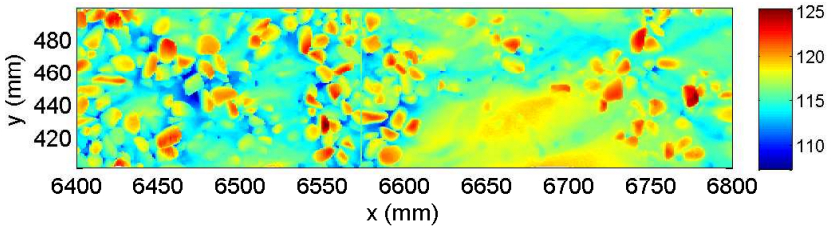

(a) état initial

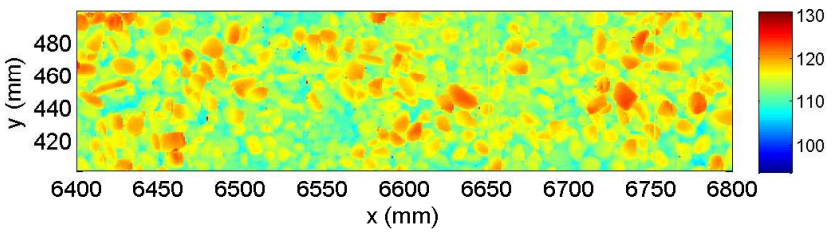

(b) état final

FIGURE 7 – Élévation du lit, expérience AE1.

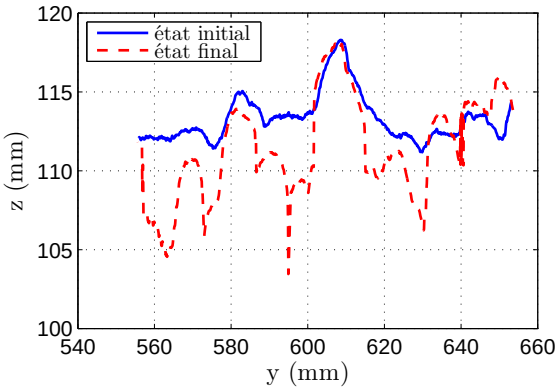

FIGURE 8 – Exemple de profil scanner, expérience AE1.

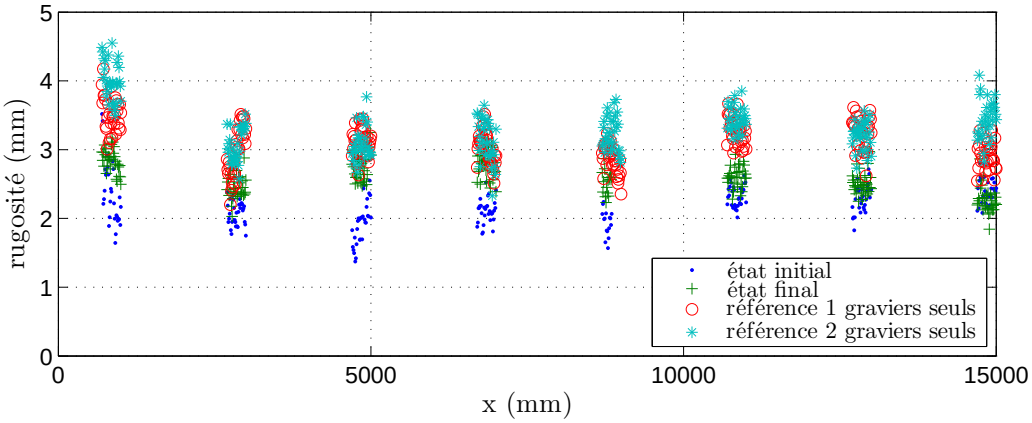

FIGURE 9 – Rugosité transversale (en millimètres) à l'échelle d'un profil (10 cm), moyennée sur 8 profils dans la largeur, expérience AE1. Deux calculs de rugosité ont été effectués sur un lit composé de graviers seulement, pour référence.

3.2 Expérience AE2

Pour l'expérience AE2, le débit et la durée de l'expérience sont les mêmes que pour l'expérience AE1. Cependant, la nature du lit est plus complexe, étant composé de graviers, de sable et de billes et l'eau qui recircule dans le canal est chargée, avec une concentration de l'ordre de 3 g/L. On peut d'ores-et-déjà constater à l'état initial un dépôt de sédiments fins (sable + billes) en surface. Ceci est dû à la présence de sable, pour lequel l'écart en diamètre avec le gravier est moins important. Les graviers sont à peine visible (voir figures 10 et 11a). A l'état final, les graviers réapparaissent à l'amont du canal, tandis qu'ils restent en partie enfouis à l'aval (voir figures 10 et 11b). Les mesures de concentrations semblent indiquer une concentration dans l'écoulement un peu plus élevée à l'amont qu'à l'aval ce qui tend à suggérer que les sédiments fins ont été mieux lavés à l'amont car la concentration y était plus faible. L'écoulement s'est chargé en sédiment fin le long du canal, et une part de ce sédiment s'est déposée dans le réservoir. Ceci se traduit en terme de rugosité transversale par une rugosité initiale de l'ordre de 3-4 mm, à peu près constante le long du canal (voir figure 12) qui diminue, en particulier à l'aval, pour atteindre 1 mm. Nous verrons par la suite que la rugosité initiale est la conséquence de formes de fond (petites dunes, voir photos de la figure 10) qui sont efficacement nettoyées par l'écoulement, et laissent place à un lit de sable très lisse en surface à l'aval du canal. Le fait qu'on obtienne une rugosité semblable à celle du gravier initialement n'est probablement ici qu'une coïncidence.

Nous présentons également des photos à travers la paroi du canal (figure 10, à droite). A l'amont du canal, le lit est colmaté sur toute la profondeur. Au fond du canal, il y a essentiellement du sable (plus jaune) et dans la couche supérieure, un mélange de sable et de billes (plus blanches). Cette répartition n'évolue pas pendant l'expérience. A l'aval du canal, deux couches se distinguent nettement. Une couche de sable en surface et une couche de billes au fond du canal. Durant l'expérience, cette couche de bille s'épaissit, le colmatage occupe maintenant presque toute la profondeur.

Pour cette expérience et les suivantes, nous avons également utilisé le scanner longitudinalement et réalisé un profil d'élévation entre 6 et 16 m de l'amont du canal. Nous avons analysé ce profil de différentes manières.

1. En calculant l'écart type de l'élévation à l'échelle de la mesure scanner (*i.e.* sur un profil de 10 cm de long environ).

2. En calculant l'écart type de l'élévation à laquelle nous avons soustrait la tendance linéaire globale à l'échelle de la mesure scanner (*i.e.* sur un profil de 10 cm de long environ).

3. En calculant l'écart type de l'élévation à l'échelle de 5 grains (*i.e.* sur un profil de 37.5 mm). Pour cet écart type, nous retirons également la tendance linéaire globale sur ces 37,5 mm.

Ces trois types de rugosité sont représentés figure 13 pour l'état initial (280815) et l'état final (010915) du lit de l'expérience AE2. L'écart entre ces trois rugosités pour l'état initial atteste la présence de formes de fond. La rugosité de grain inférieure à 1 mm atteste la présence de sédiments fins en surface. Pour référence, la rugosité du sable seul est de l'ordre de 0.3 mm. Après l'expérience, les formes de fond sont nettoyées, comme vu ci-dessus, et ces trois rugosités se rejoignent.

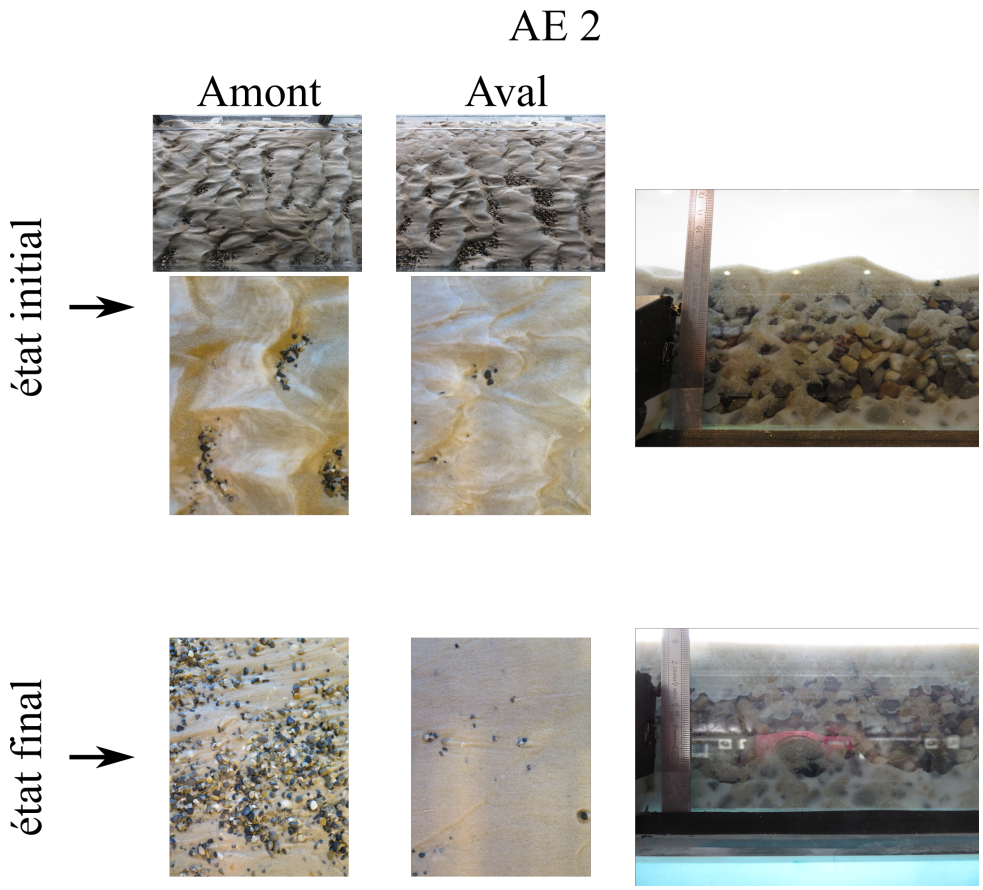

FIGURE 10 – Photographies de l'état de surface (à gauche) et par côté (à travers la vitre du canal, à droite) de l'expérience AE2, à l'état initial et à l'état final. La flèche indique le sens du courant.

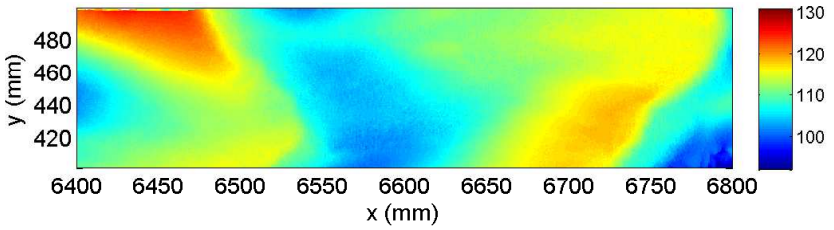

(a) état initial

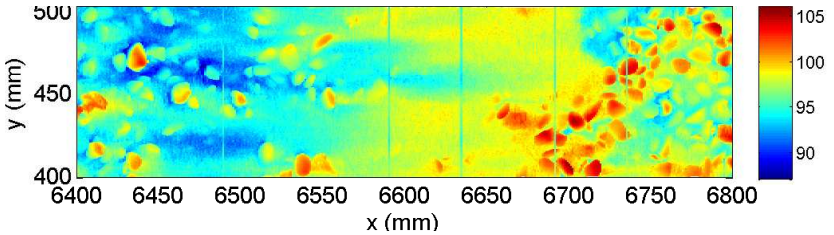

(b) état final

FIGURE 11 – Élévation du lit en $x = 6400\,\text{mm}$, expérience AE2.

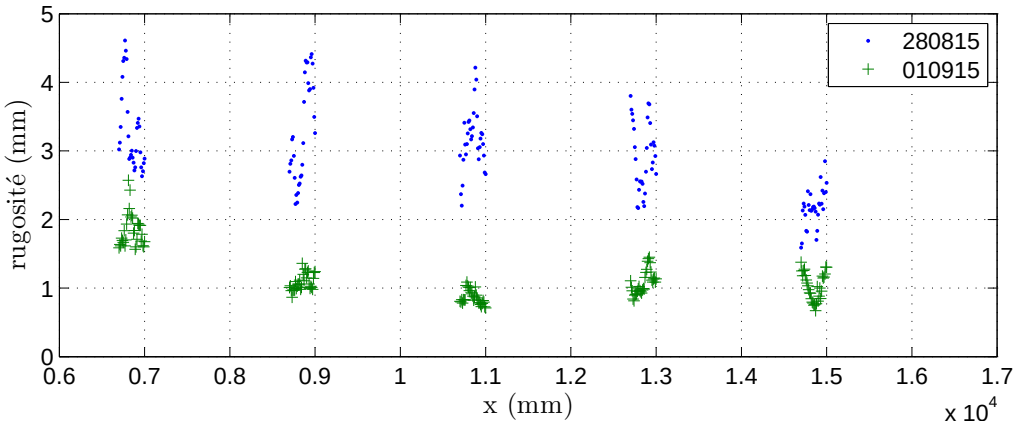

FIGURE 12 – Rugosité transversale (en millimètres) à l'échelle d'un profil (10 cm), moyennée sur 8 profils dans la largeur, avant (280815) et après (010915) l'expérience AE2.

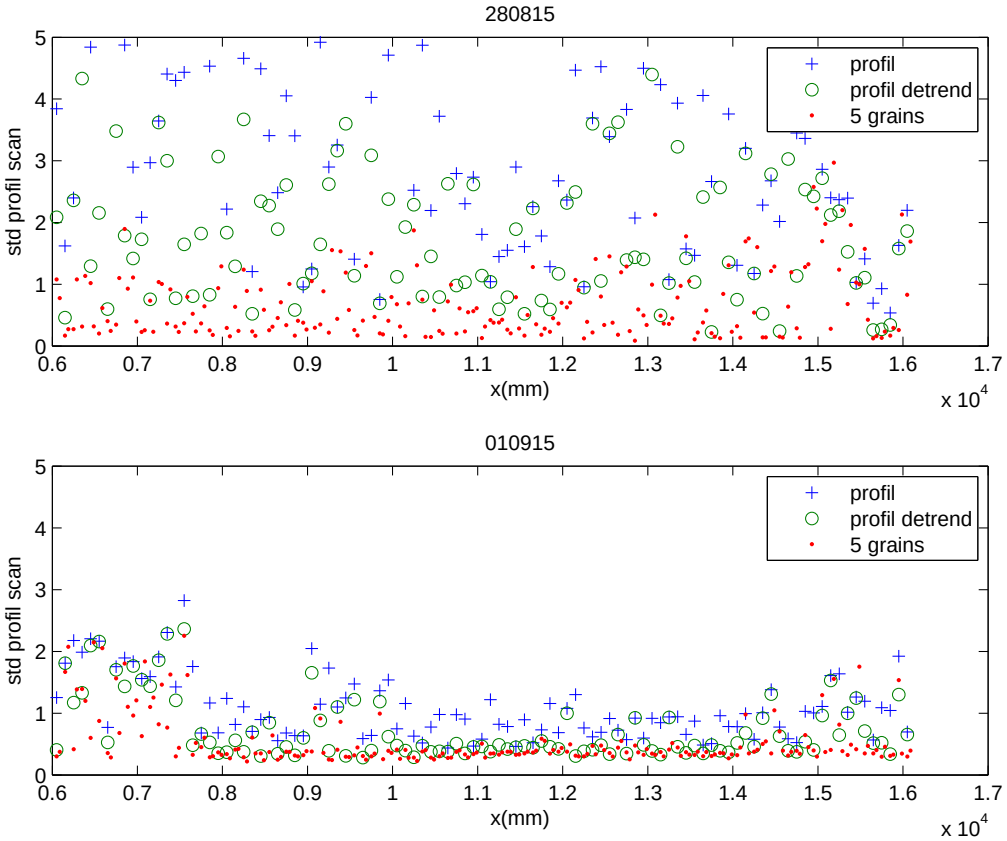

FIGURE 13 – Rugosité longitudinale (en millimètres) à l'échelle d'un profil (croix bleues), à l'échelle d'un profil après avoir soustrait une éventuelle pente globale sur le profil (ronds verts) et à l'échelle de 5 grains (points rouges), avant (en haut) et après (en bas) l'expérience AE2.

3.3 Expérience AE3

Nous avons cherché à explorer avec l'expérience AE3 l'influence du débit sur la capacité à décolmater un lit, tout en restant à volume total déversé constant (voir figure 4). Le débit pour cette expérience est supérieur au débit de l'expérience AE2, mais a été choisi cependant faible pour limiter la mise en mouvement des graviers. Il faut cependant noter que la présence de sable facilite la mise en mouvement du lit et que le transport de gravier pour un même débit liquide est plus important que pour un lit de graviers seuls.

L'état initial est légèrement différent de l'état initial pour l'expérience AE2. On observe comme pour l'expérience AE2 des dépots de sable en surface à l'amont du canal mais peu en aval (voir figure 14). De plus, les dunes de sable à l'amont sont moins marquées et plus longues (voir figure 15a) et génèrent une rugosité longitudinale moins importante (de l'ordre de 1 mm pour AE3, jusqu'à 5 mm pour AE2, voir figures 17 et 13). La rugosité longitudinale plus forte à l'aval quelle que soit l'échelle considérée (voir figure 17) indique la présence de graviers en surface. En effet, afin d'analyser les processus d'infiltration, les deux expériences d'infiltration menant à l'état initial des expériences AE2 et AE3 sont différentes (voir tableau 1). Pour ces deux expériences, le lit a d'abord été infiltré de sable puis de billes. Les conditions pour l'infiltration du sable sont différentes : pour AE2, le débit liquide était de 50 L/s et la pente de 0.1 % ; pour AE3, 40 L/s et 1 %.

L'état final semble globalement similaire. Les formes de fond sont en grande partie lessivées et la majeur partie du lit est recouverte de sable. La rugosité transversale est de l'ordre de 1 à 2 mm à l'amont, et la rugosité longitudinale inférieure à 1 mm. Elle est similaire à l'échelle d'un profil et à l'échelle d'un grain.

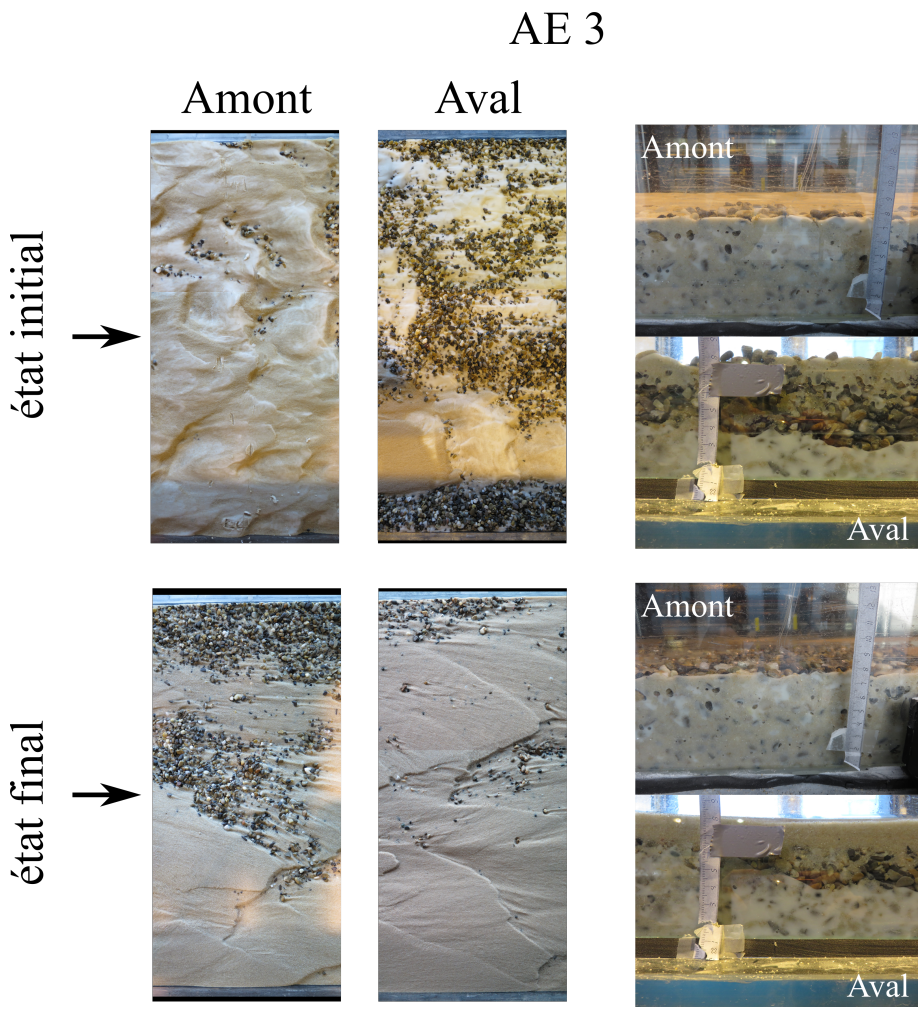

FIGURE 14 – Photographies de l'état de surface (à gauche) et par côté (à travers la vitre du canal, à droite) de l'expérience AE3, à l'état initial et à l'état final. La flèche indique le sens du courant.

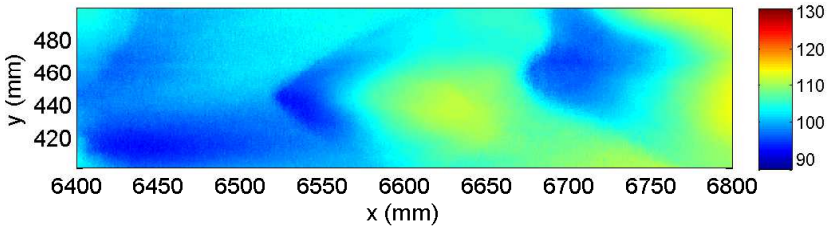

(a) état initial

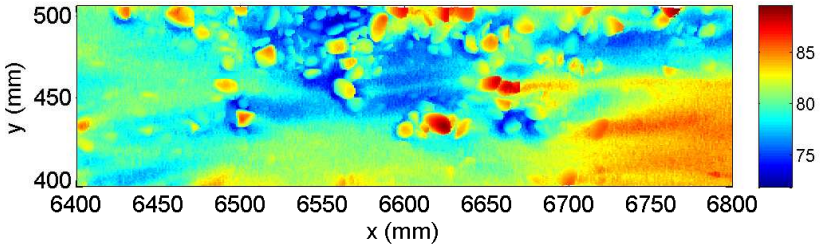

(b) état final

FIGURE 15 – Élévation du lit en $x = 6400\,\text{mm}$, expérience AE3.

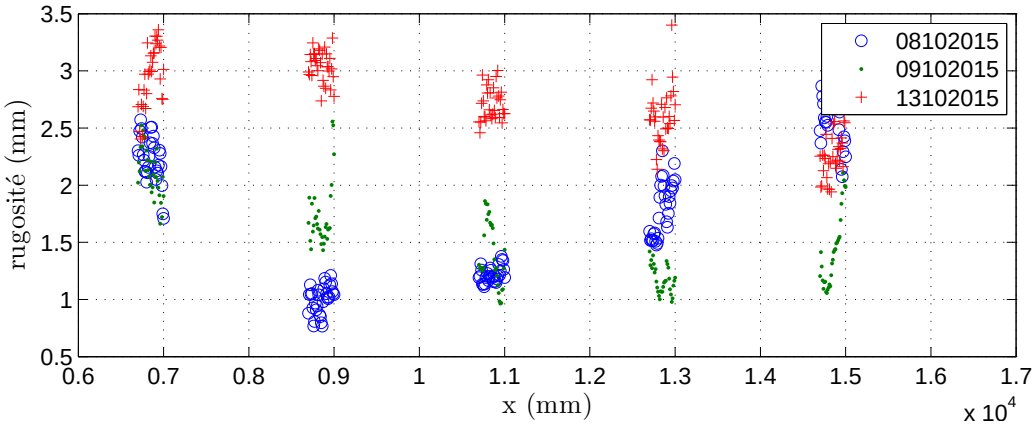

FIGURE 16 – Rugosité transversale (en millimètres) à l'échelle d'un profil (10 cm), moyennée sur 8 profils dans la largeur, avant (08102015) et après (09102015) l'expérience AE3, puis l'expérience AE4 qui suit (13102015).

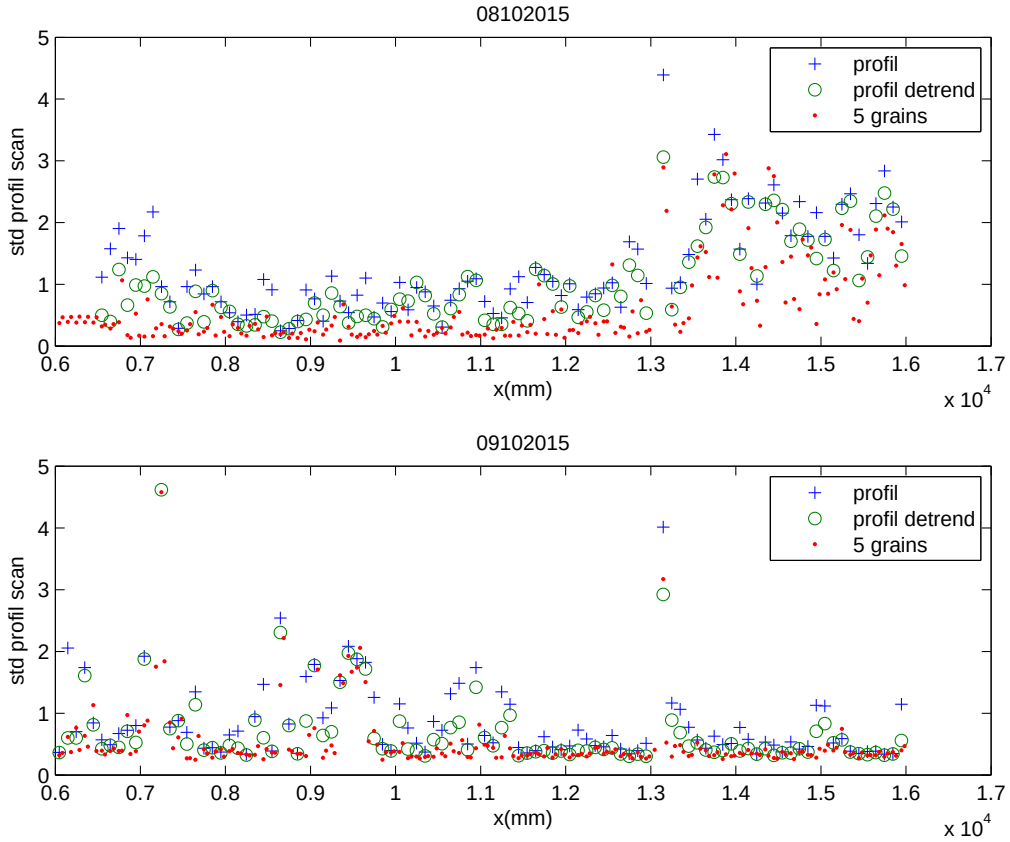

FIGURE 17 – Rugosité longitudinale (en millimètres) à l'échelle d'un profil (croix bleues), à l'échelle d'un profil après avoir soustrait une éventuelle pente globale sur le profil (ronds verts) et à l'échelle de 5 grains (points rouges), avant et après l'expérience AE3.

3.4 Expérience AE4

L'expérience AE4 fait suite à l'expérience AE3. Elle a pour objectif de quantifier la mobilité du gravier dans un lit décolmaté. Elle permet également de voir l'effet d'un débit plus important qui met en mouvement l'ensemble du lit.

Cette expérience conduit à une érosion significative du lit (voir photos de côté figure 19) et un décolmatage en surface de l'ensemble du canal. La rugosité transversale augmente pour s'approcher de 3 mm, rugosité du gravier seul (figure 16, 13102015).

Le débit solide de graviers récolté est récapitulé dans le tableau 3. Le débit liquide, la hauteur d'eau et la contrainte y sont associés. Les 16 mm d'incertitudes sur la hauteur d'eau correspondent à l'érosion détectée entre le début et la fin de l'expérience au point de mesure considéré. Cette incertitude se répercute sur la contrainte. Nous l'avons associée aux deux paliers de débit de 50 et 55 L/s compte tenu du faible transport pour le premier palier. La diminution de débit solide alors que le débit liquide augmente de 50 à 55 L/s peut être due au fait que la quantité de sable a diminué. En effet, si l'on considère un lit de graviers seuls, comme cela a été fait dans le cadre de la thèse d'Emeline Perret (thèse en cours, coencadrement Céline Berni & Benoît Camenen), un transport de graviers de $5 \cdot 10^{-7}\,\mathrm{m}^2/\mathrm{s}$ correspond à une contrainte adimensionnée variant de 0.05 à 0.06. Le transport sédimentaire pour une contrainte du même ordre dans cette expérience de décolmatage est nettement supérieur, ce que l'on interprète comme étant la conséquence d'une lubrification de l'écoulement de sédiments due à la présence de sable.

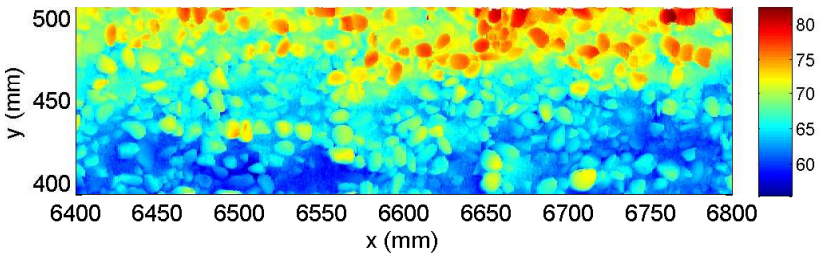

FIGURE 18 – Élévation du lit en $x = 6400$ mm, expérience AE4, état final. L'état initial est présenté figure 15b.

débit liquide (L/s)	hauteur d'eau (mm)	contrainte	débit solide (m^3/s)
45	53	0.04	$6.4 \cdot 10^{-6}$
50	57 + 16 ?	0.05-0.06	$2.1 \cdot 10^{-5}$
55	57 + 16 ?	0.05-0.06	$1.1 \cdot 10^{-5}$

TABLE 3 – Débit solide collecté lors de l'expérience AE4 ainsi que le débit liquide, la hauteur d'eau (h) et la contrainte adimensionnée ($\theta = \frac{\rho g h I}{(\rho_s - \rho) g d}$, avec I la pente, ici 1 %, d le diamètre médian des graviers, $d = 7.5$ mm, ρ la masse volumique de l'eau et $\rho_s = 2650\,\mathrm{kg/m}^3$ la masse volumique du sédiment). L'incertitude de 16 mm sur la hauteur d'eau correspond à l'érosion détectée durant l'expérience au point de mesure considéré.

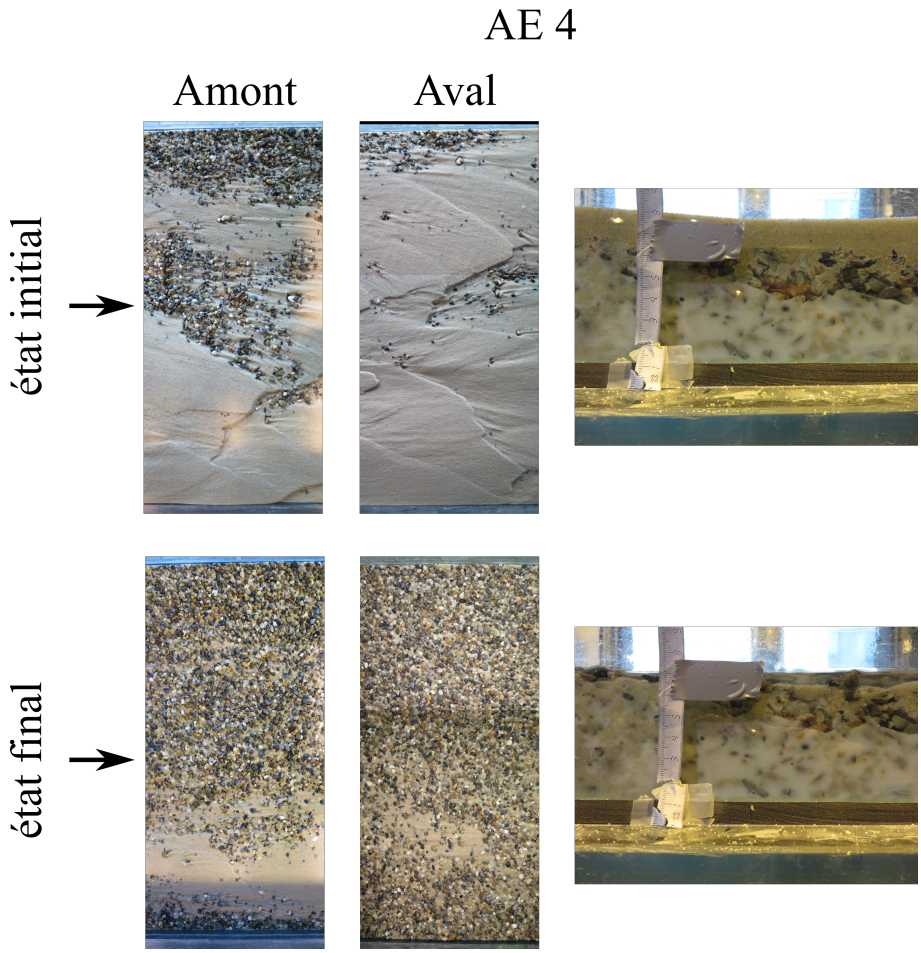

FIGURE 19 – Photographies de l'état de surface (à gauche) et par côté (à travers la vitre du canal, à droite) de l'expérience AE4, à l'état initial et à l'état final. La flèche indique le sens du courant.

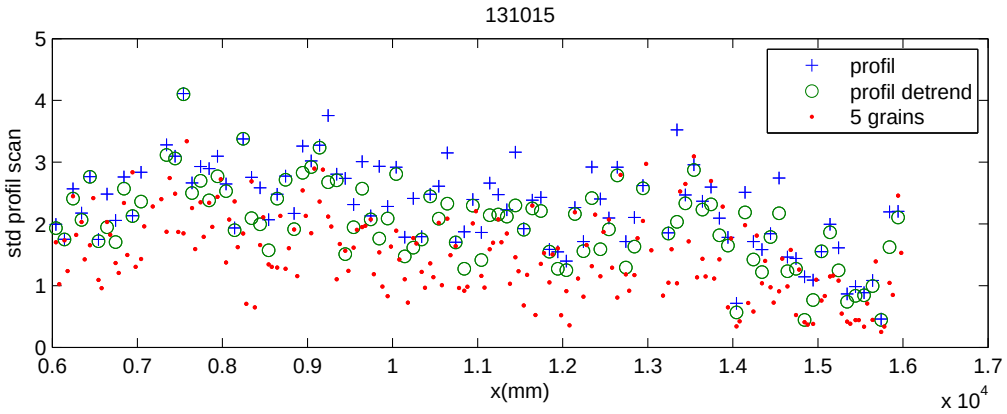

FIGURE 20 – Rugosité longitudinale (en millimètres) à l'échelle d'un profil (croix bleues), à l'échelle d'un profil après avoir soustrait une éventuelle pente globale sur le profil (ronds verts) et à l'échelle de 5 grains (points rouges), après l'expérience AE4.

3.5 Expérience AE5

Le débit liquide pour l'expérience AE5, contrairement aux précédentes expériences, augmente linéairement durant tout l'expérience pour être coupé brutalement à la fin de l'expérience (voir figure 4). Le débit solide de graviers (voir tableau 4) augmente lui aussi tout au long de l'expérience. Comme pour l'expérience AE4, il est supérieur à celui que génère la même contrainte sur un lit de graviers seuls.

Le lit est initialement constitué de graviers infiltrés de sable sur une majeure partie de la profondeur, avec des dunes de sables en surface qui laissent voir quelques graviers. (voir figure 21). Ces dunes sont relativement peu marquées et génèrent une rugosité à l'échelle du profil de l'ordre de 3 mm, qui correspond à la hauteur de dunes (voir figure 22a).

Après l'hydrogramme, à l'état final, la plupart des dunes sont nettoyées, comme le montre la photo de l'état final à l'aval (voir figure 21). Ceci se traduit par une rugosité à l'échelle du grain qui augmente sur la majeur partie du canal, de 0.4 mm à 2 mm environ. La rugosité transversale à l'échelle du profil varie moins, à part à l'aval, car la rugosité des graviers et celle des dunes qui leur précédaient sont équivalentes (voir figure 23).

Nous présentons également pour cette expérience l'analyse d'images d'un film réalisé par côté durant toute l'expérience (voir figure 25). Le niveau du sédiment fin a été relevé à différents instants. Selon les expériences et l'instant considéré, il peut s'agir du niveau du lit ou de la couche colmatée dans le lit. Le niveau du sommet des graviers est marqué par une ligne horizontale en pointillées. Si le niveau de colmatage est au-dessus de cette ligne pointillée, il y a un dépôt de sable en surface. Si ce niveau est en-dessous, nous observons ainsi sur quelle profondeur le lit est décolmaté. Lors des expériences que nous avons mené, nous ne sommes jamais parvenus à nettoyer entièrement la couche de sable pour un lit colmaté mixte. On peut ainsi suivre l'évolution du colmatage du lit (soit de surface, soit matriciel). Pour cette expérience, le lit a été particulièrement décolmaté lorsque le débit a été augmenté de 15 à 20 L/s. Il semblerait que ce niveau ait augmenté durant le palier à 15 L/s, mais cette oscillation est probablement due au passage d'une dune. Mis à part cette oscillation entre 1250 et 1750 s, la tendance est généralement à la baisse, et le lit est continuellement décolmaté durant l'expérience. Nous n'observons pas de dépôts à la fin de l'expérience.

débit liquide (L/s)	hauteur d'eau (mm)	contrainte	débit solide (m^3/s)
14	41	0.03	$1.3 \cdot 10^{-7}$
21	50	0.04	$1.4 \cdot 10^{-6}$
28	53	0.04	$6.6 \cdot 10^{-6}$
35	56	0.05	$1.6 \cdot 10^{-5}$
42	60	0.05	$3.7 \cdot 10^{-5}$

TABLE 4 – Débit solide collecté lors de l'expérience AE5 ainsi que le débit liquide, la hauteur d'eau (h) et la contrainte adimensionnée ($\theta = \frac{\rho g h I}{(\rho_s - \rho) g d}$, avec I la pente, ici 1 %, d le diamètre médian des graviers, $d = 7.5$ mm, ρ la masse volumique de l'eau et $\rho_s = 2650\,kg/m^3$ la masse volumique du sédiment).

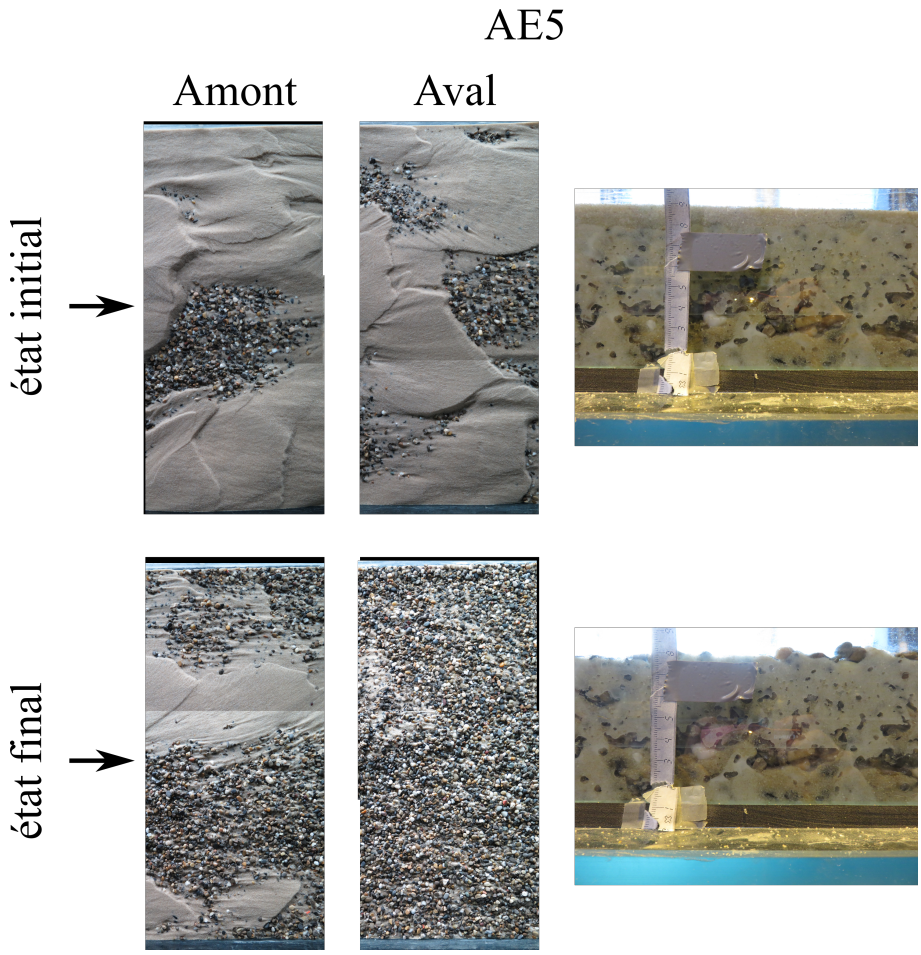

FIGURE 21 – Photographies de l'état de surface (à gauche) et par côté (à travers la vitre du canal, à droite) de l'expérience AE5, à l'état initial et à l'état final. La flèche indique le sens du courant.

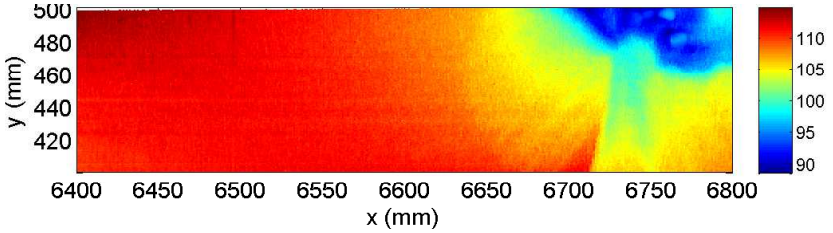

(a) état initial

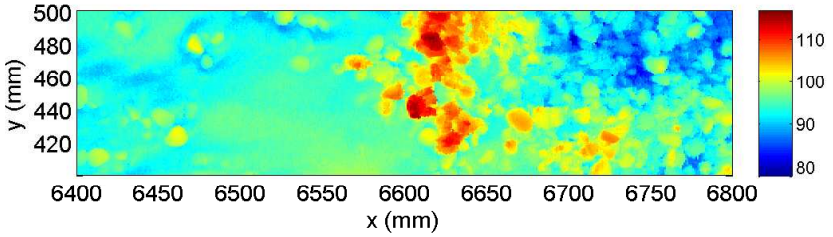

(b) état final

FIGURE 22 – Élévation du lit en $x = 6400\,\text{mm}$, expérience AE5.

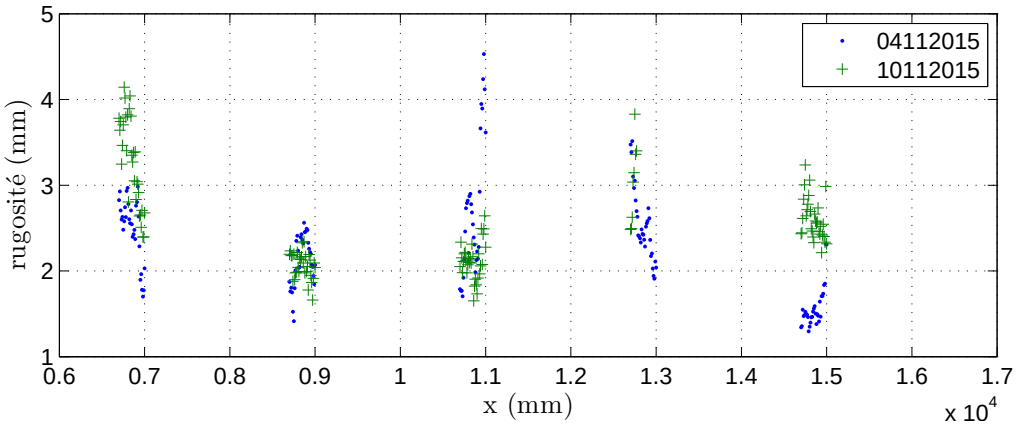

FIGURE 23 – Rugosité transversale (en millimètres) à l'échelle d'un profil (10 cm), moyennée sur 8 profils dans la largeur, avant (041115) et après (101115) l'expérience AE5.

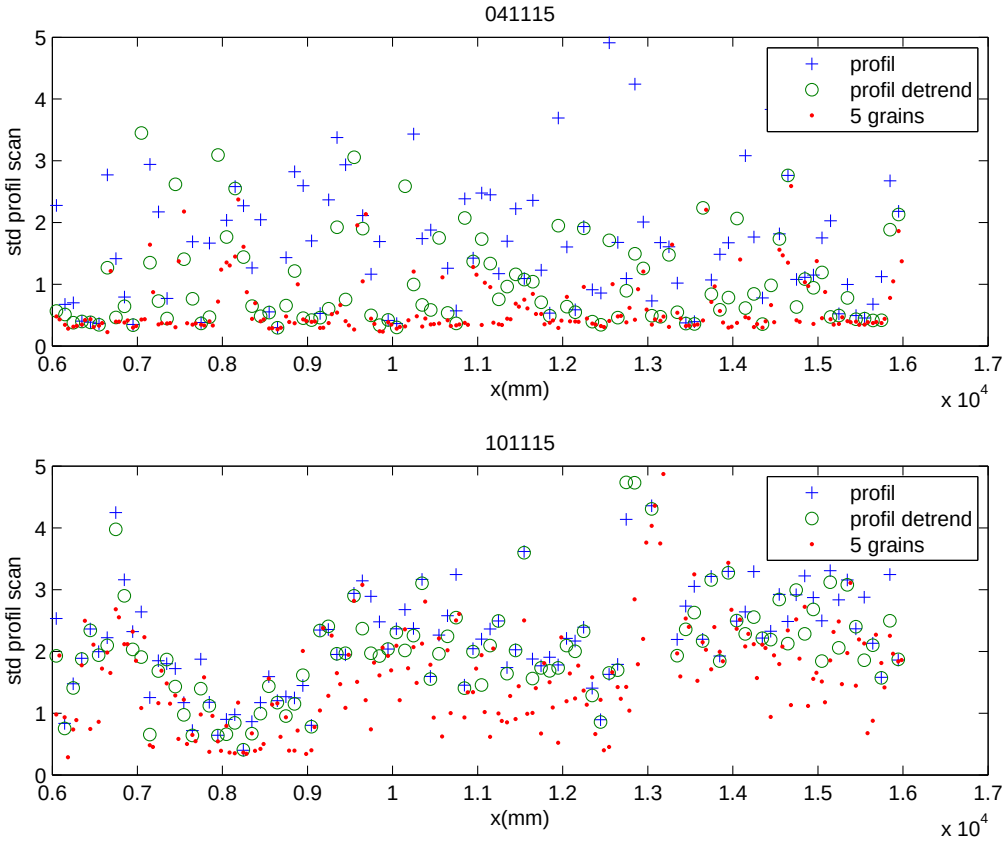

FIGURE 24 – Rugosité longitudinale (en millimètres) à l'échelle d'un profil (croix bleues), à l'échelle d'un profil après avoir soustrait une éventuelle pente globale sur le profil (ronds verts) et à l'échelle de 5 grains (points rouges), avant et après l'expérience AE5.

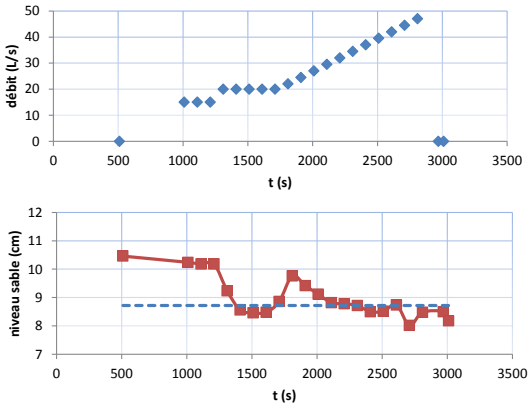

(a) Séries temporelles du débit (L/s) et du niveau de sable (cm). La ligne pointillée horizontale indique le niveau du sommet des graviers.

(b) exemple d'image analysée

FIGURE 25 – Evolution du niveau du lit pendant l'expérience AE5. Analyse d'une vidéo par côté.

3.6 Expérience AE6

Lors de l'expérience AE6, le débit a également varié, mais contrairement à l'expérience 5, il s'agit ici d'un hydrogramme descendant. Le débit a initialement été fixé à 50 L/s pour diminuer progressivement jusqu'à l'arrêt. Le débit solide de graviers (voir tableau 5) est du même ordre pour cette expérience et l'expérience AE5. Il ne diminue que très peu avec la diminution de débit.

Le lit au début de l'expérience est légèrement différent de l'expérience 5. Les dunes sont moins nombreuses, moins marquées, et le dépôt de sable en surface est principalement limité à la zone amont, comme l'attestent les photos figure 26 et les valeurs de rugosités (voir figure 29). Le colmatage est relativement uniforme sur la profondeur (voir photo par côté, figure 26).

Après l'expérience, on observe des dépôts de sable sur toute la longueur du canal. Il n'y a pas ou peu de formes de fond. la rugosité transversale est intermédiaire entre celle du sable et du gravier, comme à l'état initial (voir figure 28). Elle correspond à la rugosité d'un lit de graviers avec des fins dans les interstices de surface. Pour la rugosité longitudinale à l'échelle des grains, si elle augmente légèrement à l'amont, elle diminue sur la partie aval du canal, attestant la présence de sable (voir figure 29).

Nous avons, comme pour l'expérience 5, suivi le niveau de colmatage le long de l'expérience (au milieu du canal). Celui-ci est resté relativement stable. Il a très légèrement diminué au début pour augmenter progressivement jusqu'à la fin de l'expérience. Le niveau du sommet des graviers, pour référence est resté constant tout au long de l'expérience au point considéré, de l'ordre de 1 cm au-dessus du niveau de la couche colmatée.

débit liquide (L/s)	hauteur d'eau (mm)	contrainte	débit solide (m^3/s)
39	60	0.05	$1.5 \cdot 10^{-5}$
29	48	0.04	$1.3 \cdot 10^{-5}$

TABLE 5 – Débit solide collecté lors de l'expérience AE6 ainsi que le débit liquide, la hauteur d'eau (h) et la contrainte adimensionnée ($\theta = \frac{\rho g h I}{(\rho_s - \rho) g d}$, avec I la pente, ici 1 %, d le diamètre médian des graviers, $d = 7.5\,\text{mm}$, ρ la masse volumique de l'eau et $\rho_s = 2650\,\text{kg/m}^3$ la masse volumique du sédiment).

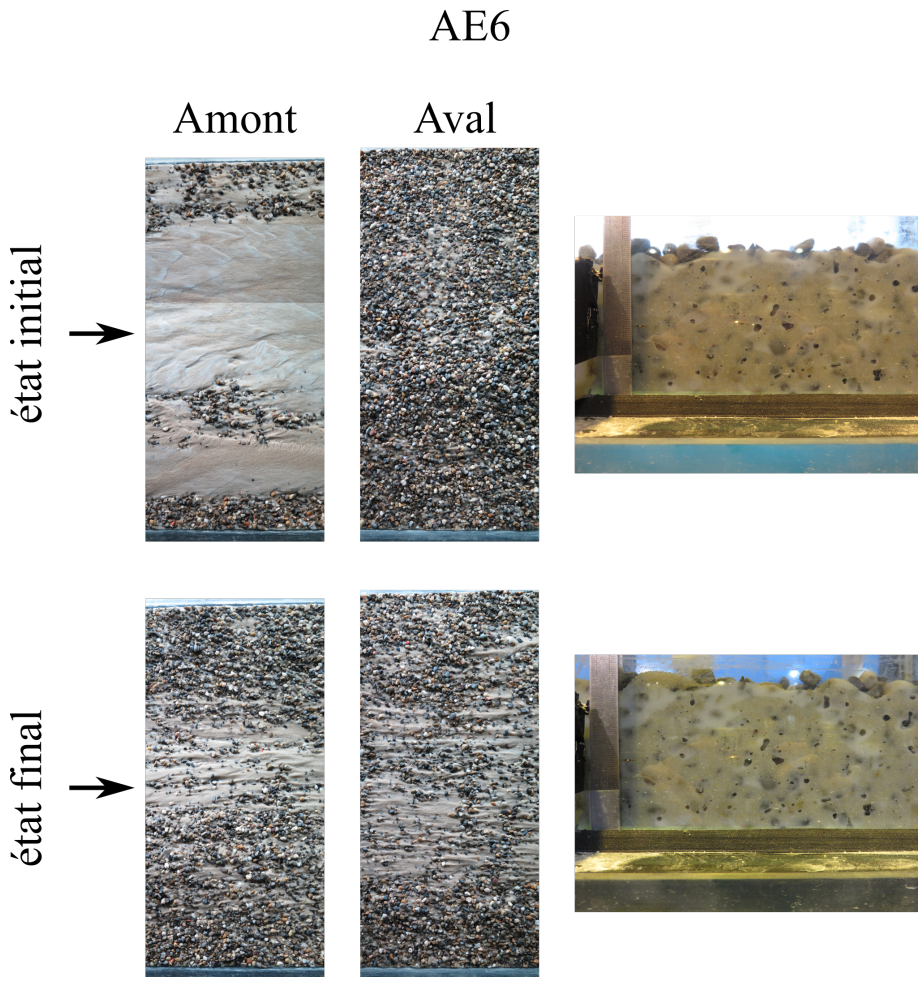

FIGURE 26 – Photographies de l'état de surface (à gauche) et par côté (à travers la vitre du canal, à droite) de l'expérience AE6, à l'état initial et à l'état final. La flèche indique le sens du courant.

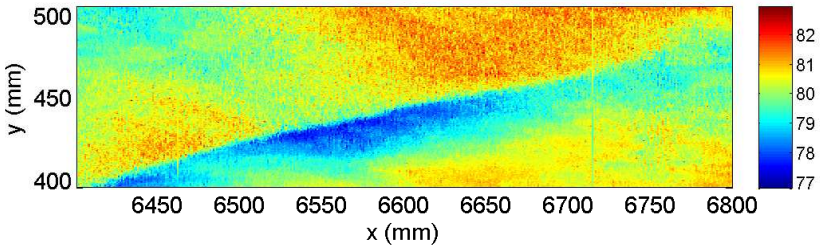

(a) état initial

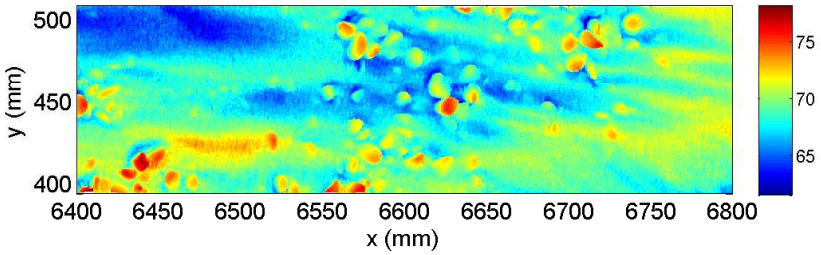

(b) état final

FIGURE 27 – Élévation du lit en $x = 6400\,\text{mm}$, expérience AE6.

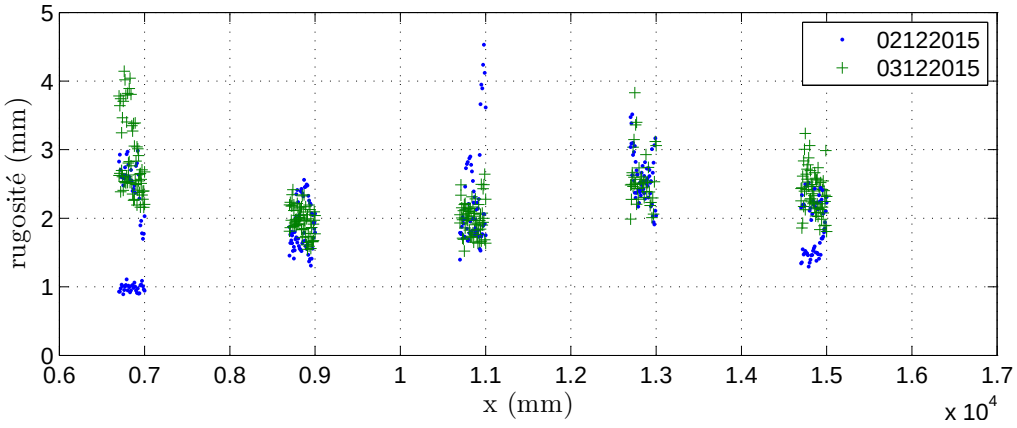

FIGURE 28 – Rugosité transversale (en millimètres) à l'échelle d'un profil (10 cm), moyennée sur 8 profils dans la largeur, avant (021215) et après (031215) l'expérience AE6.

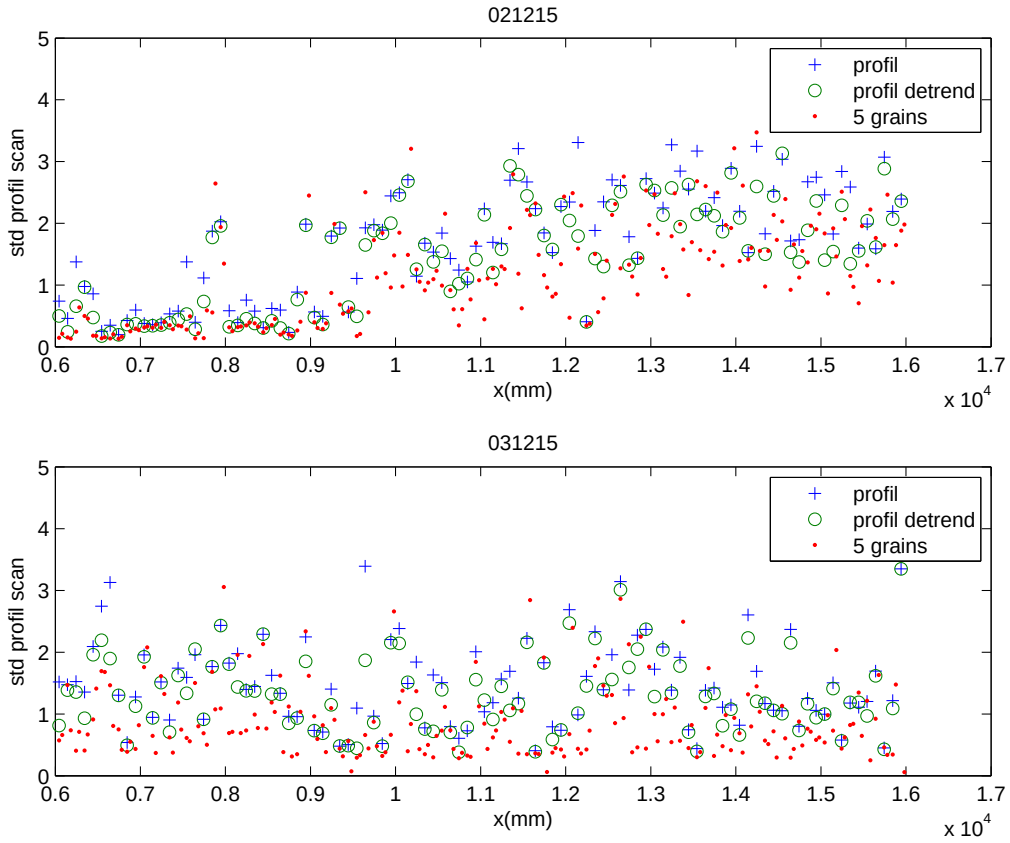

FIGURE 29 – Rugosité longitudinale (en millimètres) à l'échelle d'un profil (croix bleues), à l'échelle d'un profil après avoir soustrait une éventuelle pente globale sur le profil (ronds verts) et à l'échelle de 5 grains (points rouges), avant et après l'expérience AE6.

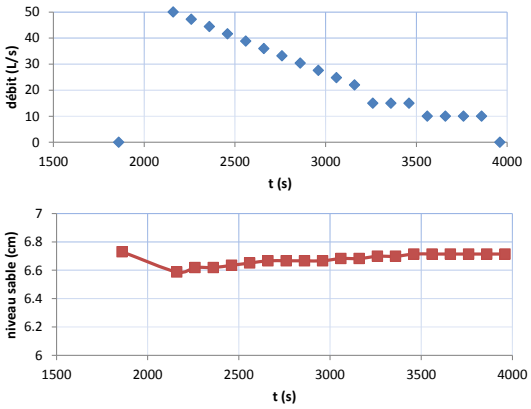

(a) Séries temporelles du débit (L/s) et du niveau de sable (cm). Le niveau du sommet des graviers est pour référence à 7.6 cm.

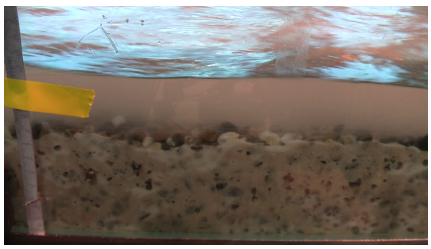

(b) exemple d'image analysée

FIGURE 30 – Evolution du niveau du lit pendant l'expérience AE6. Analyse d'une vidéo par côté.

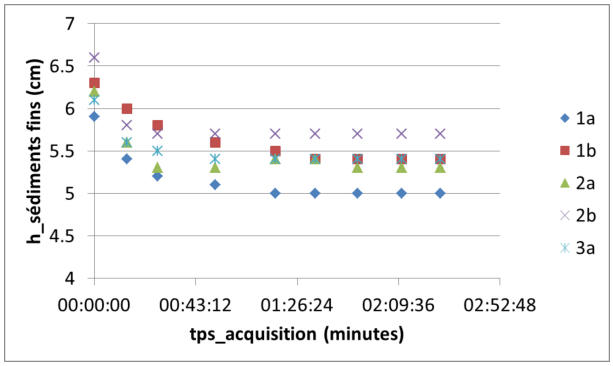

FIGURE 31 – Evolution du niveau du lit pendant l'expérience complémentaire. Les différents symboles correspondent à différentes positions le long du canal, du plus en amont (1) au plus en aval (3), à travers la vitre de gauche (a) ou de droite (b). Initialement, la couche colmatée affleure le lit de graviers.

3.7 Expérience complémentaire

Une expérience complémentaire a été effectuée dans le cadre de la thèse d'Emeline Perret. Pour cette expérience, le sédiment fin était légèrement plus fin que les billes de verre, d'un diamètre médian de 40 microns. Nous n'avons pas utilisé de sable. Il s'agit d'une expérience longue, à débit constant de 64 L/s. La contrainte adimensionnée pour cet écoulement était de 0.06 et le débit solide en gravier de l'ordre de $1 \cdot 10^{-7}\,\mathrm{m}^2/\mathrm{s}$. Nous avons relevé comme pour les expériences AE5 et AE6 le niveau de la couche colmatée tout au long de l'expérience. Ces résultats sont présentés figure 31. Durant cette expérience, le lit est décolmaté sur une profondeur de 1 cm quelle que soit la position considérée. La majeure partie de ce décolmatage s'effectue durant les 30 premières minutes.

4 Discussion

Les différentes expériences menées dans le cadre de ce projet ont été présentées successivement dans la partie précédente. Nous souhaitons dans cette partie effectuer des comparaisons et tirer les conclusions de ce travail.

Pour faciliter la lecture de ces différentes expériences, nous avons rassemblé certains indicateurs dans le tableau 6. Sont exposées dans ce tableau les rugosités longitudinales à l'échelle du profil et à l'échelle du grain, moyennées sur l'ensemble des profils qui décrivent le canal entre $x = 6\,\mathrm{m}$ et $x = 17\,\mathrm{m}$.

Nous avons également utilisé cette élévation du lit tout le long du canal pour estimer une érosion moyenne durant l'expérience. Celle-ci nous permettra de quantifier l'impact du décolmatage sur le lit de grossiers.

Nous pouvons dans un premier temps comparer les expériences AE2 et AE3 aux expériences AE5 et AE6. La concentration pour les deux premières est nettement plus forte, le débit est constant. Le décolmatage est moins efficace que pour les expériences AE5 et AE6, ce que l'on a pu constater sur les photos mais qui peut être également déduit de la rugosité de grain moyenne qui n'augmente pas et diminue même pendant ces deux expériences (voir tableau 6). Un décolmatage efficace cependant est caractérisé par une augmentation de la rugosité, afin de tendre vers la rugosité du gravier.

Si l'on compare maintenant ces deux expériences AE2 et AE3 entre-elles, nous n'observons pas de différence notable entre les deux. Les dunes de sable sont dans les deux cas lissées (plus pour l'expérience AE2 pour laquelle elles sont plus développées initialement) et laissent place

à une surface relativement lisse de sable, avec quelques graviers qui émergent. Nous constatons également que durant ces deux expériences, et plus particulièrement à l'aval pour l'expérience AE3, les sédiments fins migrent à travers le lit pour augmenter l'épaisseur de la couche colmatée du fond (voir figures 10 et 14). Ainsi, si l'on nettoie quelque peu la surface du lit lors de ces expériences, dans l'une comme dans l'autre, ceci est au détriment de la perméabilité du lit plus en profondeur. Enfin, l'érosion du lit est plus faible pour la première, ce qui est cohérent avec le fait que le débit est beaucoup plus faible. Si l'on souhaite préserver l'intégrité du lit de graviers (ou de galets en grandeur nature), un débit faible est mieux adapté.

Pour l'expérience AE2, la hauteur d'eau était de l'ordre de 45 mm, ce qui correspond à une contrainte adimensionnée $\theta_g = 0.037$ en adimensionnant avec le diamètre des grossiers et de $\theta_s = 0.35$ si l'on considère le diamètre du sable. Pour l'expérience AE3, $\theta_g = 0.055$ et $\theta_s = 0.51$, la contrainte est toujours largement suffisante pour mettre en mouvement les sables mais elle commence également à déstabiliser significativement le lit de graviers.

Si l'on compare maintenant les expériences AE5 et AE6, l'expérience AE6 est moins efficace pour le décolmatage en terme de rugosité et également visuellement en ce qui concerne l'état de surface. La rugosité de grains augmente en moyenne pour l'expérience AE5 alors qu'elle diminue pour l'expérience AE6. Au fil de l'expérience, le niveau de colmatage a légèrement augmenté contrairement à l'expérience 5 (voir figures 25 et 30). Cette conclusion est cependant à modérer car le colmatage en surface le long de la vitre au point de mesure considéré ($x \approx 9\,\mathrm{m}$) pour l'expérience AE6 était moins important ce qui laissait moins de place à l'érosion du sable en surface.

Par ailleurs, lors de l'expérience AE5, le colmatage n'était pas homogène initialement sur la profondeur et l'on n'observe pas d'augmentation de l'épaisseur de la couche colmatée de fond contrairement aux expériences AE2 et AE3. Il est difficile, compte tenu des différences de concentration, de conclure avec certitude mais il semblerait qu'un hydrogramme montant avec une descente rapide est la configuration la plus adaptée pour obtenir un décolmatage efficace du lit à volume constant. Cependant, si le lit doit être préservé au maximum et que l'on souhaite simplement réduire le colmatage sans mobiliser les grossiers, mieux vaut privilégier un écoulement à faible débit comme pour l'expérience AE2. Le choix de ce débit doit prendre en compte le fait que le sable agit comme un lubrifiant et que le transport de gravier observé durant ces expériences était loin d'être négligeable, même pour des contraintes inférieures à 0.047, la contrainte critique de mise en mouvement habituellement considérée (Meyer-Peter Müller).

Pour finir, nous pouvons revenir à l'expérience AE1. Cette expérience est différente des autres car elle ne fait pas intervenir de sable. En pratique, elle correspond à une rivière présentant des galets et des limons ou sables fins, avec très peu de sédiments d'une granulométrie intermédiaire. Cette configuration donne lieu à un colmatage homogène sur la profondeur. Ce colmatage peut être efficacement nettoyé en surface à l'eau claire, sans mobilisation des graviers. La profondeur maximale de décolmatage observée est alors de l'ordre d'un diamètre de grain (de gravier). L'expérience complémentaire a montré qu'avec un débit plus important et de l'eau chargée (2 g/L), on peut aussi décolmater le lit, sur une profondeur même un peu plus importante, de l'ordre de 1 cm, *i.e.* légèrement supérieure à la taille de grain grossier environ. Ce décolmatage s'effectue en majeur partie durant les 30 premières minutes. Ainsi dans le cas particulier d'un colmatage par des limons seuls, un écoulement chargé n'est pas un obstacle au décolmatage. En présence de sable, l'expérience AE4 montre qu'augmenter le débit ou la durée de l'expérience conduit à une érosion globale plus importante et un décolmatage de surface effectif mais que la profondeur sur laquelle le lit est décolmaté ne semble pas augmenter.

Pour conclure, sur le terrain, l'expérience de la chasse de l'Arc a montré qu'un débit constant ou diminuant lentement pendant une longue période favorise les dépôts. Selon la nécessité de préserver ou non le lit de grossier en l'état, on peut favoriser soit un débit générant une contrainte deux fois plus faible que la contrainte critique des grossiers à préserver, soit un débit qui augmente

TABLE 6 – Tableau récapitulatif des rugosités et érosions durant les expériences de décolmatage.

Expérience		rugosité à l'échelle d'un profil (mm)	rugosité moyenne à l'échelle de 5 grains (mm)	érosion moyenne durant l'expérience (mm)
AE2	init	3.2951	0.6725	
	fin	1.0707	0.53385	4.6526
AE3	init	1.7848	0.6228	
	fin	1.0413	0.5929	9.0267
AE4	fin	2.6923	1.6077	18.6656
AE5	init	2.2409	0.58315	
	fin	2.4442	1.3125	9.6938
AE6	init	2.1955	0.94655	
	fin	1.4748	0.8294	8.6109

jusqu'à la contrainte critique de mise en mouvement. Dans les deux cas, rien ne sert de faire durer l'expérience trop longtemps, et il faut veiller à ce que la descente de débit s'effectue relativement rapidement pour éviter les dépôts durant cette phase.

A Annexes

A.1 Article théorique sur les processus d'infiltration

Sand infiltration into a gravel bed: a mathematical model

A. Herrero[1,2], C. Berni[2]

[1]Catalan Institute for Water Research, Girona, Spain†.

[2] IRSTEA, Villeurbanne, France

Corresponding author: Albert Herrero (aherrero@icra.cat)

† Postal address: C/Emili Grahit, 101, 17003, Girona, Spain

Key Points:

- A stochastic model is proposed to reproduce fine sediment infiltration into a river bed
- The occurrence of bridging or unimpeded static percolation is properly reproduced
- Divergences between calculated and measured sand content may be due to subsurface water flow

Abstract

Fine sediment infiltration into a river bed is a physical process affected by different human actions and has several environmental, socioeconomic and river morphology consequences. A theoretical model is proposed herein aiming to reproduce the fine sediment content (FSC) depth profile resulting from the infiltration of fine sediment into an initially clean gravel bed. The model is based on the probability of infiltrating particles to be trapped in a pore throat formed by three bed particles. The model is tested against previous experimental results and is found to reproduce well the occurrence of the two infiltration mechanisms reported by previous studies: bridging and unimpeded static percolation. Theoretical depth profiles are found to underestimate FSC at the subsurface compared to the laboratory results. A possible interpretation of this fact lies on the influence of pore water velocity on the stability of strained infiltrated particles.

1 Introduction

Fine sediment infiltration (FSI) into a river bed formed by coarser material is a physical process that occurs frequently in mountain and piedmont streams. As a consequence, the structure and the physical properties of the bed are significantly modified. FSI modifies the hyporheic exchange at the sediment-water interface, therefore affecting the access of nutrients and oxygen to the subsurface. This fact has an impact on different aspects of the river ecosystem like fish spawning [*Greig et al*., 2007], macrophytes root length [*Wood and Armitage*, 1997] or the habitat of subsurface invertebrates [*Jones et al*., 2012]. Moreover, FSI takes part in the fate and transport of many contaminant substances that are attached to the fine particles transported by the river and infiltrated into the bed [*Walling et al.*, 2003]. Today's management of rivers often leads to fine sediment fluxes that are significantly modified by human activities [*Morris and Fan*, 1998]. In particular, water and sediment releases from dams generate fine sediment pulses that can potentially infiltrate into the river bed downstream [*Cui and Wilcox*, 2005]. Understanding the physics of FSI can help to perform optimal dam operations that minimize the harmful environmental consequences mentioned above. The change of the bed permeability that results from FSI is a second socioeconomic aspect that has to be considered as it affects the efficiency of infiltration wells that take water from aquifers connected to the river [*Wooster et al*., 2008; *Blaschke et al*., 2003]. Lastly, from a hydromorphological point of view, the infiltrated sediment does not directly affect the bed topography [*Frings et al*., 2008]. Considering and quantifying FSI can help to improve morphological models that evaluate river evolution. Moreover, infiltrated sediment changes bed roughness, both by modifying the bed surface structure and by changing water exchange at the sediment-water interface [*Manes et al*., 2011; *Blois et al*., 2012] and affects the incipient motion of the coarse sediment that forms the bed substrate [*Wilcock et al*., 2001; *Wilcock and Crowe*, 2003].

Following the different points that motivate its study, FSI has been the main focus of different laboratory analyses [*Einstein*, 1968; *Schälchli*, 1992; *Wooster et al*., 2008; *Gibson et al*., 2009, 2010, 2011] and field works [*Lisle*, 1989; *Evans and Wilcox*, 2013]. Their observations highlight the occurrence of two different infiltration mechanisms: (1) the formation of a surface clogged layer due to the straining of fine particles at the pore throats (bridging process); (2) the infiltration of fine sediment down to an eventual impermeable layer an subsequent filling of the bed pores over the whole depth (unimpeded static percolation) [*Kleinhans*, 2002]. The occurrence of one mechanism or the other has been observed to depend mainly on the size ratio

between the bed substrate and the infiltrating sediment [*Gibson et al*., 2010] and the standard deviation of both grain size distributions (GSD) [*Huston and Fox*, 2015].

Some studies have tried to cope with this issue from a mathematical point of view [*Lauck*, 1991; *Cui et al*., 2008]. They are mainly based on the introduction of a trapping coefficient that describes the probability of fine sediment being trapped when travelling a vertical unit distance across the bed. Assuming a constant value for the trapping coefficient, leads to fine sediment content (FSC) depth profiles with an exponentially decaying shape. *Wooster et al*. [2008] found this hypothesis consistent with their laboratory observations and proposed an equation to compute the trapping coefficient as a function of the characteristic size and the standard deviation of the coarse and fine sediment. On the other hand, *Leonardson* [2010] analyzed the FSC depth profiles obtained by *Gibson et al*. [2009] and *Gibson et al*. [2010] and observed that they were better reproduced assuming a trapping coefficient dependent on FSC.

Based on the ideas of *Lauck* [1991], this work proposes a mathematical model to reproduce the fine sediment infiltration process and calculate the FSC depth profile of a clogged bed at equilibrium. The development of the mathematical model is carried out first. Then, the model is tested against previous laboratory experiment results [*Gibson et al*., 2009; *Gibson et al*., 2010]. The different hypotheses and the performance of the model are discussed next and some final conclusions are drawn.

2 Development of the mathematical model

The mathematical model that is developed here aims at quantifying the fine sediment content within a gravel bed, that can be infiltrated when sand-sized sediment-laden flow pass on the top of it. GSDs of both gravel and sand are known and respectively characterized by $\left(D_i^0, G_i^0\right)$ and $\left(d_j, g_j\right)$. D_i^0 and d_j are the diameters resulting from the discretization of the GSD after the sieving process for gravel and sand respectively, and G_i^0 and g_j are the weight fraction finer than the corresponding diameter for gravel and sand respectively. As a consequence of being transported over the bed surface, sand infiltrates across it at a rate equal to $q_{Tot,0}$. This infiltration rate is divided into the mass fluxes corresponding to each sand size fraction, $q_{j,0}$, based on sand GSD (g_j). The bed is discretized in several horizontal layers. One specific layer, noted as layer *l*, where sand-sized sediment enters through the upper boundary is first considered. The mass flux of sand that enters into this layer is q_l (sand volume per bed surface unit and time unit), which is subdivided in $q_{j,l}$, the mass flux associated with each diameter d_j (Figure 1). As sand grains infiltrate into the layer they get trapped in the pore throats that are too small to let them pass, therefore modifying the GSD of the bed layer $\left(D_i, G_i\right)$, with *i* varying from 1 to *n*, *n* being the number of classes of both fine and coarse sediment. When advancing down the bed, the mass flux then decreases and $q_{j,l} > q_{j,l+1}$. Sand infiltration within the *l*-th layer continues until this layer or one above is clogged which prevents further sand grains from entering it.

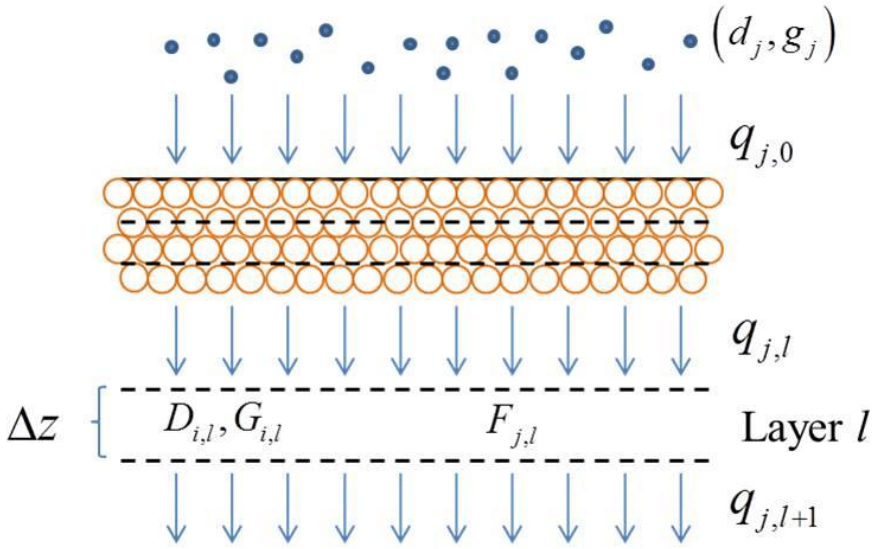

Figure 1. Scheme of the infiltration process

Following *Lauck* [1991], the model is based on the probability of an infiltrating fine grain with a certain diameter d_j to be trapped in a pore throat formed by three bed grains. This probability is called from here on trapping coefficient and is denoted by β_j. Based on this concept, the probability for this fine grain to go through N pore throats without being trapped is $(1-\beta_j)^N$.

The distance between two pore throats can be calculated as [Leonardson, 2010]:

$$\Delta z_p = \frac{2D^g}{3(1-\theta)} \tag{1}$$

where D^g and θ are the geometrical diameter and the porosity of the bed sediment, respectively. The average number of pores found by a fine particle when it goes through a layer of thickness equal to Δz, is $N = \Delta z / \Delta z_p$. Therefore, the fine sediment mass flux of size d_j passing through the *l*-th layer is:

$$q_{j,l+1} = q_{j,l}\left(1-\beta_j\right)^{\Delta z/\Delta z_p} \tag{2}$$

It should be noted that the change in the GSD of the bed layer that results from the deposition of infiltrated sediment, modifies the trapping coefficient affecting sand that infiltrates later on.

It is therefore necessary to quantify the trapping coefficient, β_j, for fine sediment with a specified diameter, d_j, going through a bed layer with a GSD characterized by D_i and G_i, combining both coarse and fine sediment distributions.

117 2.1 Trapping coefficient

118 The probability of a fine sediment particle of diameter d_j being trapped in a pore throat
119 is assumed to be equal to the probability of a stochastic pore throat being smaller than d_j. In
120 other words, it is equal to the cumulative probability distribution of pore throat size, P_p,
121 evaluated at d_j. The diameter, x,of a pore throat formed by three bed grains which are assumed
122 to be spherical can be obtained using Heron's formula (Figure 2):

123 $$\sqrt{(D_1+D_2+D_3)D_1D_2D_3} = \sqrt{(D_1+D_2+x)D_1D_2x} + \\ +\sqrt{(D_1+x+D_3)D_1xD_3} + \sqrt{(x+D_2+D_3)xD_2D_3} \quad (3)$$

124 where D_1, D_2 and D_3 are the diameters of the three particles forming it. Based on
125 equation (3), the probability density function (PDF) of pore throat size, $p_p(x)$, can be obtained
126 from the joint probability distribution of the size of three bed particles to form a pore,
127 $p_3(D_1, D_2, D_3)$, which in turn depends on the PDF of bed sediment size, $p_b(D)$, that describes
128 the probability of choosing a particle with a specific diameter, *D*.

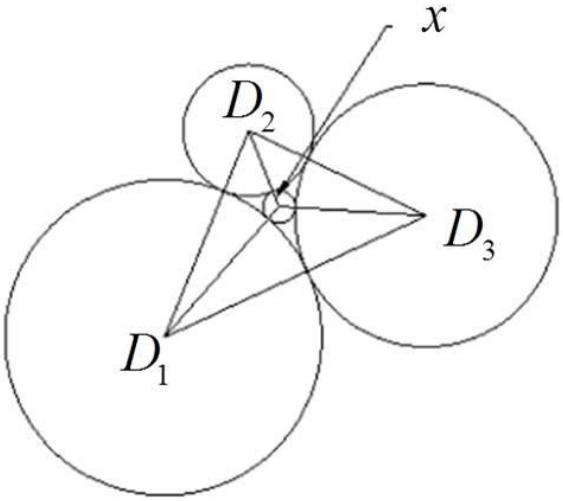

129
130 **Figure 2**. Pore throat size between three bed particles calculated through Heron's formula.
131

132 The PDF $p_b(D)$ is initially unknown and has to be obtained from the GSD, G_i, which is
133 expressed in terms of weight. Considering a bed sample of one weight unit, both distributions are
134 related as:

135 $$G_{i+1} - G_i = \int_{D_i}^{D_{i+1}} \gamma D^3 N p_b(D)\,\mathrm{d}D \quad (4)$$

136 where γ is a coefficient so that γD^3 is the weight of a particle of diameter *D* (assuming
137 spherical particles, $\gamma = \rho_g \pi / 6$, being ρ_g the sediment density), and *N* is the number of bed
138 particles per weight unit, so that $Np_b(D)\mathrm{d}D$ is the number of particles per weight unit with a
139 diameter between *D* and *D*+d*D*. As no information is available about the GSD within each

interval (D_i, D_{i+1}), $p_b(D)$ is assumed to be uniform for each range of diameters. The constant value, denoted by $p_{b,i}$, can be obtained as :

$$p_{b,i} = \frac{4}{N\gamma} \frac{G_{i+1} - G_i}{D_{i+1}^4 - D_i^4} \tag{5}$$

The normalization of $p_b(D)$ implies that

$$\sum_{i=1}^{n-1} p_{b,i} (D_{i+1} - D_i) = 1 \tag{6}$$

And *N* can be obtained as:

$$N = \sum_{i=1}^{n-1} \frac{4}{\gamma} \frac{G_{i+1} - G_i}{D_{i+1}^4 - D_i^4} (D_{i+1} - D_i) \tag{7}$$

Some considerations must be taken into account before obtaining $p_3(D_1, D_2, D_3)$ from $p_b(D)$. $p_3(D_1, D_2, D_3)$ is meant to be used to calculate the pore throat size PDF. It is defined as the probability to choose a pore formed by three particles of diameters D_1, D_2 and D_3 between the variety of pores occurring in the bed. The fact that particles of different sizes are associated with a different number of pores needs to be taken into account when evaluating $p_3(D_1, D_2, D_3)$ (that is, p_3 cannot be calculated simply as $p_b(D_1) \cdot p_b(D_2) \cdot p_b(D_3)$). It could be assumed that the number of pore throats in which a grain participates is proportional to the number of contacts with other grains, which in turn is proportional to the grain surface [*Lauck*, 1991]. Consequently, large particles would participate in more pore throats and their choice should be enhanced when defining $p_3(D_1, D_2, D_3)$. Therefore, a bias should be introduced in the calculation of $p_3(D_1, D_2, D_3)$:

$$p_3(D_1, D_2, D_3) = C \cdot p_b(D_1)(D_1)^{\alpha}\ p_b(D_2)(D_2)^{\alpha}\ p_b(D_3)(D_3)^{\alpha} \tag{8}$$

where *C* is a normalizing constant and α is the bias exponent. Positive or negative values of α enhance the choice of large or small particles respectively. The argument exposed above suggests the suitability of assuming $\alpha = 2$ (Figure 3A). However, other aspects could be taken into account, making the choice of this parameter uncertain. It should be noted, for example, that the number of fine particles per unit of vertical length is larger than the number of coarse particles (Figure 3B). Therefore, an infiltrating sand particle finds more fine particles than coarse particles when going through a bed layer with a fixed thickness. This factor suggests the enhancement of the choice of fine particles through the introduction of an additional bias of -1. On the other hand, very fine particles, such as sand when compared to gravel, can be deposited on the top of the coarser grains and rest without being part of the bed sediment matrix (Figure 3C). This aspect again suggests higher values of α. Thus, it can be concluded that the choice of an appropriate value of the bias exponent is far from being simple. This point is discussed further in the results section.

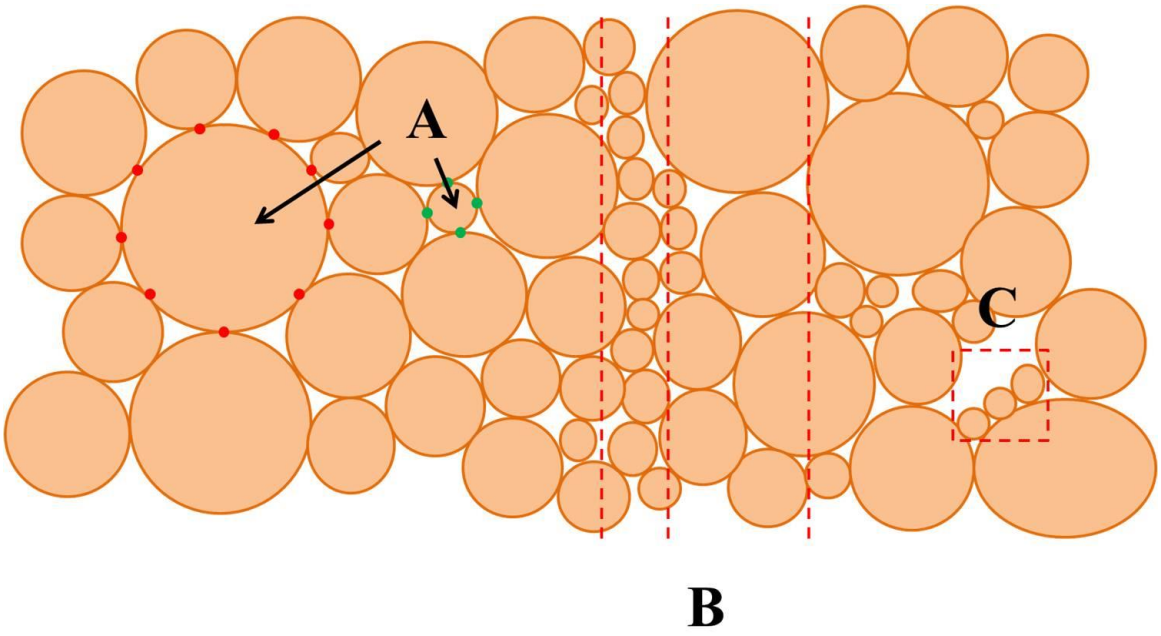

Figure 3. Scheme of sediment patterns that have an influence on the value of the bias parameter, α . A: the number of pores associated with a single grain is proportional to the grain surface; B: the number of particles per depth unit is inversely proportional to the particle size; C: some particles do not directly form the bed framework.

Equation (3) and $p_3(D_1, D_2, D_3)$ can be used to obtain the pore throat size PDF, $p_p(x)$. As *x* cannot be determined explicitly from equation (3), the following procedure is adopted. First, the range of possible bed sediment diameters is discretized and equation (3) is used to compute the pore throat size associated with each combination of three sizes. The smallest pore throat size is that formed by three bed particles with the smallest possible diameter and the largest is the one formed by three bed particles with the coarsest size. The range of pore throat sizes is then discretized in possible values, x_k , and the pore throat size PDF, $p_p(x)$, is assumed to be constant in each interval and denoted by $p_{p,k}$. The value of $p_{p,k}$ is calculated as the addition of the probabilities of all the combinations of particles that form pores with a diameter between x_k and x_{k+1} :

$$p_{p,k} = \sum_{x \in (x_k, x_{k+1})} p_3(D_1, D_2, D_3)(\Delta D)^3 \quad (9)$$

where ΔD is the interval of discretization of the bed layer GSD.

Based on $p_p(x)$, the cumulative distribution of the pore throat size can be calculated as:

$$P_p(x) = \int_0^x p_p(x')\, dx' \quad (10)$$

Finally, the trapping coefficient (β_j) associated with fine sediment of diameter d_j is:

$$\beta_j = P_p(d_j) \quad (11)$$

194 2.2 Time iteration

195 The previous reasoning is now used to calculate the evolution of the depth profile of FSC
196 in a gravel channel bed with a specified thickness (h_b) where sand-sized sediment enters through
197 the upper boundary. The bed is subdivided in horizontal layers with a thickness (Δz) equal to the
198 geometrical diameter of the gravel, D^g. The GSD of the *l*-th layer is characterized by $D_{i,l}$ and
199 $G_{i,l}$. Considering the mass balance in the *l*-th layer, the amount of fine sediment of size d_j,
200 $\left(\Delta F_j\right)_l$, accumulated during an interval of time Δt is:

201 $$\left(\Delta F_j\right)_l = \frac{q_{j,l} - q_{j,l+1}}{\Delta z}\Delta t \qquad (12)$$

202 Equation (2) together with equation (1) are used in equation (12) to evaluate the amount
203 of sand that is trapped in each layer during an interval of time Δt. Sand deposition changes the
204 GSD of each bed layer. It should be noted that in equation (2), the trapping coefficient, β_j, and
205 the mean distance between pore throats, Δz_p, need to be recalculated at each time step,
206 considering the FSC updated by adding ΔF_j. The new values are used again in equation (2) to
207 obtain new depth profiles of sand mass fluxes which are introduced in equation (12) to calculate
208 the new FSC in each layer.

209 The deepest layer is considered to be impermeable, hence the trapping coefficient is set to
210 one for all sand sizes. FSC at any layer cannot increase indefinitely but is limited by a specified
211 maximum value that corresponds to a fully clogged layer. This value is calculated as
212 [*Leonardson*, 2010]:

213 $$F_{\max} = \theta_g\left(1-\theta_s\right)\left[1-2.35\frac{d^g}{D_{15}}+1.35\left(\frac{d^g}{D_{15}}\right)^2\right] \qquad (13)$$

214 where $F_{\max}$ is the maximum FSC, θ_g is clean gravel porosity, θ_s is sand porosity, d^g is
215 sand geometric diameter and D_{15} is the diameter for which 15 percent (in weight) of the gravel is
216 finer. Once the total FSC in a bed layer reaches this value, this layer is considered to become
217 impermeable for sand and the trapping coefficient is assumed to be one. The model stops when
218 the FSC at the surface bed layer reaches $F_{\max}$.
219

220 **3 Results**

221 A numerical code written in MATLAB was developed based on the theoretical model
222 described in the previous section. Input data of the model consist in GSD of bed (gravel) and
223 infiltrating (sand) sediments in terms of the weight fraction of each interval resulting from the
224 sieving process. The model is initialized with a bed formed only by clean gravel. Time step is
225 defined as:

226 $$\Delta t = \lambda\frac{F_{\max}\Delta z}{q_{Tot,0}} \qquad (14)$$

where $q_{Tot,0}$ is the total infiltrating sediment that enters at the surface layer (including all the possible sizes) and λ is a parameter that determines the accuracy of time discretization. A value of 0.2 was adopted as a base value. This means that Δt is such that the fine sediment retained in one layer during one time step cannot exceed 20% of the maximum FSC at that layer. After each time step, the GSD of each layer was updated based on the fine sediment retained. The model stopped once the surface layer reached the theoretical maximum FSC specified by equation (13).

Firstly, a sensitivity test of the theoretical model was carried out to analyze the influence of the discretizations of the GSD and the time. Concerning the discretization of the GSDs of the bed sediment and the infiltrating material, N_a is the number of subdivisions in each interval of the GSD that results from the sieving process. Increasing N_a generates a higher number of possible sizes of both infiltrating and bed material. Subsequently a better representation of pore size PDF is possible and the convolution with infiltrating sediment size PDF provides a better reproduction of the retained fine sediment. A base value of 3 was adopted for N_a. Concerning the time step, Δt, the results of the sensitivity analysis show that higher accuracies do not provide significantly different results for the depth profiles (Figure 4). As Δt is defined in terms of $q_{Tot,0}$, this results implies that as far equation (14) is used, the calculated depth profile is not sensible to $q_{Tot,0}$. Therefore, the base values of N_a and λ were considered for all the calculations presented herein, as they implied a reasonable computation time. On the other hand, $q_{Tot,0}$ was arbitrarily set to one.

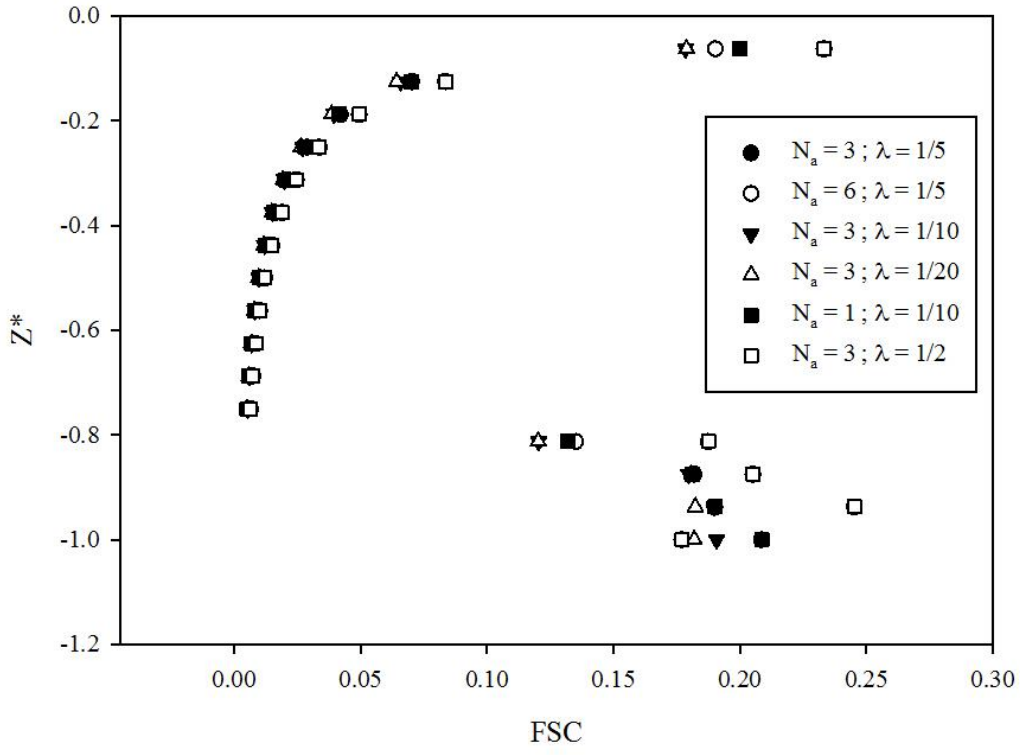

248 **Figure 4**. Fine sediment content depth profiles with different discretizations of the grain size
249 distribution (N_a) and the time (λ)
250

251 Secondly, the mathematical model was tested against the experimental results obtained
252 by *Gibson et al*. [2009]. These laboratory analyses studied the depth profile of FSC as a function
253 of the GSD of both bed and infiltrating sediment. This work focused on determining a threshold
254 value for coarse to fine sediment diameter ratio that separates the occurrence of bridging and
255 unimpeded static percolation. Three different infiltrating sediments (sand-sized) were tested over
256 the same gravel bed. Their GSD's are detailed in Figure 5. During their experiments, Gibson et
257 al. (2009) performed two analogous tests with each combination of bed and infiltrating sediment
258 in open channel flow and still water conditions. The open channel flow experiments were
259 performed in a tilting channel with upstream fine sediment feeding and under specified
260 conditions of discharge and slope. The still water experiments were carried out in plastic bins
261 where fine sediment was sprinkled over a layer of gravel.

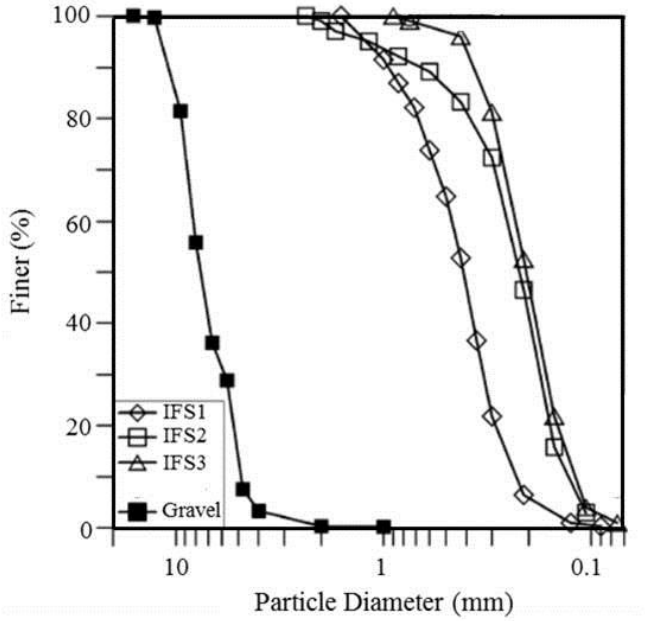

262
263 **Figure 5**. GSD's used in the laboratory experiments performed by *Gibson et al*. [2009] (IFS:
264 Infiltrated Fine Sediment)
265

266 Figure 6 shows the fine sediment depth profile resulting from the experiment 1 (IFS1) of
267 *Gibson et al*. [2009] and from the theoretical model considering the same GSD's. Theoretical
268 profiles with different values of the bias parameter, α, are shown. The results show a higher
269 amount of infiltrated sediment at the deep layers for high values of α. For the highest value (
270 $\alpha = 3.5$) the depth profile is modified significantly and changes from a bridging profile to an
271 approximately uniform profile characteristic of unimpeded static percolation. With regard to the
272 experimental results of *Gibson et al*. [2009], infiltration under free flow conditions shows higher
273 FSC than the corresponding still water experiment. On the other hand, Figure 7 shows the
274 comparison between the modeled and the experimental FSC depth profiles for the different

GSDs used by *Gibson et al*. [2009]. Model results consider a value of 3 for the bias parameter (the value for which a best fit is observed between model and laboratory results, see Discussion section) and experimental results correspond to the still water experiments. Experimental results show bridging profiles for the types of sand IFS1 and IFS2 and unimpeded static percolation for IFS3. Experimental and model results agree well except for the deepest part of the depth profile of experiment IFS2, that is a consequence of the influence of the impermeable boundary condition imposed in the model, which is not observed in the experimental results.

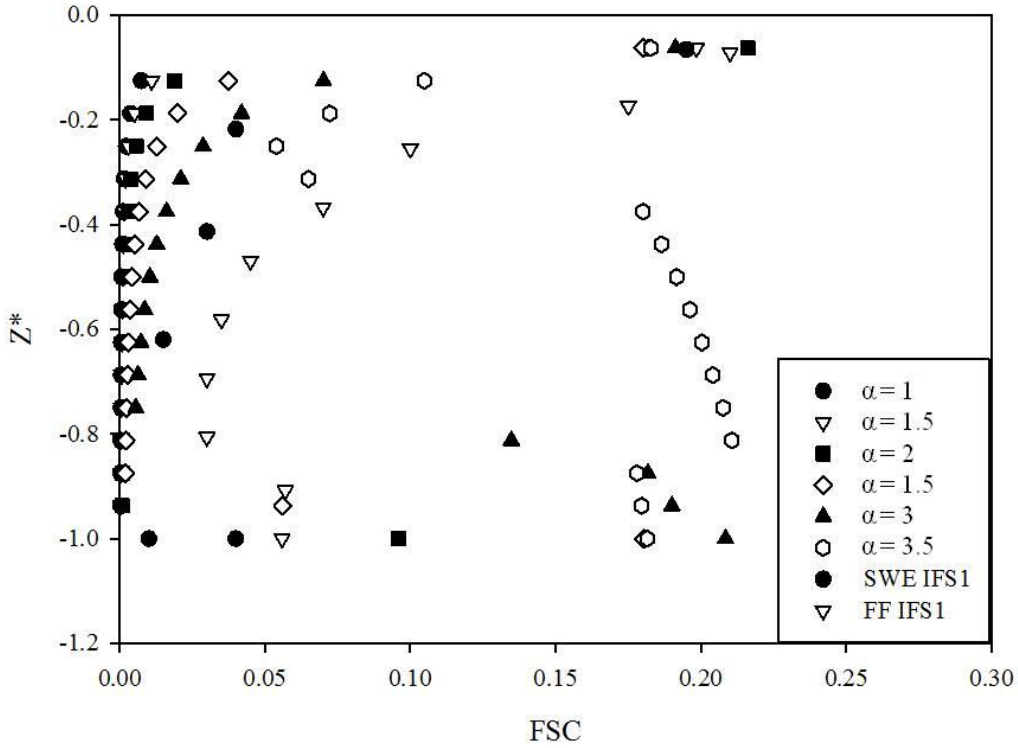

Figure 6. Fine sediment content depth profiles for different values of the bias parameter α compared to experimental results of *Gibson et al*. [2009] in experiment 1 under free flow conditions (FF IFS1) and in still water conditions (SWE IFS1).

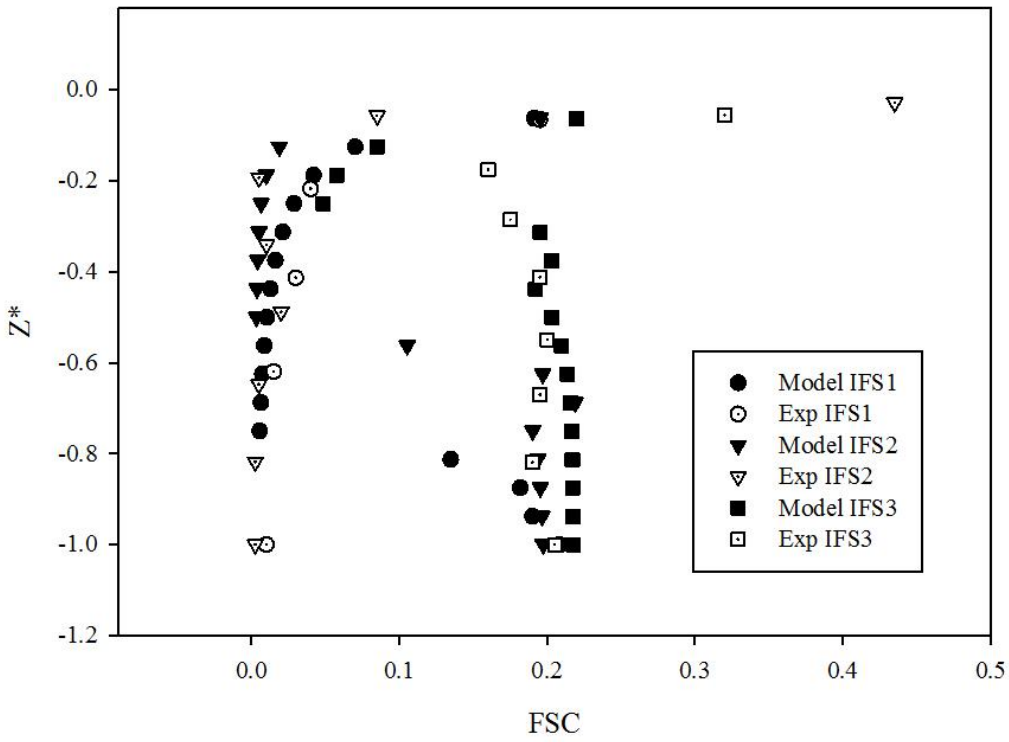

Figure 7. Comparison between the results of the theoretical model (full symbols) and the experimental results obtained by *Gibson et al*. [2009] (empty symbols).

Gibson et al. [2010] performed a similar experimental work involving different types of gravel and infiltrating sediment with seven and ten GSD's respectively (D_{50} ranged from 2.9 to 9.2mm for the gravel and d_{85} ranging from 0.05 to 1.05mm for the sand), with the aim of determining more precisely a threshold value that separates bridging and USP situations. The model proposed herein was used to calculate theoretical depth profiles of FSC for the different combinations of bed and infiltrating sediment. Coherently with *Gibson et al*. [2010], equilibrium FSC depth profiles were classified in bridging, transitional and USP profiles. All the theoretical profiles follow a qualitatively similar trend. The surface layer is saturated with F_{max} and FSC decreases with depth down to a clogged layer, formed at the bottom as a consequence of the impermeable boundary condition. The thickness of this clogged layer at equilibrium depends on the time during which fine sediment is able to infiltrate before FSC at the near-surface layers prevent further fine sediment from infiltrating. Bridging profiles are defined as those where the shallowest layer is saturated and FSC decreases with depth down to the bottom clogged layer. Transitional profiles include FSC depth profiles where the FSC in any of the layers is below 15% and above 5% in all of them. USP profiles are defined as those where the clogged layer covers the whole bed. Figure 8 shows the classification of the different profiles resulting from the experimental work [*Gibson et al*. 2010] and the theoretical model for a value of $\alpha = 3$.

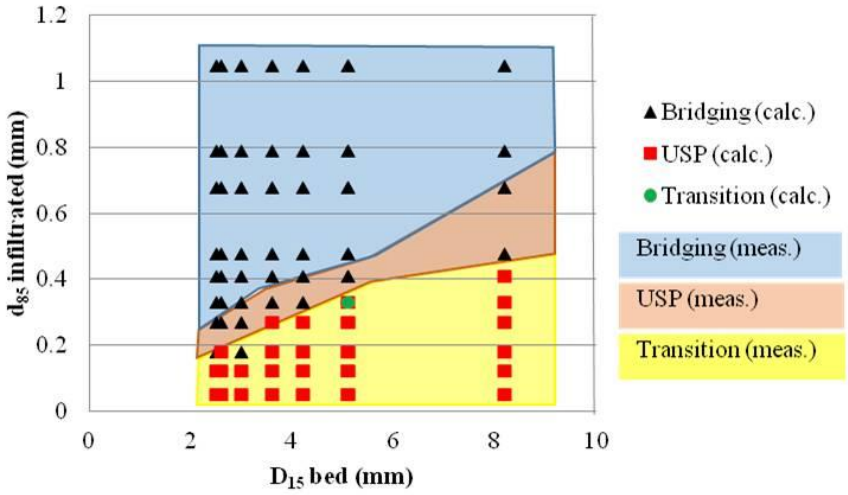

Figure 8. Comparison of bridging and USP threshold calculated using the theoretical model and that observed by *Gibson et al*. [2010]. Symbols are the results of the model presented herein with a bias parameter α equal to 3, whereas the shades in background summarize the experimental results of *Gibson et al*. [2010].

4 Discussion

Figure 6 shows the comparison of the calculated profiles for different values of the bias parameter, α. An increase in the bias parameter results in higher fine sediment infiltration down to the deepest layers. This is a consequence of the higher probability to choose coarser particles that form larger pores. The theoretical profile that reproduces the experimental results best is the one corresponding to $\alpha = 3$. This indicates that the probability for a bed particle to participate in a pore throat is proportional to its volume. It may be considered that the number of pore throats in which a bed grain participates is proportional to the number of contact points with adjacent grains, which in turn may be proportional to the grain surface and therefore to the square of its diameter, therefore suggesting a value of $\alpha = 2$. A higher value of α could indicate that fine bed grains contribute in fewer pore throats than indicated by their surface. A possible interpretation is that part of the finest bed grains do not form the bed matrix but they are deposited in the pores formed by the coarser grains (Figure 3C). This situation may be more likely as the standard deviation of the bed sediment GSD increases.

Figure 8 showed how the results of the mathematical model are consistent with the experimental results obtained by *Gibson et al*. [2010]. A threshold value between 14 and 16 for D_{15} / d_{85} separates the occurrence of bridging and USP for both the experimental data and the model results. It can be noted though that this threshold does not perfectly separate both mechanisms. *Huston & Fox* [2015] suggested another parameter to define this threshold, namely the ratio between geometrical diameters of coarse and fine sediment divided by the variance of the coarse sediment GSD: $D^g/(d^g \sigma)$. Both parameters aim to compare the pore size of the gravel bed and the diameter of the fine sediment. D^g/σ and D_{15} are used as surrogates of the characteristic pore size by *Huston and Fox* [2015] and *Gibson et al*. [2010], respectively. In

order to discuss the suitability of each threshold parameter, first the mathematical model presented herein is applied on the data of *Gibson et al*. [2010] to discuss the best way to reproduce the pore size. The choice for the characteristic diameter of the fine sediment will be addressed afterwards.

The median pore size of the eight types of gravels used in *Gibson et al*. [2010] were computed with the model presented herein (eq. (10) and $P_p(x) = 0.5$), using $\alpha = 3$ and $N_a = 3$. Results are presented in Figure 9 as a function of D^g/σ and D_{15}. The correlation coefficients r^2 of the linear fit through data points are indicated on each panel. Both parameters similarly reproduce the median pore diameter for such GSDs and the different slopes of respectively 0.24 and 0.20 for D^g/σ and D_{15} partially explain the different values for the clogging threshold that they obtain. It should be noted though that natural GSDs can present multiple modes and such parameters then fail in reproducing a characteristic pore size diameter.

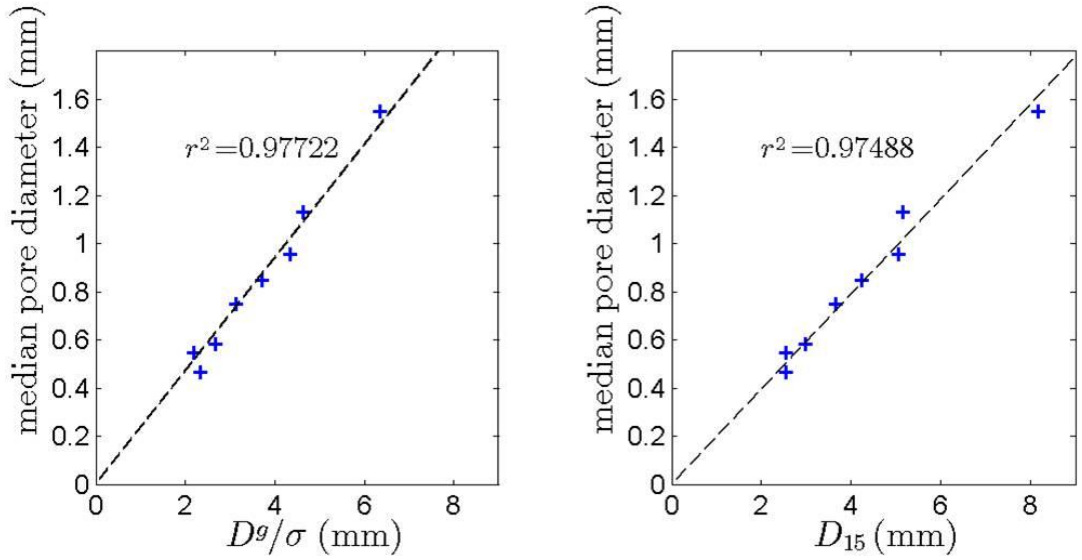

Figure 9. Median pore size of gravels used in *Gibson et al*. (2010) as a function of the ratio between the geometrical diameter and the standard deviation D^g/σ and the D_{15} of the gravels.

A characteristic diameter for fine sediment also takes part in the definition of the clogging threshold criteria. *Huston and Fox* (2015) use the geometric mean diameter while *Gibson et al*. [2010] consider d_{85}. In the model presented herein, each class of fine sediment can be retained independently and this parameter is not critical. The suitability of one or the other option to describe the bridging threshold may be discussed. The threshold proposed by *Huston and Fox* [2015] ($D^g/(d^g\,\sigma) = 27$) can be reinterpreted as a ratio between median pore size and fine geometric diameter of $0.24 \cdot 27 = 6.5$. This ratio above one could be the consequence of several particles smaller than the pore throat arriving simultaneously and forming a bridge that can be retained in the pore. Multi-particle bridging has been indeed proposed as a mechanism responsible of surficial clogging [*Huston and Fox*, 2015; *Valdes and Santamarina*, 2006]. Nevertheless, the ratio of 6.5 is too high to be explained by multi-particle bridging. Multi-particle bridging indeed is not stable for pore spaces that are 3 to 4 times the fine particle diameter [*Valdes and Santamarina*, 2008]. On the other hand, reinterpreting the threshold value

of *Gibson et al*. [2010] leads to a ratio between pore size and fine sediment size of 2.7. The difference in these threshold values is quite consistent with the difference between d_{85} and d^g for the fine sediments used in *Gibson et al*. [2010] (1.96 in average). A possible interpretation of these results is that a pore is blocked by a bridge formed by fine particles belonging to the coarsest fraction of the infiltrating sediment (i.e. 2-3 particles of size d_{85} and not 6-7 of size d^g). This idea supports the choice of a characteristic size of the coarsest fraction of the infiltrating sediment to represent it in the clogging threshold parameter, in agreement with the proposition of *Gibson et al*. [2010]. We therefore consider the threshold parameter proposed by *Huston & Fox* [2015] as less suitable than the one proposed by *Gibson et al*. [2010]. On the other hand, the influence of multi-particle bridging may be a function of the rate at which fine sediment is infiltrated into the bed which would likely affect the probability of two or more particles arriving simultaneously at a pore throat. This discussion underlines a limitation of the model proposed herein that relies on the fact that fine particles arrive to a specific pore throat one by one so that multi-particle bridging is not taken into account.

On the other hand, the pore size calculated with Heron's formula (equation 3) is based on the hypothesis that the pore is formed by three bed grains. However, real bed pore throats may often be formed by four or even more adjacent grains. In this case, pore throat size is larger than in the case of a pore formed by three grains. This can be easily illustrated considering the pore throats formed by three or four identical particles of diameter *D* (Figure 10). The size of the four-grain pore throat is 2.5 times larger than the three-grain pore throat. Obviously, the four-grain case can give rise to more variable geometries but it seems however that the geometry assumed by Heron's formula may underestimate the representative real pore throat size.

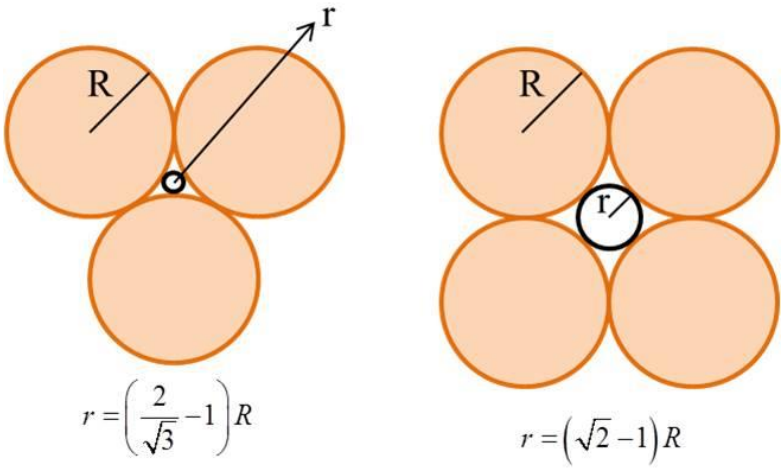

Figure 10. Theoretical pore throats formed by three and four bed grains

Another aspect that may have an impact on pore throat size and subsequently on the straining of infiltrating particles is the shape of the bed grains. The approach proposed herein assumes that a pore throat is formed by three spherical particles. It seems plausible to think that particles with a longer elliptical shape may form smaller pore throats between them. This implies that Heron's formula would overestimate the realistic pore throat size therefore justifying somehow the threshold value for clogging obtained by *Huston & Fox* (2015). This effect should be more important for coarse bed material, as past studies have shown that sphericity of gravel

decreases as particle size increases [*Peronius and Sweeting*, 1985; *Zou and Yu*, 1996; *Cho et al*., 2006].

When considering the experimental results of *Gibson et al*. [2009] (Figure 6), higher FSC is observed at the deep layers for the free flow experiment compared to the still water experiment. A possible explanation of this fact is based on the hydraulic sorting process that occurs in the free flow experiment, by which fine particles are transported faster and can infiltrate before coarser particles clog the surface grains and stop the infiltration process. During the still water experiment coarse and fine particles arrive almost simultaneously to the bed surface and less sediment is able to infiltrate into the bed before the surface becomes clogged.

Pore scale processes can also explain differences between the model results and the experimental observations. The mathematical model proposed herein considers the blockage of infiltrated grains only at the pore throats. However, fine grains can also be deposited on the top of bed gravel grains. The authors performed a series of laboratory analysis on silt and sand infiltration (article in prep.) where this process was observed. During the first stage of the tests silt and sand piles were observed on the top of the bed grains, being more stable in the case of silt infiltration. This process is not considered in this model and may explain the higher fine sediment content observed in the laboratory. Another consequence of this process is that fine sediment depth profiles corresponding to lower α values may match better the laboratory results of the still water experiments by *Gibson et al*. [2009].

Another possible interpretation of this trend is based on the influence of interstitial flow. *Huston and Fox* [2015] suggest the impact of pore water velocity on the dispersion of fine particles towards deep layers. Shear stress associated with pore water velocity may be high enough to destabilize some of the deposits that clog the surface layer, causing small landslides that transport fine sediment downwards. Based on this, we consider that the destabilization may occur as a consequence of velocity fluctuations associated with turbulent sweeps. This phenomenon is related with the momentum exchange affecting the effective bed roughness as stated by *Manes et al*. [2011]. This pattern has been observed by the authors in the laboratory (results not published yet). These aspects may explain the difference between the theoretical and the experimental results. The mathematical model proposed herein is based on a geometrical approach that reproduces well the still water experiments but do not take into account the influence of the flow. The better correspondence of theoretical results with still water experiments than with free flow experiments is observed in Figure 6. Although reproducing this process is out of the scope of this article, a plausible approach would be to introduce a downward flux of the previously deposited sediment related to turbulent sweeps and their time scale compared to the specified time step. The influence of these turbulent events should be depth dependent [*Detert and Parker*, 2010].

Previous works highlight the occurrence of a significant expansion of the bed frameworks in flow conditions just prior to entrainment [*Allan and Frostick*, 1999; *Middleton et al*., 2000]. This aspect can modify fine sediment distribution within the bed by allowing fine particles to penetrate deeper into the bed. However, the flow conditions used in the experiments of *Gibson et al*. [2009] and *Gibson et al*. [2010] are far from the incipient motion of the gravel bed (15 to 25 per cent). Therefore, it does not seem plausible that this mechanism could be responsible of the higher FSC observed within the bed in the experimental results compared to the model results.

Based on a statistical analysis over a large data set of previous laboratory experiments, *Huston and Fox* [2015] proposed the following equation to reproduce the FSC depth profile:

$$f = f_s \exp(-kz) \tag{15}$$

In equation (15), f_s is calculated as $f_s = \theta_g (1-\theta_s)$, z is the vertical coordinate considered positive upwards and k is a coefficient defined as:

$$k = \frac{\ln(0.01/f_s)}{Z_C} \tag{16}$$

where Z_C represents the depth of the clogged layer. Based on the same statistical analysis, *Huston and Fox* (2015) proposed the following equation to calculate Z_C:

$$Z_C^* = 2.3 \cdot 10^4 \theta_g^{0.6} R^{*0.1} + 2.0 \cdot 10^4 \tag{17}$$

Where Z_C^* is the dimensionless clogging depth defined as $Z_C^* = (Z_C u_*)/\nu$ (u_*: shear velocity; ν: kinematic viscosity) and R^* is the roughness Reynolds number defined as $R^* = (u_* k_s)/\nu$ (k_s: roughness length). Figure 11 shows the comparison between the FSC depth profile predicted by the theoretical model and the statistical analysis. The gravel-sand combinations G6-S7 and G8-S7 of *Gibson et al*. [2010] are considered. FSC predicted by the theoretical model are lower than the ones predicted by the statistical analysis (equation 14). Again, a possible interpretation of this fact is the influence of the surface and subsurface flow on fine sediment distribution within the bed that occurs in the clogging laboratory experiments on which the statistical analysis is based. On the other hand, the exponential coefficient introduced in equation (15) considers that the clogging depth, Z_C, corresponds to the depth at which FSC is 1% of the theoretical maximum value. This is a subjective definition that has further influence on the obtained results.

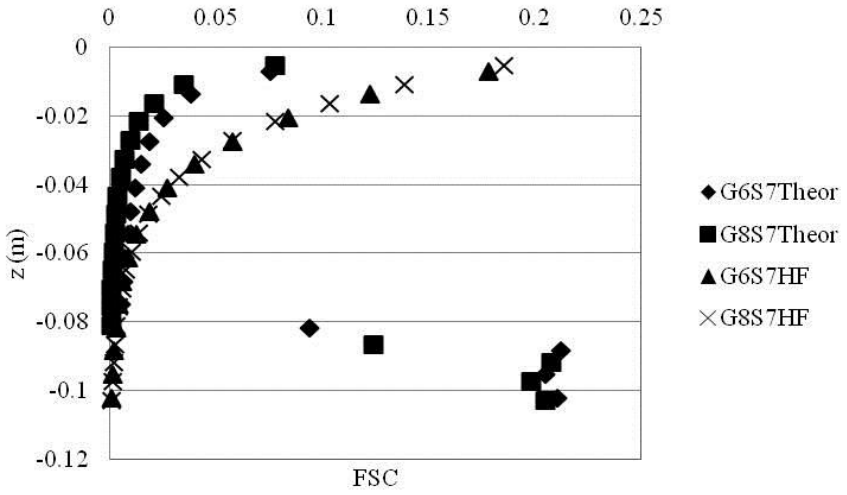

Figure 11. Comparison between the theoretical results calculated with the mathematical model presented herein and the profiles proposed by *Huston and Fox* (2015) based on their statistical analysis

5 Conclusions

This study presents the development of a mathematical model of fine sediment infiltration into a bed formed by coarser material, in order to calculate the depth profile of FSC at the equilibrium situation. The model is based on the definition of a trapping coefficient that describes the probability of an infiltrating grain being trapped in a pore throat formed by three bed grains. The bed is subdivided into horizontal layers and the GSD of each layer is updated considering the retained fine sediment, therefore modifying the trapping coefficient. The equilibrium is attained when the FSC at the surface layer reaches a theoretical maximum value based on fine and coarse sediment porosity.

The model is tested against laboratory experiments carried out by *Gibson et al*. [2009] and *Gibson et al*. [2010], where the FSC depth profile and the mechanism of infiltration (bridging or unimpeded static percolation) were analyzed for different GSD's of the bed and the infiltrating sediment. The mathematical model reproduces well the threshold value obtained in the laboratory to separate the cases where bridging occurs from those where unimpeded static percolation is observed. Nevertheless, the experimental depth profiles show higher FSC at the subsurface. A possible interpretation of this fact lies on the influence of pore water velocity and the destabilization it can cause on the fine grains retained at the pore throats.

Acknowledgments and data

The authors would like to express their gratitude to IRSTEA and the French water agency (Agence de l'Eau Rhône Méditerranée Corse) for the funding of this work and Stanford Gibson for letting use the results from their analyses. The authors will be glad to provide details or the full model code to anyone interested in it (personal communication).

References

Allan, A. F., and L. Frostick (1999), Framework dilation, winnowing, and matrix particle size: the behavior of some sand-gravel mixtures in a laboratory flume, Journal of Sedimentary Research, 69(1), 21-26.

Blaschke, A. P., K. H. Steiner, R. Schmalfuss, D. Gutknecht, and D. Sengschmitt (2003), Clogging processes in hyporheic interstices of an impounded river, the Danube at Vienna, Austria. International Review of Hydrobiology, 88(3-4), 397-413, doi:10.1002/iroh.200390034.

Blois, G., G. S. Smith, J. L. Best, R. J. Hardy, and J. R. Lead (2012), Quantifying the dynamics of flow within a permeable bed using time-resolved endoscopic particle imaging velocimetry (EPIV). Experiments in fluids, 53(1), 51-76, doi:10.1007/s00348-011-1198-8.

Cho, G. C., J. Dodds, and J. C. Santamarina (2006), Particle shape effects on packing density, stiffness, and strength: natural and crushed sands, Journal of Geotechnical and Geoenvironmental Engineering, 132(5), 591-602, doi: 10.1061/(ASCE)1090-0241(2006)132:5(591).

505 Cui, Y., and A. C. Wilcox (2005), Numerical modeling of sediment transport upon dam removal:
506 Application to Marmot Dam in Sandy River, Oregon, Sedimentation Engineering, ASCE
507 Manual, 54.

508 Cui, Y., J. K. Wooster, P. F. Baker, S. R. Dusterhoff, L. S. Sklar, and W. E. Dietrich (2008),
509 Theory of fine ediment infiltration into immobile gravel bed, Journal of Hydraulic
510 Engineering, 134(10), 1421-1429, doi: 10.1061/(ASCE)0733-9429(2008)134:10(1421)

511 Detert, M., and G. Parker (2010), Estimation of the washout depth of fine sediments from a
512 granular bed, Journal of Hydraulic Engineering, 136(10), 790-793, doi:
513 10.1061/(ASCE)HY.1943-7900.0000263

514 Einstein, H. (1968), Deposition of suspended particles in a gravel bed. Journal of Hydraulic
515 Division - American Society of Civil Engineers, 94(5), 1197-1205.

516 Evans, E., and A. C. Wilcox (2014), Fine sediment infiltration dynamics in a gravel-bed river
517 following a sediment pulse, River Research and Applications, 30(3), 1421-1429,
518 doi:10.1002/rra.2647

519 Frings, R. M., M. G. Kleinhans, and S. Vollmer (2008), Discriminating between pore-filling load
520 and bed-structure load: a new porosity-based method, exemplified for the river Rhine,
521 Sedimentology, 55(6), 1571-1593, doi: 10.1111/j.1365-3091.2008.00958.x.

522 Gibson, S., D. Abraham, R. Heath, and D. Schoellhammer (2009), Vertical gradational
523 variability of fines deposited in a gravel framework, Sedimentology, 56(3), 661-676, doi:
524 10.1111/j.1365-3091.2008.00991.x.

525 Gibson, S., D. Abraham, R. Heath, and D. Schoellhammer (2010), Bridging Process Threshold
526 for Sediment Infiltrating into a Coarse Substrate, Journal of Geotechnical and
527 Geoenvironmental Engineering, 136(2), 402-406, doi:10.1061/(ASCE)GT.1943-
528 5606.0000219.

529 Gibson, S., D. Abraham, R. Heath, and D. Schoellhammer (2011), Visualization and analysis of
530 temporal trends of sand infiltration into a gravel bed. Water Resources Research, 47(12),
531 doi:10.1029/2011WR010486.

532 Greig, S. M., D. A. Sear, and P. A. Carling (2007), A review of factors influencing the
533 availability of dissolved oxygen to incubating salmonid embryos, Hydrological
534 Processes, 21(3), 323-334, doi: 10.1002/hyp.6188.

535 Huston, D. L., and J. F. Fox (2015), Clogging of Fine Sediment within Gravel Substrates:
536 Dimensional Analysis and Macroanalysis of Experiments in Hydraulic Flumes, Journal
537 of Hydraulic Engineering, 04015015, doi:10.1061/(ASCE)HY.1943-7900.0001015.

538 Jones, J. I., A. L. Collins, P. S. Naden, and D. A. Sear (2012), The relationship between fine
539 sediment and macrophytes in rivers. River Research and Applications, 28(7), 1006-1018,
540 doi:10.1002/rra.1486.

541 Kleinhans, M.G. (2002) Sorting out sand and gravel: sediment transport and deposition in and-
542 gravel bed rivers. Neth. Geogr. Stud., 293, 317 pp.

543 Lauck, T. (1991), A simulation model for the infiltration of sediment into spawning gravel, M. S.
544 Thesis, Humboldt State University, Arcata, California, USA.

545 Leonardson, R. (2010), Exchange of fine sediments with gravel riverbeds, PhD Dissertation,
546 Berkeley University, Berkeley, California, USA.

547 Lisle, T. E. (1989), Sediment transport and resulting deposition in spawning gravels, North
548 Coastal California, Water Resources Research, 25(6), 1303-1319.

549 Manes C., D. Pokrajac, V. I. Nikora, L. Ridolfi, and D. Poggi (2011), Turbulent friction in flows
550 over permeable walls, Geophysical Research Letters, 38(3), doi:10.1029/2010GL045695

551 Middleton, R., J. Brasington, , B. J. Murphy, and L. E. Frostick (2000), Monitoring gravel
552 framework dilation using a new digital particle tracking method, Computers &
553 Geosciences, 26(3), 329-340.

554 Morris, G. L., and J. Fan (1998), Reservoir sedimentation handbook, McGraw Hill Book Co.,
555 New York.

556 Peronius, N., and T. J. Sweeting (1985), On the correlation of minimum porosity with particle
557 size distribution, Powder technology, 42(2), 113-121, doi:10.1016/0032-5910(85)80043-
558 7.

559 Schälchli, U. (1992), The clogging of coarse gravel river beds by fine sediment, Hydrobiologia,
560 235-236(1), 189-197,

561 Valdes, J. R., and J. C. Santamarina, (2006), Particle clogging in radial flow: Microscale
562 mechanisms. SPE Journal, 11(02), 193-198.

563 Walling D. E., P. N. Owens, J. Carter, G. J. L. Leeks, S.Lewis, A. A.Meharg, and J.Wright
564 (2003), Storage of sediment-associated nutrients and contaminants in river channel and
565 floodplain systems. Applied Geochemistry, 18(2), 195-220, doi:10.1016/S0883-
566 2927(02)00121-x.

567 Wilcock P. R., S. T. Kenworthy, and J. C. Crowe (2001), Experimental study of the transport of
568 mixed sand and gravel, Water Resources Research, 37(12), 3349-3358,
569 doi:10.1029/2001WR000683.

570 Wilcock P. R., and J. C. Crowe (2003), Surface-based transport model for mixed-size sediment.
571 Journal of Hydraulic Engineering, 129(2), 120-128, doi: 10.1061/(ASCE)0733-
572 9429(2003)129:2(120)

573 Wood P. J., and P. D. Armitage (1997), Biological effects of fine sediment in the lotic
574 environment. Environmental Management, 21(2), 203-217, doi: 10.1007/s002679900019.

575 Wooster J. K., S. R. Dusterhoff, Y. Cui, L. S. Sklar, W. E. Dietrich, and M. Malko (2008),
576 Sediment supply and relative size distribution effects on fine sediment infiltration into
577 immobile gravels, Water Resources Research, 44(3), doi:10.1029/2006WR005815.

578 Zou, R. P., and A. B. Yu (1996), Evaluation of the packing characteristics of mono-sized non-
579 spherical particles, Powder technology, 88(1), 71-79, doi:10.1016/0032-5910(96)03106-
580 3.

581

A.2 Résultats expérimentaux sur les processus d'infiltration

LABORATORY ANALYSIS ON SILT INFILTRATION INTO GRAVEL BED

ALBERT HERRERO[(1)], CELINE BERNI[(2)] & BENOIT CAMENEN[(3)]

Irstea, UR HHLY Hydrology-Hydraulics, 5 rue de la Doua – CS 70077 – F-69626 Villeurbanne, France,
albert.herrero@irstea.fr, celine.berni@irstea.fr, benoit.camenen@irstea.fr

ABSTRACT

Fine sediment infiltration into a gravel bed may have significant impact on environmental, socioeconomic and river morphodynamics issues. Several human activities enhance fine sediment flux, either in the production zone due to changes in land use or within the river system due to reservoir flushes or dredging. Understanding the mechanisms that control this phenomenon can help to minimize impacts of such anthropic actions. A set of experiments has been performed in the new tilting flume (18 meter long and 1 meter wide) of Irstea-Lyon hydraulics laboratory. Silt sized silica (10-30 microns) and gravels (3-12 mm) are used as fine and coarse sediments, respectively. Fine sediments are introduced for a specified concentration in a flow with fixed discharge, water depth and bed slope. All the explored conditions correspond to fine sediment travelling in homogeneous suspension (wash load). Keeping the concentration constant during each test, the process of infiltration of fine sediments into the gravel bed is analyzed and the influence of flow velocity and fine sediment concentration is discussed. Fine sediment deposition takes place as a progressive filling of the bed starting from the base of the channel and ending one to three diameters below the bed surface. The thickness of the surface layer that remains unclogged in the equilibrium situation depends mainly on the bed shear stress. On the other hand, a positive correlation is found between the suspended sediment concentration and the rate of infiltration with time. Water mass exchange and turbulent structures that occur at the flow-bed interface seem to be the key mechanisms that control fine sediment infiltration

Keywords: infiltration, silt, gravel, hyporheic exchange, laboratory work

1. INTRODUCTION

Human activities and land use changes modify sediment dynamics at the catchment and at the reach scale. As sediment input to rivers changes, the composition of river beds is altered. When the river bed is formed by relatively coarse sediment, fine sediment transported either in suspension or as bed load can infiltrate within the bed, therefore modifying its characteristics. This alteration has different environmental, socioeconomic and hydromorphological impacts.

From an environmental point of view, the formation of a clogged bed modifies the exchange of water, oxygen and nutrients across the sediment-water interface (Grant et al. 2012), therefore affecting the survival rate of fish eggs (Wood and Armitage 1997, Greig et al. 2007), the habitable regions for benthic invertebrates (Jones et al. 2012a) and the root length of machophytes (Jones et al. 2012b). When infiltration affects only the bed surface layer, oxygen is able to penetrate to the fish eggs but fries are prevented from emerging once they are born (Koski 1966). Moreover, modification of the surface decreases the possibilities to find a shelter and to refuge from predators for some species. Concerning socioeconomic issues, the decrease in permeability associated with fine sediment infiltration has an impact on the recharge process of the aquifers connected to the affected river, therefore increasing the cost of pumping operations for water (Blaschke et al. 2003). On the other hand, the presence of a clogged layer can act as a filter for some harmful substances transported by the water, hence improving the quality of the water arriving to the aquifer (Ray et al. 2002). Dam is one of the antrophogenic structures that influences on sediment dynamics along rivers, the mentioned consequences oblige to apply a regulation on dam operations (Cui et al. 2006). Finally, fine sediment infiltration modifies the flow dynamics by decreasing bed roughness and increasing flow velocities which, in turn, may affect the suitability of the habitat for some specific species (Jones et al. 2012a). Moreover, infiltrated fine sediments do not contribute directly to the morphological changes of the river, a fact that has to be taken into account when evaluating the channel evolution and sediment budgets (Frings et al. 2008).

Previous studies highlight two possible infiltration mechanisms depending on the relative size between the fine sediment transported by the flow and the coarse sediment forming the bed matrix (Gibson et al. 2009). When both sizes are significantly different, fine sediment is able to penetrate deep into the bed until some layer below, which is relatively impermeable, and the bed is clogged from the bottom upwards (unimpeded static percolation). On the other hand, when fine sediment is coarse enough to be strained in the pore throats formed by the bed grains, a clogged layer is formed at the surface that prevents any deeper infiltration. The amount of fine sediment infiltrated is influenced by different hydrodynamic and sediment parameters as the bed shear stress (Evans and Wilcox 2013), suspended sediment concentration (Khullar et al. 2013), fine sediment cohesion (Packman et al. 2000), the arrangement of bed surface grains (Cooper and Tait 2009), the occurrence of bed forms (Packman and MacKay 2003), the existence of an vertical hydraulic gradient within the bed (Schälchli 1992) and the presence of a biofilm (Arnon et al. 2010). Nevertheless, divergent conclusions have been highlight by different authors, especially concerning the role of bed shear stress on the infiltration process.

The infiltration of silt-sized sediment into a gravel bed gives place to a clogging process following the mechanism of unimpeded static percolation. Different studies analyzing deposition rates in these conditions also provided divergent results. Einstein (1968) proposed a mathematical model in which he assumed that deposition rate occurs at the Stokes settling velocity. Taking this situation as a reference, those conditions generating higher deposition rates are classified as "enhanced settling" and those causing lower deposition rates are classified as "decreased settling" (Fries and Trowbridge 2003). Fries and Trowbridge (2003) and Fries and Taghon (2010) observed enhanced settling rates although the correlation with bed shear stress had opposite sign in each of these studies. On the other hand, Hamm et al. (2011) observed decreased settling rates, especially for increasing bed shear stress.

The importance of the impacts associated with fine sediment infiltration and the uncertainty of the state of knowledge in this topic are two facts that encourage the scientific community to deepen into this area of sediment dynamics. This study presents laboratory experiments that aim to cast some light into the mentioned points and opens the door to further discussion and the development of a mathematical model that is currently in process.

2. EXPERIMENTAL SETUP

The experimental work performed during this analysis was carried out in the Hydraulics and Hydromorphology Laboratory of Irstea-Lyon (France). The tests were done in an 18meter long, 1meter wide and 0.8 m high tilting flume (Figure 1). The flume outlet is connected to a 35 m^3 reservoir where two pumps are able to recirculate water and fine sediment in suspension back to the channel inlet. A 6cm thick gravel layer was displayed along the channel. Gravel size ranged from 3 to 12 mm (D_{50}= 8 mm). Concerning fine sediment, silt-sized silica with diameters ranging from 10 to 30 microns was used in all the tests.

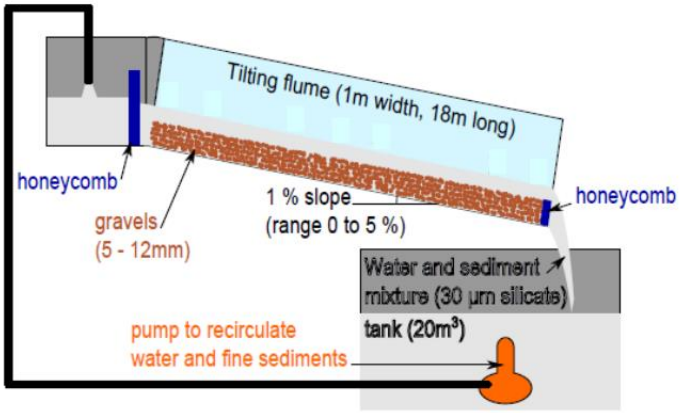

Figure 1. Recirculating flume used for the infiltration experiments

For each run, water discharge, suspended fine sediment concentration and bed slope were specified. The values of these variables are shown in Table 1 for each of the performed experiments. At the beginning of each test, the amount of fine sediment corresponding to the desired concentration was added in the reservoir, and left there long enough to be well-mixed, thanks to a stirring system installed in there. Suspended sediment concentration was kept constant during each experiment. In order to make it possible, sediment was added periodically in order to correct the suspended concentration decrease associated with fine sediment infiltration and retention within the bed. This operation was carried out based on the concentration measurement of two turbidimeters installed near the inlet and the outlet of the channel. Suspended concentration was kept constant during the tests because it was interpreted as a more realistic reproduction of natural conditions. Indeed, sediment infiltration in a natural river reach does not generate a decrease in the concentration of the flow affecting that reach. However, in a recirculation channel as the one used in this analysis the concentration evolves as a consequence of fine sediment infiltration, and unrealistic conditions are obtained if suspended concentration is not corrected.

Table 1. Experimental conditions corresponding to the different tests (Q: water discharge; C: suspended sediment concentration; S: bed slope)

Test	**1**	**2**	**3**	**4**	**5**
Q (l/s)	30	30	30	30	55
C (g/l)	4.0	5.5	4.0	7.2	4.3
S (%)	1	0.1	0.1	0.1	0.1

During each test, water depth is measured with ultrasonic sensors placed at three positions along the channel (inlet, central and outlet). An ADV profiler placed seven meters downstream of the channel inlet is used to measure near bed flow velocities which are then used to calculate bed shear stress. Water samples are taken periodically and fine sediment

contained in them are filtered so that sediment concentration can be obtained. The samples are taken next to the turbidimeters position, as well as from the reservoir at the downstream end of the flume. In order to avoid uncertainty from the turbidimeter calibration, the representative values of concentration corresponding to each test are those obtained from the water samples.

In order to quantify fine sediment content in the bed, six cylinders were placed within it before starting each test. The cylinders were made of a metallic grid with holes of 1 mm so that the influence on horizontal interstitial flow and fine sediment trajectories within the bed is minimized. The cylinders were placed in pairs at the longitudinal positions x=6 m, x=9 m and x=12 m (the flume inlet is considered as the origin of x coordinate) and at a distance of 30 cm from the channel walls. Three of the cylinders, one at each longitudinal position, were extracted after the first eight hours of experiment and the other three at the end of the test. The content of the cylinders is afterwards analyzed. One centimeter thick layers are separated and gravel is separated from silt in such a way that fine sediment content can be determined at each layer. Additionally, lateral photos of one central section of the flume were taken in order to observe the evolution of fine sediment accumulation within the pores. Fine sediment clogged the bed from the base of the flume upwards and the photos allowed following the evolution of the clogged layer. In order to evaluate the wall effects and the validity of the lateral observations, two sections were analyzed carefully after one of the experiments. The depth of the clogged layer was found to be quite uniform in the transversal direction. Therefore, it was concluded that the results obtained from the lateral photos were representative of the whole section.

The duration of each experiment lasted until the whole gravel bed was clogged with fine sediment or when no further evolution of the clogged layer was observed through the lateral walls.

3. RESULTS

Firstly, the qualitative observations of the infiltration processed are summarized. As the sediment-laden flow was introduced over initially clean gravel, water infiltrates within the bed and small piles of fine sediment are visible on the top of the gravel grains. The piles stop growing after 15 to 20 minutes of experiment and small destabilizations start occurring that push fine sediment towards the base of the flume. A clogged layer starts to form from the bottom upwards and grows as fine sediment fills the pores between the gravel grains. It should be noted that the ratio between coarse and fine sediment diameters is approximately 200 for the materials used in this experiments, therefore far from the threshold above which unimpeded static percolation is predicted (Gibson et al. 2010). Clogged layer thickness grows at an approximately constant rate until it reaches the near bed layer (3-5 gravel diameters). At this point, the rate of growth of the clogged layer starts decreasing. For some of the tests (2, 3 and 4) infiltration continues until the clogged layer reaches the bed surface. However, for tests 1 and 5, the clogging process stops before and there is a surface layer of 1 to 3 gravel diameters that remains free of sediment in the equilibrium situation. Figure 2 presents four lateral photos that show the evolution of the clogged layer during Test 2.

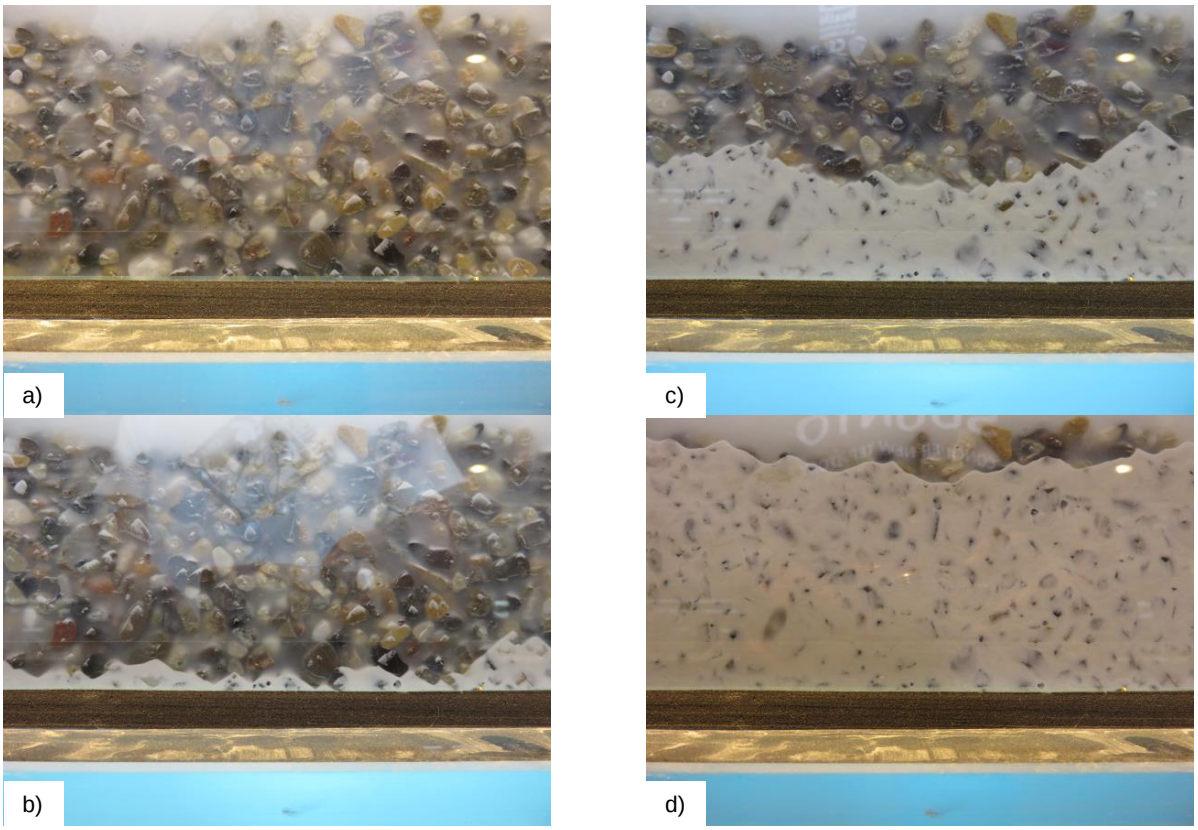

Figure 2. Lateral view of the infiltrated gravel bed at four different times during test 2

The average level of the clogged layer surface is measured referred to the base of the flume. The evolution in time of this level is shown in Figure 3 for the different tests. There is an initial and short phase during which no accumulation is observed at the bottom of the flume yet. This period corresponds to the phase of growth of fine sediment piles on the top of the gravel grains. There is also a small level difference between the base of the flume and the visible part of the walls that introduce a short lag between the beginning of the clogged layer formation and the moment when it is visible. After the initial phase, the clogged layer grows at a rate which is approximately constant, as shown by the good correspondence with the linear regression. Once the clogged layer reaches a certain level the rate of growth decreases until the equilibrium situation, in which the clogged layer surface remains stationary. This phase starts at a height between 30 and 35mm above the bottom of the channel, which corresponds to 3 to 5 gravel diameters below the bed surface.

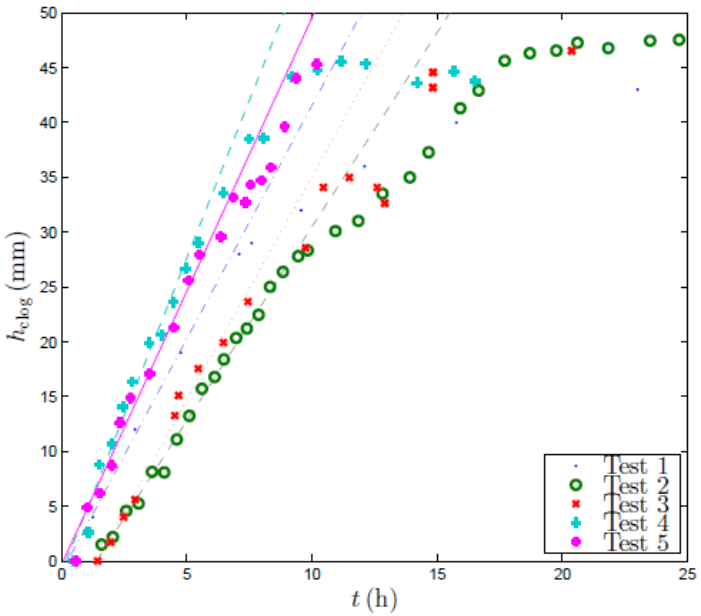

Figure 3. Height of the clogged layer for the different tests. The different lines show the linear regression corresponding to the phase of uniform growth.

The evolution in time of the clogged layer height can be used to evaluate fine sediment infiltration rate. If it is assumed that the observed values are representative of the average evolution along the flume, this rate can be computed as:

$$J_z = \rho_f \frac{\left(1-\theta_g\right)c}{1-c} S \tag{1}$$

where J_z is the fine sediment mass flux (mass of fine sediment that penetrates into the bed per area and time unit), ρ_f is fine sediment density, θ_g is gravel porosity, c is fine sediment content defined as $V_f / \left(V_f + V_g\right)$ (V_f : fine sediment volume; V_g : gravel volume) and $S = dh_{\text{clog}} / dt$ is the slope of the clogged layer height versus time curves.

The cylinders installed within the bed provide a different way to quantify fine sediment infiltration rate. Figure 4 shows, for each test, the comparison between the fine sediment content of the cylinders extracted after the first eight hours and at the end of the experiment. Each represented profile corresponds to the average of the three cylinders extracted at the associated moment. Even if measurements were performed carefully, it should be noted that the higher values at the deeper layer can be at some point influenced by the methodology used to separate de different layers. The comparison between the two profiles of each test shows the evolution of fine sediment accumulation within the bed. The equilibrium profiles show how fine sediment content tends to a uniform value. It is interesting to compare it with the theoretical value corresponding to the complete clogging of gravel pores by fine sediment:

$$c = \frac{V_f}{V_f + V_g} = \frac{\left(1-\theta_f\right)\theta_g}{\left(1-\theta_f\right)\theta_g + \left(1-\theta_g\right)} \tag{2}$$

The porosity values of gravel and silt used in these experiments are 0.38 and 0.55 respectively. Therefore, maximum fine sediment content in a totally clogged layer is 0.22. This value corresponds quite well with the observations at equilibrium. On the other hand, taking into account the period of time from the beginning of the experiment to the extraction of the first cylinder, these data provide another way to calculate fine sediment infiltration rate:

$$J_z = \frac{m}{A_c \Delta t} \tag{3}$$

where m is the fine sediment mass between in the first cylinder of each test, A_c is the area of the cylinder and Δt is the time between the extraction of both cylinders.

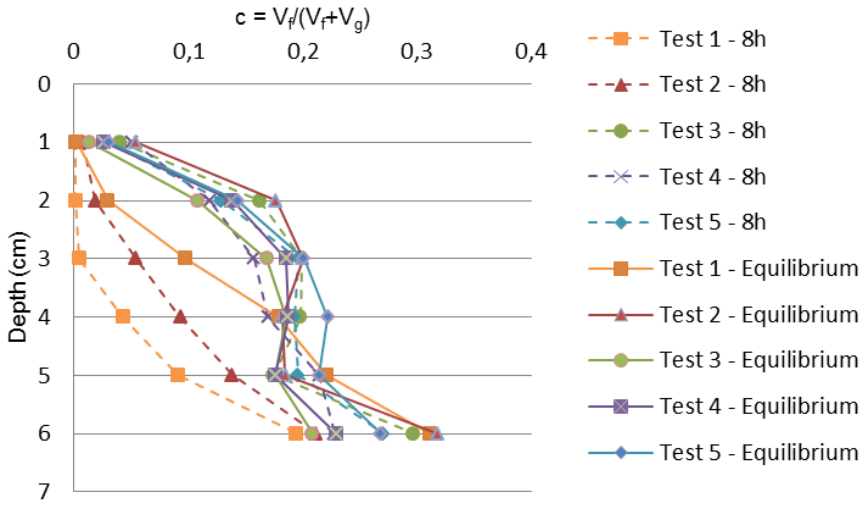

Figure 4. Fine sediment content profile with depth after eight hours of experiment and at the end of the test. The values are obtained from the cylinders introduced before the experiment and divided in layers of 1cm

A third method to quantify fine sediment infiltration rate is based on the suspended concentration measurements performed at the upstream and downstream ends of the flume. As the sediment-laden flow goes through the channel, fine sediment is infiltrated into the bed. Therefore, part of the incoming fine sediment is absent at the flume outlet and a decrease in suspended sediment concentration is expected when comparing upstream to downstream values. Based on this concentration difference, the sediment infiltration rate can be computed by means of the mass balance equation:

$$J_z = \frac{Q\Delta C}{A} \tag{4}$$

where J_z is the fine sediment mass flux, Q is the water discharge, ΔC is the difference in suspended sediment concentration between the upstream and downstream ends of the channel and A is the surface through which fine sediment is infiltrated.

Taking into account the previous results, fine sediment infiltration rate was calculated based on the clogged layer height evolution, the fine sediment content observed in the cylinders and the difference in suspended sediment concentration between the upstream and downstream ends of the flume, using equations (1), (3) and (4) respectively. The results are shown in Figure 5.

4. DISCUSSION

Some discrepancy is observed between the values of fine sediment infiltration rate obtained from the different methods. The values calculated from the longitudinal difference of concentration are higher than the ones obtained following the other two methods. The difference in concentration between the upstream and the downstream samples was often observed to be variable in time even if downstream values were always lower than upstream ones. This uncertainty could be a possible reason of the observed discrepancy. On the other hand, the measurements of clogged layer height were performed in a section close to the center of the flume, so the hypothesis of them being representative of the global average along the channel seems plausible.
It is interesting to compare the obtained results with the deposition rate obtained from considering settling due to gravity with the Stokes fall velocity (Einstein 1968). These theoretical values are also included in Figure 5. Experimental values

are clearly lower than the theoretical prediction in all the tests, therefore corresponding to decreased infiltration rates. Apart from the physical reasons of this behavior, according to the authors' opinion, Einstein's model lacks from considering bed porosity in the predicted deposition rate. Only the part of the bed corresponding to pores between the gravel grains contribute to the downwards infiltration rate (Grant et al. 2012). If the theoretical infiltration rates are corrected by multiplying them by the porosity, the obtained results are much closer to the experimental ones (Figure 5).

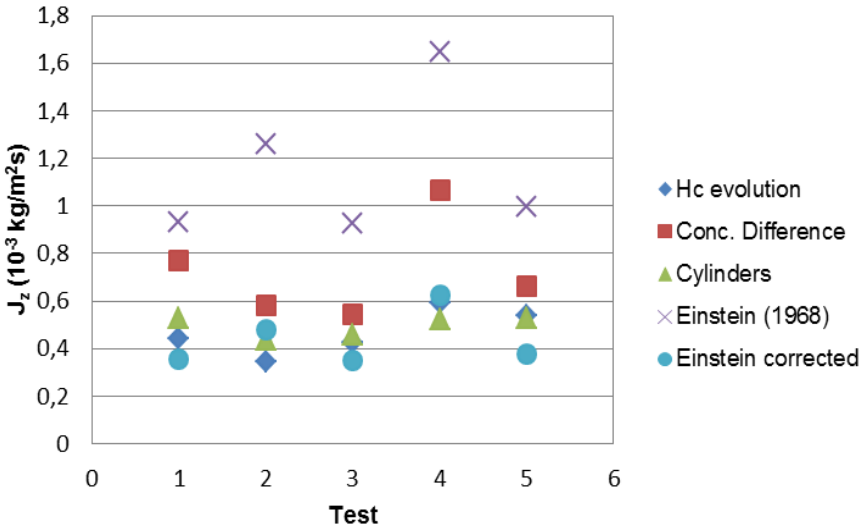

Figure 5. Fine sediment infiltration rates calculated from the clogged layer height evolution (diamonds), the concentration difference between the upstream and downstream ends of the channel (squares) and the mass of sediment retained in the cylinders (triangles). Theoretical values obtained following the model of Einstein (1968) are represented by crosses and their correction considering bed porosity are plotted as circles.

However, a certain trend towards enhanced settling is observed, especially when considering infiltration rates calculated from the concentration difference between the upstream and downstream ends of the flume. One reason for this enhancement can be the ability of the bed to trap infiltrated fine particles and to avoid their resuspension. Fine sediment entrainment is lower in permeable beds than in impermeable ones, due to the effect of bed gravel grains sheltering fine grains and decreasing the shear stress exerted on them (Hoyal et al. 1997). Moreover, enhanced settling can also be caused by fluid incursions towards the bed at different scales. Although these incursions must be compensated by ejections that make the mass balance possible, the asymmetry between the two kinds of events in terms of frequency and intensity can generate a net flux of fine sediment towards the bed (Fries and Trowbridge 2003, Fries and Taghon 2010).

The only variable that changed between tests 2, 3 and 4 was suspended sediment concentration. Measured infiltration rates may be expected to be proportional to suspended concentration. Rates obtained from concentration difference follow quite well this pattern (Figure 6). Data obtained from the cylinders and from clogged layer height evolution do not correspond to it exactly although a certain increasing trend is observed in fine sediment infiltration rates for increasing suspended sediment concentrations. A certain positive correlation is observed concerning bed slope when comparing the results from test 1 and test 3, with increased infiltration rates for the higher slope of test 1. This fact would be consistent with the positive correlation between bed shear stress and fine sediment infiltration observed in some previous studies (Fries and Taghon 2010). However, the different methods used to estimate the infiltration rate show diverging results. This divergence has also been observed in previous works so the influence of shear stress is not completely clear. With regard to water discharge, the comparison between tests 3 and 5 show a positive correlation between this variable and the infiltration rate. A higher discharge is also associated with a higher bed shear stress. Therefore, it could be inferred that the infiltration rate is positively correlated with bed shear stress. However, further observations on the flow patterns influence on fine sediment trajectories near the bed, are needed to clarify this point.

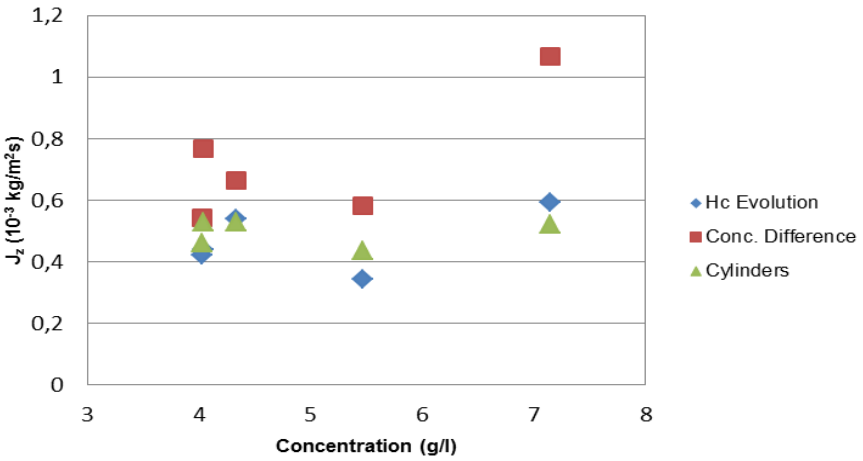

Figure 6. Fine sediment infiltration rate as a function of suspended sediment concentration

5. CONCLUSIONS

A series of experiments on silt-sized sediment infiltration into an initially clean gravel bed is presented. As predicted by previous studies (Gibson et al. 2010), the clogging of the bed occurs as unimpeded static percolation and the bed pores are filled from the bottom upwards. Three phases are distinguished during the infiltration process: an initial phase during which fine sediment deposits on the top of the gravel grains; an intermediate phase where fine sediment falls to the impermeable bottom and a clogged layer is formed at a constant growth rate; a final stage when the rate of fine sediment accumulation with time decreases until the system reaches an equilibrium where the clogged layer surface is one to three diameters from the bed surface. The final position of the clogged layer depends mainly on the bed shear stress of the flow.

When compared to a previous theoretical model proposing an infiltration rate based on Stokes velocity, the obtained results are found to be significantly lower. This fact is interpreted as a consequence of the theoretical model not taking into account bed porosity, which determines the area through which fine sediments can be infiltrated. Moreover, bed filtration and fluid incursions at different scales are proposed as other mechanisms that can influence on fine sediment infiltration rate.

ACKNOWLEDGMENTS

Irstea is acknowledged for the funding of Albert Herrero in post-doctoral position at Irstea Lyon-Villeurbanne.

REFERENCES

Arnon S., Marx L.P., Searcy K.E., and Packman A.I. (2010). Effects of overlying velocity, particle size, and biofilm growth on stream-subsurface exchange of particles. *Hydrological Processes*, 24 (1), 108-114.

Blaschke A.P. Steiner, K.H., Schmalfuss R., Gutknecht D., and Sengschmitt D. (2003). Clogging processes in hyporheic interstices of an impounded river, the Danube at Vienna, Austria. *International Review of Hydrobiology*, 88 (3-4), 397-413.

Cooper J.R., and Tait S.J. (2009). Water-worked gravel beds in laboratory flumes - a natural analogue? *Earth Surface Processes and Landforms*, 34 (3), 384-397.

Cui Y., Parker G., Braudrick C., Dietrich W.E., and Cluer B. (2006). Dam removal express assessment models (DREAM). Part 1: model development and validation. *Journal of Hydraulic Research* 44 (3), 291-307.

Einstein H. (1968). Deposition of suspended particles in a gravel bed. *J. Hydraul. Div. Am. Soc. Civ. Eng* 94 (5): 1197-1205.

Evans E., and A.C. Wilcox. (2013). Fine sediment infiltration dynamics in a gravel-bed river following a sediment pulse. *River Research and Applications.*

Fries J.S., and Taghon G.L. (2010). Particle Fluxes into Permeable Sediments: Comparison of Mechanisms Mediating Deposition. *Journal of Hydraulic Engineering* 136 (4), 214-221.

Fries J.S., and Trowbridge J.H. (2003). Flume observations of enhanced fine-particle deposition to permeable sediment beds. *Limnology and Oceanography* 48 (2), 802-812.

Frings R.M., Kleinhans M.G., and Vollmer S. (2008). Discriminating between pore-filling load and bed-structure load: a new porosity-based method, exemplified for the river Rhine. *Sedimentology* 55 (6), 1571-1593.

Gibson S., Abraham D., Heath R., and Schoellhamer D. (2009). Vertical gradational variability of fines deposited in a gravel framework. *Sedimentology* **56** (3), 661-676.

Gibson S., Abraham D., Heath R., and Schoellhamer D. (2010). Bridging Process Threshold for Sediment Infiltrating into a Coarse Substrate. *Journal of Geotechnical and Geoenvironmental Engineering* 136 (2), 402-406.

Grant S.B. Stewardson M.J., and Marusic I. (2012). Effective diffusivity and mass flux across the sediment-water interface in streams. *Water Resources Research* 48 (5).

Greig S.M., Sear D.A., and Carling P.A. (2007). A review of factors influencing the availability of dissolved oxygen to incubating salmonid embryos." *Hydrological Processes* 21 (3), 323-334

Hamm N.T., Dade, W.B., and Renshaw C.E. (2011). Fine particle deposition to porous beds. *Water Resources Research* 47.

Hoyal D., Bursik M.I., Atkinson J.F., and Depinto J.V. (1997). Filtration enhances suspended sediment deposition from surface water to granular permeable beds. *Water Air and Soil Pollution* 99 (1-4), 157-171.

Jones J.I., Collins, A.L. Naden P.S., and Sear D.A. (2012). The relationship between fine sediment and macrophytes in rivers. *River Research and Applications* 28 (7), 1006-1018.

Jones J.I., Murphy J.F., Collins A.L., Sear D.A., Naden P.S. and Armitage P.D. (2012). The impact of fine sediment on macro-invertebrates. *River Research and Applications* 28 (8), 1055-1071.

Khullar N.K., Kothyari U.C., and Raju K.G.R. (2013). Study of deposition of fine sediment within the pores of a coarse sediment bed stream. *International Journal of Sediment Research* 28 (2), 210-219.

Koski K.V. (1966). The survival of coho salmon (Oncorhynchus kisutch) from egg deposition to emergence in three Oregon coastal streams, *Master Thesis*, Oregon State University.

Packman A.I., Brooks N.H., and Morgan J.J. (2000). Kaolinite exchange between a stream and streambed: Laboratory experiments and validation of a colloid transport model. *Water Resources Research* **36** (8), 2363-2372.

Packman A.I., and MacKay J.S. (2003)."Interplay of stream-subsurface exchange, clay particle deposition, and streambed evolution. *Water Resources Research* 39 (4).

Ray C., Soong T.W., Lian Y.Q., and Roadcap G.S. (2002). Effect of flood-induced chemical load on filtrate quality at bank filtration sites. *Journal of Hydrology* 266 (3), 235-258.

Schälchli, U. (1992). The clogging of coarse gravel river beds by fine sediment. *Hydrobiologia* 235-236 (1), 189-197.

Wood P.J., and Armitage P.D. (1997). Biological effects of fine sediment in the lotic environment. *Environmental Management* 21 (2), 203-217.

A.3 Chasse de l'Arc

FIELD EXPERIMENT ON THE DYNAMICS OF FINE AND COARSE SEDIMENTS OVER A GRAVEL BAR IN AN ALPINE RIVER

BENOIT CAMENEN, ALBERT HERRERO, GUILLAUME DRAMAIS, FABIEN THOLLET, CHLOE LE BESCOND, EMELINE PERRET, CÉLINE BERNI

Irstea, UR HHLY Hydrology-Hydraulics, 5 rue de la Doua – CS 70077 – F-69626 Villeurbanne, France,
benoit.camenen@irstea.fr, albert.herrero@irstea.fr, guillaume.dramais@irstea.fr, chloe.le-bescond@irstea.fr, fabien.thollet@irstea.fr, emeline.perret@irstea.fr, celine.berni@irstea.fr

ABSTRACT

Alpine gravel-bed rivers are characterized by very poorly sorted sediments and significant grain sorting is generally observed on gravel bars. The grain size variability may significantly influence the inception of movement for each of the classes represented over a gravel bar. The purpose of this paper is to present some field measurements achieved on the Arc en Maurienne River, France. The main objective is to characterize the dynamics of fine and coarse sediments for conditions close to the incipient motion of gravels and for different degrees of clogging of the river bed. The field campaign was carried out on a gravel bar located 10 km downstream of St Jean de Maurienne during the dam flushing event on June 17th, 2014. Six patches including tagged pebbles (using PIT-tag) were built up with three different characteristics: clean patches formed with gravels and pebbles only, patches with a natural mixture where tagged pebbles were substituted to naturally arranged ones, and patches artificially clogged with fine sediments. These patches were located on the side of a secondary channel on the gravel bar. Surface grain size analyses of the gravel (using the Woolman method and photo analyses using BaseGrain) as well as topographic measurements were achieved the day before the event. During the flushing event, surface velocities over the gravel bar were measured thanks to video analysis (LSPIV). Water levels and mean slope in the secondary channel were measured thanks to pressure gauges positioned on the side of the secondary channel. An estimation of the bed shear stresses over the patches was thus possible all along the event. Intense water sampling was also carried out both upstream and downstream the secondary channel. During the post-event survey the day after, the PIT-tag search showed that the coarse particles did not move. On the other hand, a significant amount of fine sediments were deposited on the patches and infiltrated on the clean patches. Grain size analysis showed that deposited sediments were much coarser than sediments in suspension. An estimation of the fine sediment deposition rate and a discussion on the sediment dynamics is proposed from these measurements.

Keywords: *sediment mixture, gravel bar, infiltration, incipient motion*

1. INTRODUCTION

Alpine gravel-bed rivers are often characterized by very poorly sorted sediments and significant grain sorting is observed on gravel bars with relatively coarse sediments on the bar head and transverse channel and fine sediments on the bar tail (Lisle et a., 1991, 1993, Diplas, 1994, Lanzoni, 2000, Eekhout et al., 2013). The grain size variability significantly influences the inception of movement for each of the classes represented over a gravel bar (Konrad, 2002). In particular, fine sediment infiltration in the bed and fine sediment deposits are often observed over gravel bars in alpine rivers (Diplas 1994, Lisle & Hilton, 1999). Depending on the fine sediment content, fine sediments may limit or enhance gravel mobility (Diplas & Parker, 1992). The purpose of this paper is to present some field measurements performed on the Arc en Maurienne River, France. Main objectives are to characterize the dynamics of fine and coarse sediments for conditions close to the incipient motion of gravels and for different degrees of clogging of the river bed. The field campaign was carried out on a gravel bar located 10 km downstream of St Jean de Maurienne during the dam flushing event on June 17th, 2014. Patches with different degrees of clogging were built with tag gravels. Main hydraulic parameters measured during the event were water surface levels and surface velocities. Sediment characteristics of the patches were estimated before and after the event. A discussion of the impact of this event on the bed evolution, more especially on the infiltration dynamics is provided.

2. EXPERIMENTAL SITES AND DATA

2.1 Description of the experimental site

The fieldwork took place in the Arc River, located in the French Alps (Figure 1). The catchment area is 1957 km^2 (grey area in Fig. 1) with a nival hydrologic regime and a mean water discharge from 6-8 m^3/s in winter to 15-20 m^3/s in summer (Jodeau, 2007, Jaballah, 2013). The river bed has been largely modified and artificially straightened in many places in order to allow the 1 km wide valley to contain a road, a highway and a railway. Consequently, only 5% of the river reaches remain with their natural flow patterns and morphology. In addition the flow is regulated by many hydraulic constructions (several dams and pipes) for hydroelectricity production. The present regulated flow regime has significantly altered the natural river discharges and sediment transport. Although its bed is made of gravel, the Arc en Maurienne River has unusually high fine sediment transport, supplied by tributaries. The main ones are the Arvan and Glandon streams, which supply large amounts of predominantly black Lias schist.

The area of interest is a system of alternate bars located 18 km from the downstream reservoir at Sainte-Marie-de-Cuines (see Figure 1). This system is apparently forced due to the presence of a bend and a bridge pier at the downstream boundary (Jaballah et al., 2015). Lateral limits are set by 5 m high embankments made of boulders and scattered young trees leading to a river width of 50m in average. The mean slope of this reach is approximately 0.6 %. The fieldwork was more precisely carried out on a gravel bar located on the left side of the river 2.5 km upstream the confluence with the Glandon tributary (2 km upstream the bridge).

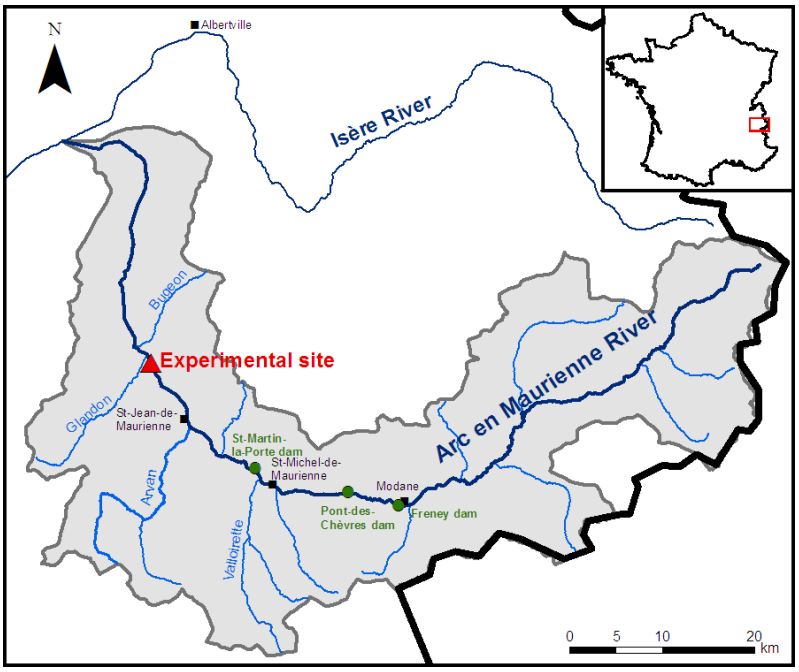

Figure 1. Map of the study site (green circles correspond to the three river dams).

2.2 Experimental set-up

A procedure is proposed here to study incipient motion of gravel particles for different conditions of clogging. Six patches were built on a gravel bar, which separates a secondary channel from the main channel (see Fig. 3). This secondary channel diverts a low percentage of the main channel flow discharge (about 10%). The gravel bar is totally covered for high flow conditions (over 110 m^3/s approximately). The six patches included 20 tracers (natural particle with a Pit-tag inserted) laid following a regular grid (Fig. 3, Camenen et al., 2010). Their size was one square meter approximately. The six patches were prepared in two rows parallel to the flow on the side of the secondary channel (cf. Fig; 3d). They were built in order to obtain three different characteristics:

- two clean patches made of cobbles of 4 to 10 cm in diameter (approx.), see Fig. 2a.
- two unmodified patches where natural cobbles are substituted by tagged cobbles, see Fig. 2b.
- two clogged patches for which a large amount of very fine sediments surrounds the tagged cobbles, see Fig. 2c.

Preparation of the different patches is detailed as follows. For unmodified patches, the bed structure was not modified and twenty cobbles initially present in the bed were manually substituted by tagged cobbles. The tagged cobbles were distributed in four rows of five cobbles each, with a distance of more than 20-25 cm between them. For the other type of patches, a surface of approximately one square meter was first excavated to a depth of approximately 10 cm. In case of clean patches, the resulting hole was then filled with cobbles and pebbles between 5 and 10cm in diameter including twenty tagged cobbles distributed similarly as for the unmodified patches. In case of clogged patches, it was filled with silt and clay sized material found in nearby (fine deposits on the gravel bar); and eventually, twenty tagged cobbles were introduced within this layer forming four rows of five cobbles each. The position and code of each tagged particles was identified within each patch. Coordinates (in the Lambert 93 system) of the four corners of each patch were measured using DGPS tool. A topographic survey of the gravel and secondary channel was also achieved before the flushing event.

An estimation of the grain size distribution for each of these patches was made using photo analysis thanks to the software Basegrain (Detert & Weitbrecht, 2012) to be compared with the Wolman (1954) pebble count procedure achieved on several places of the gravel bars. The median grain size varies from 1 to 3 cm around the patches with a standard deviation of approximately 3.5; detailed results are not presented in this paper.

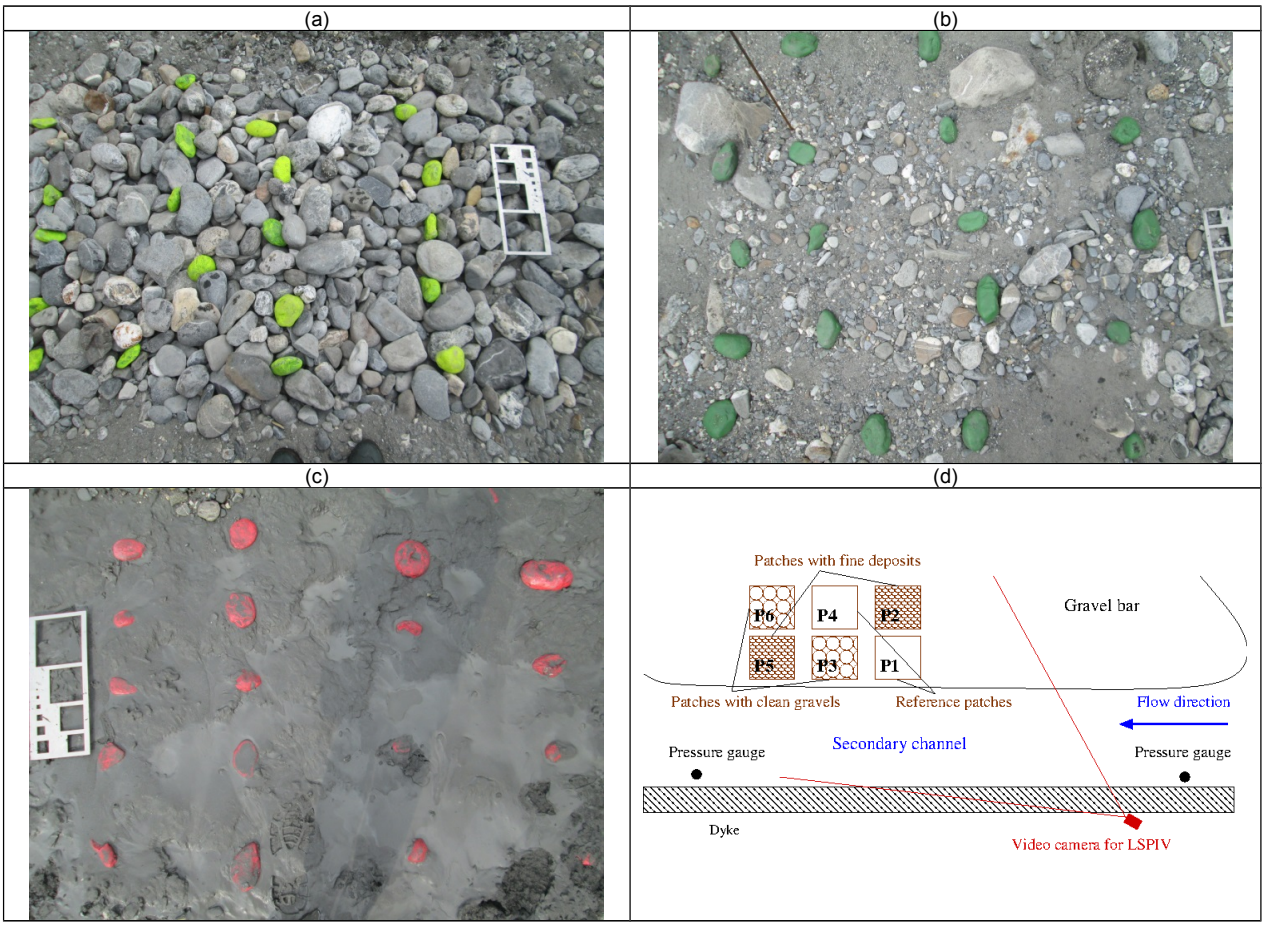

Figure 2. Photos of the different patches built: (a) cleaned patch P6 (b) natural patch P1 (c) clogged patch P5, and (d) schematic view of the experimental set-up.

During the flushing event, several measurements were achieved to obtain a better idea of the hydro-sedimentary conditions over the patches. A system for video analysis was implemented using a camera fixed at the top of a telescopic mast on the side embankment (Fig. 3). The Large Scale Particle Image Velocimetry (LSPIV) method was used to measure the surface flow velocities during the event. Ground Reference Points (GRPs) were positioned in the view field using square targets (red and white) on the gravel bar and on the bank. They allow a geometrical correction of the pictures (Jodeau et al., 2008). The software Fudda-LSPIV (Le Coz et al., 2014) was eventually used to process the movies in order to get the velocity field and estimate the discharge within the secondary channel. 10 movies of 30 s were eventually taken during the event, which corresponds to a movie every 40 minutes in average.

Two pressure gauges were installed upstream and downstream the secondary channel in order to obtain an estimation of the water level and slope within the secondary channel. Atmospheric pressure effects were taken into account using a third pressure gauge outside water.

Since fine sediment concentrations may be very high during these events (up to 30 g/l, Antoine et al., 2011), a possible deposition of fine particles was expected along the secondary channel during the event. Intense water sampling (every half an hour) was performed at both upstream and downstream ends of the secondary channel. Sediment concentration was measured for each sample using the filtration method and grain size analysis was made by laser diffractometry.

After the event, we intended to make a search of the tagged particles using a specific antenna to detect each particle with their own code together with a DGPS to note the location of each particle detected (Camenen et al, 2010). However, as discussed later, the flushing event was interrupted unexpectedly and the discharge did not reach 130 m^3/s as planned. As a consequence, three of the patches remained outside water during the event and velocities were too low over the three other patches to transport coarse particles. None of the tagged particles moved but a significant infiltration / deposition of fine particles was eventually observed.

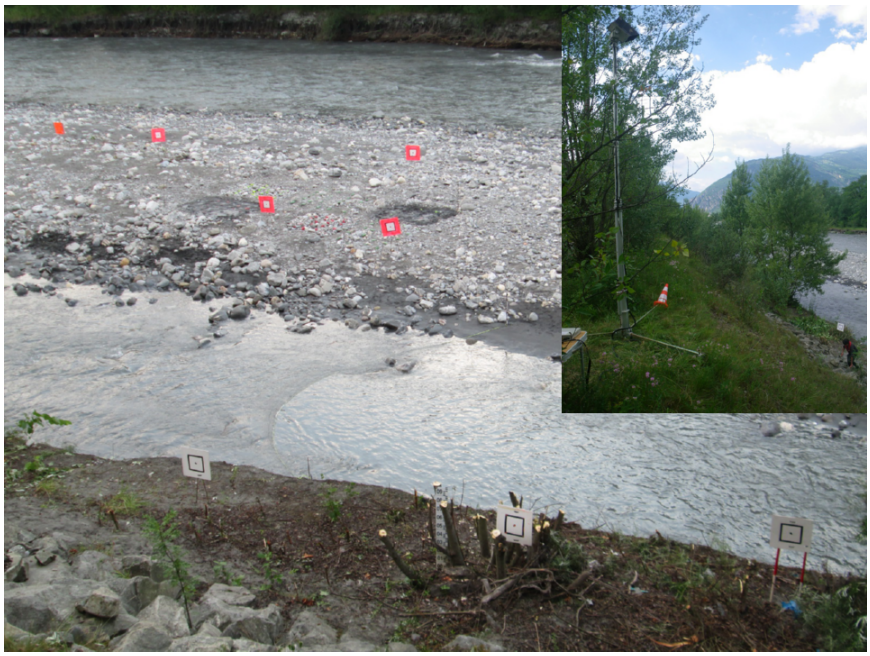

Figure 3. Photo of the set-up for video analysis showing GRPs (photo inserted: mast on which the camera is fixed).

3. EXPERIMENTAL RESULTS

3.1 Discharge and sediment concentrations

The discharge was measured at the hydrometric station of Pontamafrey located 9 km upstream. It was estimated that the time for the wave to travel from Pontamafrey to Sainte-Marie-de-Cuine is Δt = 45mn. Flushing operations are conducted yearly in June with the exception of years for which a large flood occurred previously. Since the same procedure is followed, similar discharge time series are generally observed with a first plateau at 80-100 m^3/s lasting approximately 4 hours and a second plateau at 120-130 m^3/s lasting approximately 4 hours (see red line in Fig. 4a corresponding to the 2011 flushing event). It appears clearly that the 2014 flushing event was shorten with nearly no existence of the second plateau, which obviously affected our experiment. This was explained later due to an incident in one of the dam reservoirs.

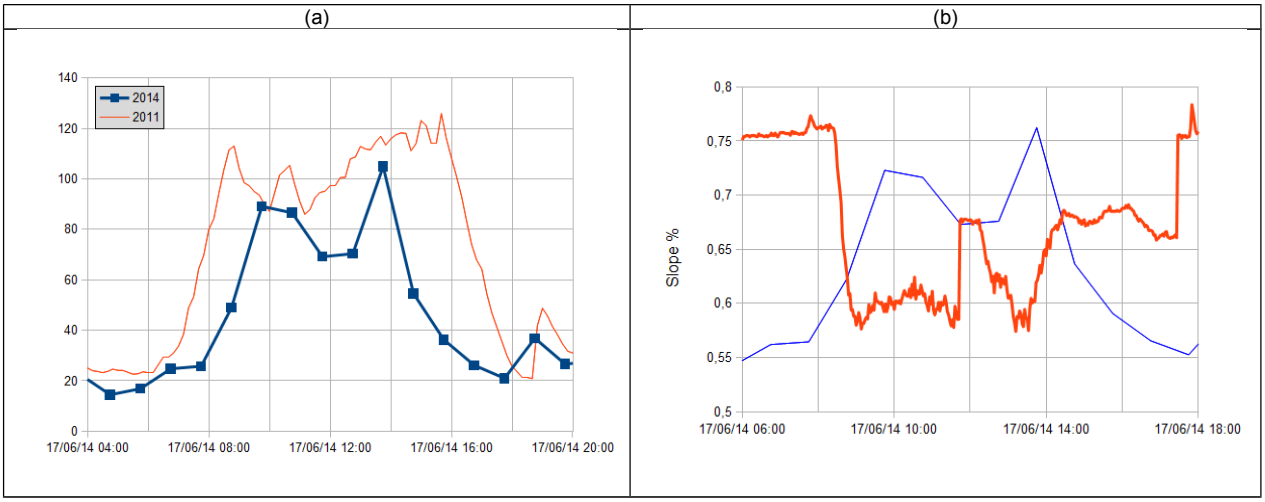

Figure 4. Discharge time series (TU+2) measured at the hydrometric station of Pontamafrey with Δt = 45mn (a) and water slope on the secondary channel (red line, the blue line corresponds to the discharge) (b).

In Fig. 4b, the slope in the secondary channel during the event is presented, as estimated from the two pressure gauges installed. Interestingly, it appeared that the slope first decreased with the increase of discharge, maybe due to the downstream boundary influenced by the main channel level. It varied between 0.6 and 0.7% during the event. From the water level and LSPIV measurements, we also estimated the duration for which patches P1, P3 and P5 were under water:

$T = 60$ mn.

Results for concentration measurements are presented in Fig. 5. Concentration levels clearly follow the discharge time-series. A plateau at 4 g/l is observed during the first plateau for *Q* followed by a pick at 12 g/l at the pick of discharge for which supercritical flow occurs in dam reservoirs. This may explain the much larger concentrations observed. However, these concentrations remain relatively low compared to previous flushing events (Antoine et al., 2011). Grain size analyses (Fig. 5b) show that the composition of the suspension did not evolve significantly during the event (d_{50} = 17 µm). One can observe a small pick at the pick discharge with (d_{50} = 20 µm).

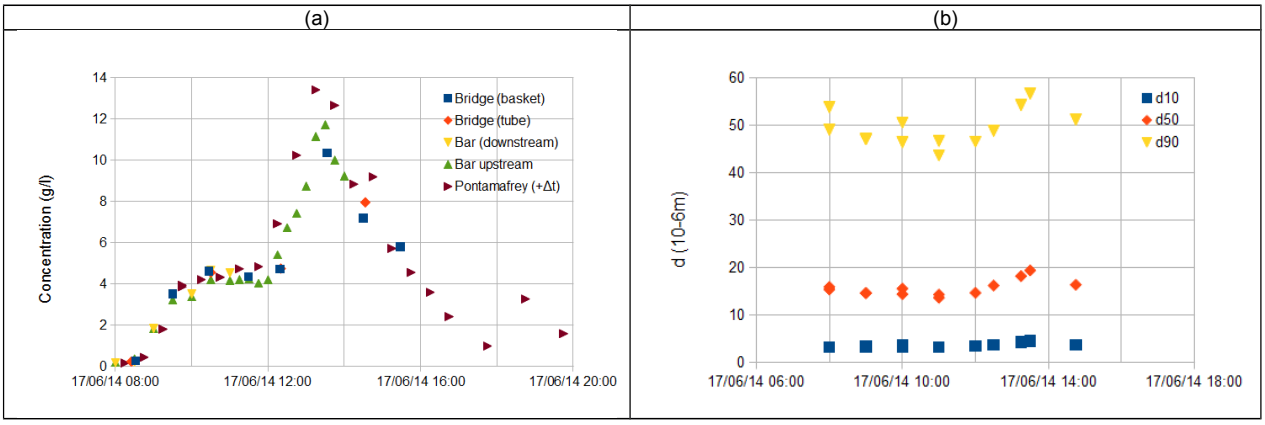

Figure 5. Concentration time series measured upstream and downstream the gravel bar, 1km downstream from a bridge and 10 km upstream at the hydrometric station of Pontamafrey with Δt = 45mn (a) and grain size analysis of samples next to the gravel bar (b).

3.2 Surface velocity and bed shear stresses

LS-PIV is an image-based method, which consists in calculating the most likely displacements of patterns between two successive images using statistical identification (Fujita et al., 1998, Jodeau et al., 2008). Fig. 6 presents some typical results from the LSPIV post-processing using Fudaa-LSPIV (Le Coz et al., 2014). If a cross-section of the river bed is available (see yellow line in Fig. 6a), it is also possible to estimate the discharge assuming a ratio between the depth averaged velocity and the surface velocity of 0.85 (rough bed). Similarly, assuming a roughness length $k_s = 2d_{90} \approx 8$ cm, it is also possible to estimate the local bed shear stress. Focusing on the side of the secondary channel next to the patches (Fig. 6b), it is interesting to see the deflection of the surface velocities toward to side of the channel. It actually corresponds to small waves propagating toward the gravel bar with a celerity of 10 cm/s approximately. Because of mass conservation, a small undertow current should be present with a main direction toward the center of the channel.

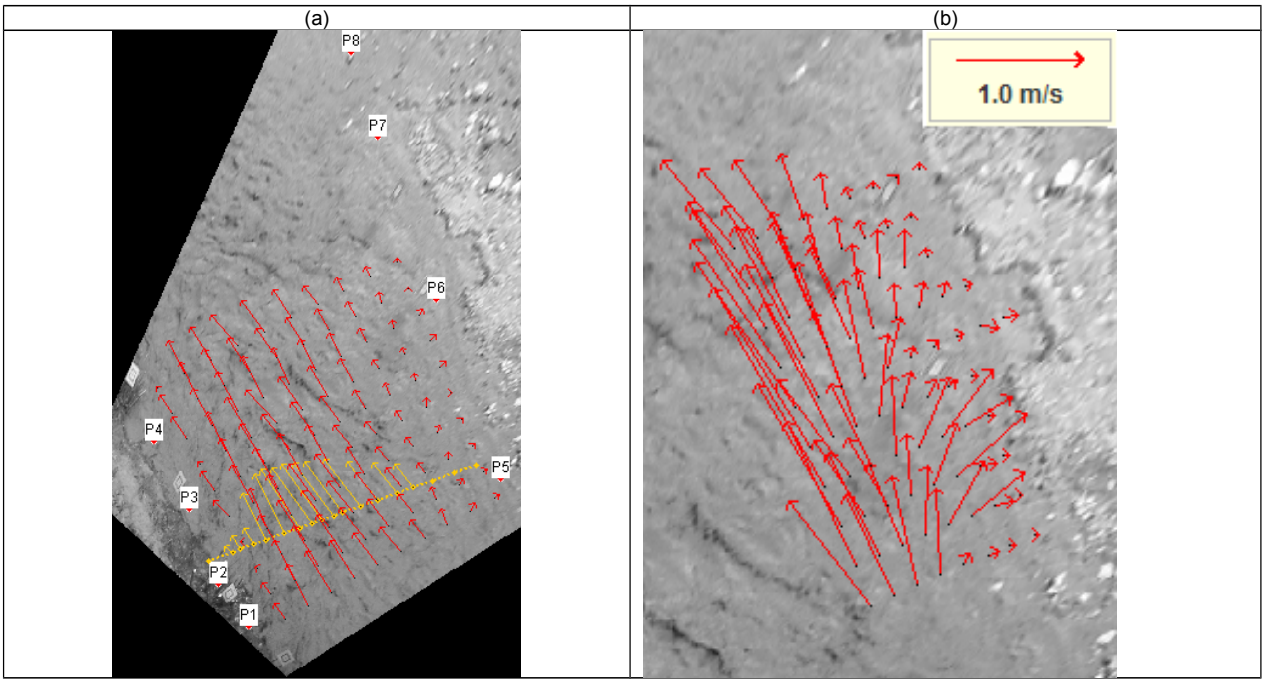

Figure 6. Estimation of the surface velocity using LSPIV in the secondary channel at 13:30 over the whole section (a) and making a zoom close to the patches (b).

Best shear stress estimates using both LSPIV and water level measurements are presented in Fig. 7. As discussed before, LSPIV allows an estimation of local bed shear stress as soon as bed topography measurements are available. Fig. 7a presents the bed shear stress distribution throughout a secondary channel section. Values over 100 Pa were observed in the middle of the secondary channel that is sufficient to mobilize the coarsest particles forming the bed. Section-averaged bed shear stress are presented in Fig. 7b, either using the "law of the wall" method with data from Fig. 7a or using the reach averaged method:

$$\tau = \rho C_f V^2 = \rho g R_h I \qquad [1]$$

with ρ the water density, $C_f = f(R_h, k_s)$ the friction coefficient, V the section-averaged velocity, g the acceleration of gravity, R_h the hydraulic radius, and I the water slope. The "law of the wall" method was applied locally using the local depth-averaged velocity and assuming $R_h = h$ with h the local water depth. Good agreement is observed between the two methods used to estimate the section averaged bed shear stress in the secondary channel. Results from the LSPIV measurements are however very sensitive to the water level estimation, especially when water depths are shallow. This explains the very low value obtained at t = 07:23. In the zone over the patches, it was difficult to estimate the local bed shear stress. By extrapolation to what we could measure, we estimate it close to zero. However, some possible erosion of fine sediments could have been possible because of the propagation of the small waves described above.

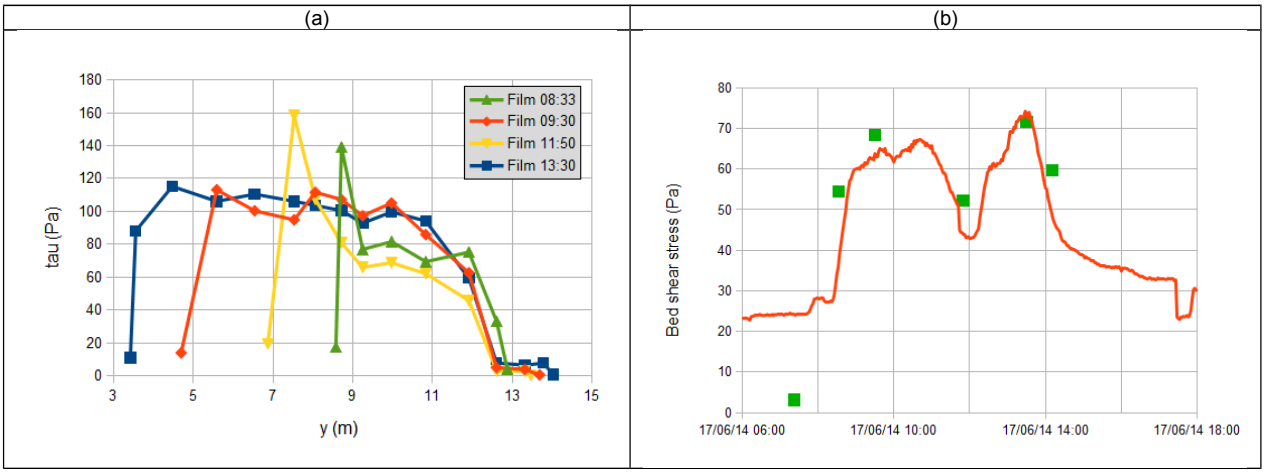

Figure 7. Local bed shear stress distribution throughout the secondary channel next to the patches from LSPIV measurements (a) and mean bed shear stress in the secondary channel from slope measurement and LSPIV measurement (green square) (a).

3.3 Fine sediment infiltrated

Although no movement of the tagged particle could be observed, a significant amount of fine sediments infiltrated the clean patch P3. An estimation of the amount of fine sediments infiltrated was made using the following method (Fig. 8): a surface of approximately 0.2 m² (0.45 × 0.45 m) was selected within patch P3. All fine sediments infiltrated in cobble layer (approximately 10 cm thick, see Fig. 8c) were collected in a basket. Coarse particles were taken out and cleaned in the same basket. Eventually, a sample of 5.23 kg was collected. Since some sandy particles may have been collected at the bottom of the layer, this sample was sieved at 0.5 mm. It remained 4.56 kg.

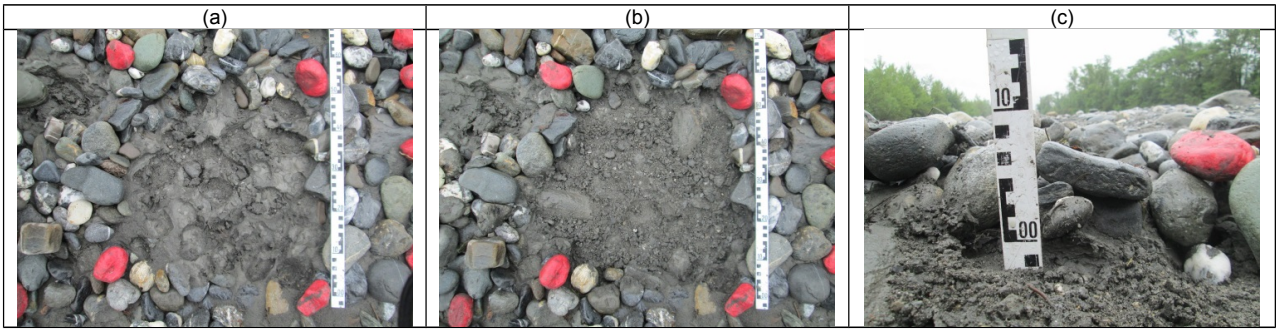

Figure 8. Estimation of the fine sediment infiltration in patch P3; photos of the sampling surface after taking off pebbles (a) and cleaning all deposits (b), side picture of the sampling surface (c).

When fine sediments are much smaller than coarse sediments, fines can percolate without getting trapped as they pass through the pore throats, therefore being deposited only on the top of coarse grains or on an eventual impermeable layer located under the gravel bed. In this situation, the bed is filled from the bottom upwards and tends to a relatively uniform distribution of fines over the bed depth. This infiltration mechanism that corresponds typically to our case is commonly known as unimpeded static percolation (Gibson et al., 2009, Evans & Wilcox 2013). Assuming an initial porosity of 0.4 for the patch P3, and a porosity of 0.4 for the fine sediments infiltrated, the maximum amount of fine sediments that could infiltrate the 0.2 m² is $M = 2650 \times 0.4^2 \times 0.1 \times 0.2 = 8.5$ kg. This means that approximately 50% of the pores were clogged with fine sediments in 60 minutes.
In Fig. 9, the grain size distributions of the suspended sediments and of the sediments infiltrated in the patch 3 are plotted. For the sediment in suspension, 6 classes predominate:

- one class of clay with $d \approx 5$ µm,
- one class of fine silts with $d \approx 12$ µm,
- four classes of coarse silts with $d \approx 25$, 35, 47, and 68 µm, respectively

The very same classes are observed for the sediments infiltrated in patch 3 but with different proportions. A class of poorly sorted fine sands with d ≈ 120 µm is also present in the deposits. It clearly shows the grain sorting occurring over the bed for the infiltration process. Coarser particles with larger settling velocity do settle and infiltrate easier even when bed shear stresses are very low. The presence of the fine sand class indicates that this sediment fraction travels in a graded suspension with concentration much larger close to the bottom. Surface water sampling on the side of the river do not allow to detect this class of sediments.

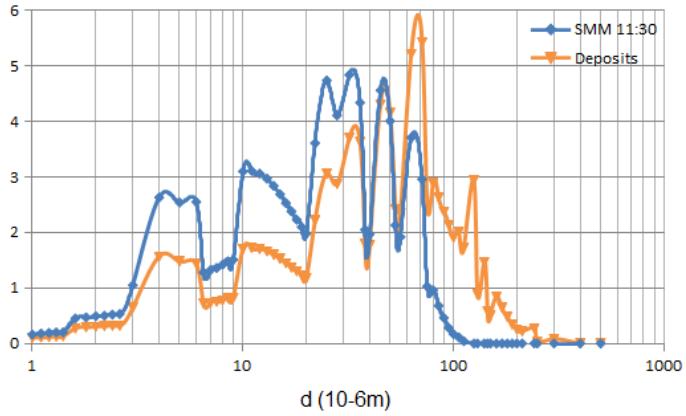

Figure 9. Grain size distribution comparison between the sediments in suspension and the sediments infiltrated in the patch 3.

4. CONCLUSIONS

A field survey to study the dynamics of fine and coarse sediments in an alpine river during a flushing event is presented. It included flow velocity measurements and surface water sampling during the event and characteristics of the bed and reference patches before and after the event.

The proposed methodology appeared successful to better understand the local dynamics of a mixture of sediment. Estimation of bed shear stress in the secondary channel using both pressure gauges and LSPIV measurements were in good agreement. An intense sampling frequency for the fine sediment in suspension is necessary for such event since the concentration values can change rapidly.

However, the flushing event was interrupted unexpectedly and bed shear stress remained too low to transport coarse particles. None of the tagged particles moved but a significant infiltration / deposition of fine particles was eventually observed. The infiltration rate was estimated at 50% in the clean patch after a period under water of 60 minutes only. Grain size analyses of both fine sediment in suspension and infiltrated sediment gave an interesting view of the fine sediment dynamics over the gravel bar.

A similar experiment is planned for the 2015 flushing event with the objective of better estimating the inception of motion of coarse particles for different fine sediment contents.

REFERENCES

Antoine, G., Camenen, B., Jodeau, M. & Esteves, M. (2011). *Assessment of the suspended sediment load due to dam flushing along the Arc and Isère rivers, France.* Proc. 7th IAHR symposium on River, Coastal and Estuarine Morphodynamics, 1-10

Camenen, B., Le Coz, J., Paquier, A. & Lagouy, (2010). *An estimation of gravel mobility over an alpine river gravel bar (Arc en Maurienne, France) using PIT-tag tracers.* River Flow, Proc. 5th Int. Conf. on Fluvial Hydraulics, Braunschweig, Germany. M. Dittrich, A.; Koll, K.; Aberle, J. & Geisenhainer, P. (Eds.), pp. 953-960.

Detert, M., Weitbrecht, V. (2012). Automatic object detection to analyze the geometry of gravel grains – a free stand-alone tool. River Flow, , Proc. 6th Int. Conf. on Fluvial Hydraulics, R.M. Muños (Ed.), ISBN 978-0-415-62129-8, pp. 595-600.

Diplas, P. (1994). *Modelling of fine and coarse sediment interaction over alternate bars*. Journal of Hydrology, 159:335–351.

Diplas, P. & Parker, G. (1992). *Deposition and removal of fines in gravel-bed streams*. In Billi, P., Hey, R., Thorne, C. & Tacconi, P., editors : Dynamics of gravel bed rivers, pages 313–329. Wyley & Sons. 11

Eekhout, J. P. C. , Hoitink, A. J. F. & Mosselman, E. (2013). *Field experiment on alternate bar development in a straight sand-bed stream*, Water Resources Research, 49:1-12.

Evans, E. & Wilcox, A. C. (2013). *Fine sediment infiltration dynamics in a gravel-bed river following a sediment pulse*. River Research and Applications, 30, 372-384

Gibson, S., Abraham, D., Heath, R. & Schoellhamer, D. (2009). *Vertical gradational variability of fines deposited in a gravel framework Sedimentology*, 56:661-676.

Fujita I., Muste M. & Kruger A. (1998). Large-scale particle image velocimetry for flow analysis in hydraulic engineering applications. Journal of Hydraulic Research, 36:397–414.

Jaballah, M. (2013). *Alternate bar morphodynamics in an engineered mountainous river*. PhD thesis, C. Bernard University, Lyon 1. 2013

Jaballah, M.; Camenen, B. & Paquier, A. (2015). *Alternate bar development in an alpine river following engineering works*. accepted in “Advances in Water Resources”

Jodeau, M. (2007). *Morphodynamique d’un banc de galets en rivière aménagée lors de crues [Gravel bar morphodynamics in an engineered river during high flow events].* PhD thesis, C. Bernard University, Lyon I. (in French).

Jodeau, M., Hauet, A., Paquier, A., Le Coz, J. & Dramais, G. (2008). *Application and evaluation of LS-PIV technique for the monitoring of river surface velocities in high flow conditions.* Flow Measurement & Instrumentation, 19, 117-127

Konrad, C. P., Both, D. B., Burges, S. J., and Montgomery, D. R. (2002). *Partial entrainment of gravel bars during floods*. Water Resources Research, 38(7):1-16.

Lanzoni, S. (2000). *Experiments on bar formation in a straight flume: 2. Graded sediment*, Water Resources Research, 36:1-11.

Le Coz, J, Le Boursicaud, R, Jodeau, M, Hauet, A. & Marchand, B. (2014). *Image-based velocity and discharge measurements in field and laboratory river engineering studies using the free FUDAA-LSPIV software*, River Flow, Proc. 7th Int. Conf. on Fluvial Hydraulics Lausanne, Switzerland.

Lisle, T. et Hilton, S. (1999). *Fine bed material in pools of natural gravel bed channels*. Water Resources Research, 35:1291-1304.

Lisle, T., Ikeda, H. et Iseya, F. (1991). *Formation of stationary alternate bars in a steep channel with mixed-size sediment : a flume experiment.* Earth Surface Processes and Landforms, 16:463–469.

Lisle, T., Iseya, F. et Ikeda, H. (1993). *Response of a channel with alternate bars to a decrease in supply of mixed-size bed load : a flume experiment.* Water Resources Research, 29:3623-3629.

Wolman, M. G. (1954). *A method of sampling coarse river-bed material.* Transactions American Geophysical Union. 35(6):951-956.

Références

Einstein H.A. Deposition of suspended particles in a gravel bed. *J. Hydraul. Eng.*, 94(5): 1197–1205, 1968.